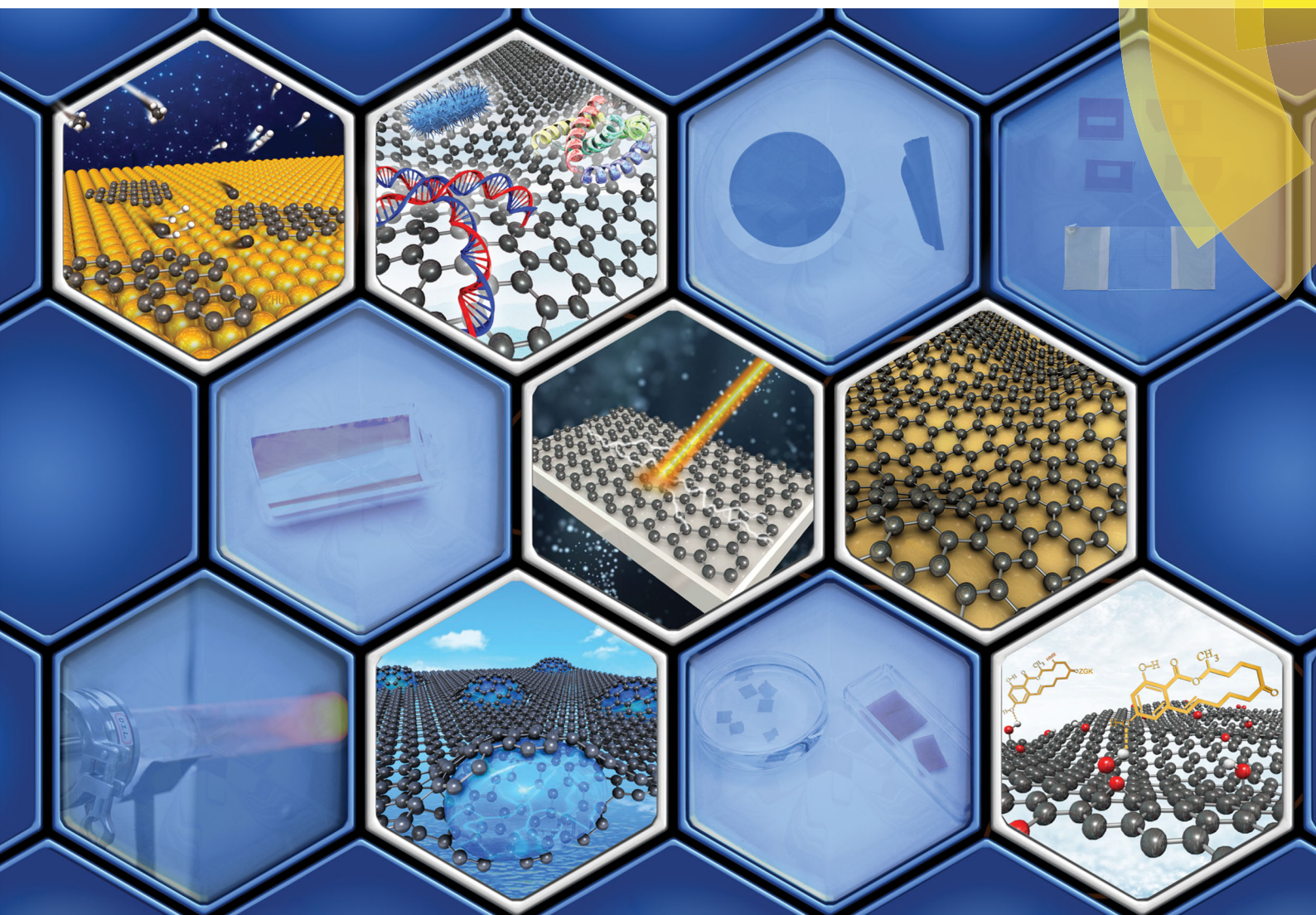


Chem Soc Rev

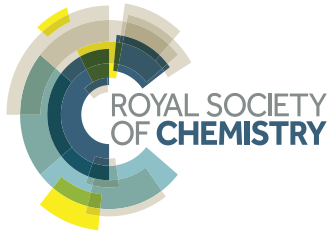
Chemical Society Reviews

rsc.li/chem-soc-rev



Includes a collection of articles on the theme of Graphene Chemistry

ISSN 0306-0012



REVIEW ARTICLE

Jian-Bin Xu, Rodney S. Ruoff, Hongwei Zhu et al.
The physics and chemistry of graphene-on-surfaces

REVIEW ARTICLE



Cite this: *Chem. Soc. Rev.*, 2017,
46, 4417

The physics and chemistry of graphene-on-surfaces

Guoke Zhao,^{†[a](#)} Xinming Li,^{ID †[b](#)} Meirong Huang,^{†[a](#)} Zhen Zhen,^a Yujia Zhong,^a Qiao Chen,^a Xuanliang Zhao,^a Yijia He,^a Ruirui Hu,^a Tingting Yang,^a Rujing Zhang,^a Changli Li,^a Jing Kong,^c Jian-Bin Xu,^{ID *[b](#)} Rodney S. Ruoff^{*[d](#)} and Hongwei Zhu^{ID *[a](#)}

Graphene has demonstrated great potential in next-generation electronics due to its unique two-dimensional structure and properties including a zero-gap band structure, high electron mobility, and high electrical and thermal conductivity. The integration of atom-thick graphene into a device always involves its interaction with a supporting substrate by van der Waals forces and other intermolecular forces or even covalent bonding, and this is critical to its real applications. Graphene films on different surfaces are expected to exhibit significant differences in their properties, which lead to changes in their morphology, electronic structure, surface chemistry/physics, and surface/interface states. Therefore, a thorough understanding of the surface/interface properties is of great importance. In this review, we describe the major “graphene-on-surface” structures and examine the roles of their properties and related phenomena in governing the overall performance for specific applications including optoelectronics, surface catalysis, anti-friction and superlubricity, and coatings and composites. Finally, perspectives on the opportunities and challenges of graphene-on-surface systems are discussed.

Received 10th April 2017

DOI: 10.1039/c7cs00256d

rsc.li/chem-soc-rev

^a State Key Lab of New Ceramics and Fine Processing, School of Materials Science and Engineering, and Center for Nano and Micro Mechanics, Tsinghua University, Beijing 100084, China. E-mail: hongweizhu@tsinghua.edu.cn

^b Department of Electronic Engineering, The Chinese University of Hong Kong, Hong Kong SAR, China. E-mail: jbxu@ee.cuhk.edu.hk

^c Department of Electrical Engineering and Computer Sciences, Massachusetts Institute of Technology, Cambridge, Massachusetts 02139, USA

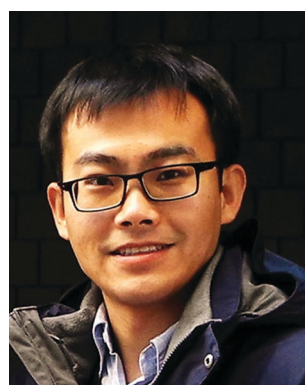
^d Center for Multidimensional Carbon Materials, Institute for Basic Science (IBS), and Department of Chemistry, Ulsan National Institute of Science and Technology (UNIST), Ulsan, Republic of Korea. E-mail: ruofflab@gmail.com

† These authors contributed equally to this work.



Guoke Zhao

Guoke Zhao received her bachelor's degree from Northwestern Polytechnical University in 2016. She is currently a PhD candidate with Prof. Hongwei Zhu at the School of Materials Science and Engineering, Tsinghua University, China. Her research mainly focuses on nanocrystals.



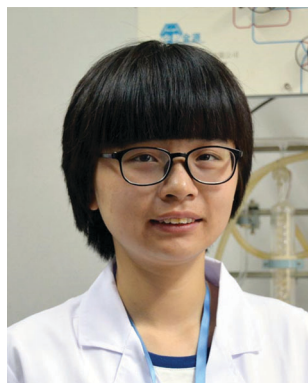
Xinming Li

Xinming Li obtained his PhD in Materials Science and Engineering from Tsinghua University in 2013, after receiving his BS in Mechanical Engineering from the same university. He was a visiting scholar at Massachusetts Institute of Technology (2011–2012) and an Assistant Professor (2013–2016) at National Center for Nanoscience and Technology, China. He is currently a postdoctoral research fellow at The Chinese University of Hong Kong. His research interests include the synthesis and structural engineering of carbon nanomaterials and 2D materials, and their applications in energy conversion, optoelectronics, sensors, and flexible devices.

1. Introduction

Graphene, a two-dimensional (2D) structure with carbon atoms arranged in a honeycomb lattice, was successfully mechanically exfoliated in 2004.¹ The history of graphene can be traced back to the early reports of graphene oxide (GO).² Later, with the development of the chemical/thermal reduction of GO and the epitaxial growth of graphene, single layers of graphite were observed and defined as “graphene” by the International Union of Pure and Applied Chemistry in 1995.³ Graphene possesses excellent physicochemical, electronic, optical,

thermal, and mechanical properties,^{4–9} that are mainly due to its atomic thickness and structure. However, it cannot stand alone without a supporting substrate in real applications. Therefore, graphene occurs in combination with various substrates, such as metals, semiconductors, ceramics, polymers, biomaterials, and even liquids,^{10–14} to form graphene-on-surface systems and the interfacial structure and interactions may cause modifications, and even add new features to the intrinsic characteristics of graphene. Therefore, investigating and understanding the physics and chemistry of the interfaces in these graphene-on-surface systems is very important.



Meirong Huang

Meirong Huang received her bachelor's degree from China University of Petroleum (Beijing) in 2016 and is currently conducting her PhD studies under the supervision of Prof. Hongwei Zhu at Tsinghua University. Her current research focuses on photocatalysis.



Jian-Bin Xu

Jian-Bin Xu received his BSc and MSc from Nanjing University in 1983 and 1986, respectively. Since 1988, he has been privileged to study in the University of Konstanz. His doctoral dissertation was focused on nanoscopic heat transport associated with electronic processes. He earned his doctorate (Dr.rer.nat.) in 1993. Afterwards, he joined the Department of Electronic Engineering, The Chinese University of Hong Kong. His research interests include 2D materials; advanced solar energy technology; scanning probe techniques; interface engineering for materials and devices; physics and technology of organic semiconductors; functional oxides, etc.



Rodney S. Ruoff

Rodney S. Ruoff, Distinguished Professor, UNIST Department of Chemistry and the School of Materials Science and Engineering, is director of the Center for Multi-dimensional Carbon Materials (CMCM), an IBS Center located at the Ulsan National Institute of Science and Technology (UNIST) campus. Prior to joining UNIST he was the Cockrell Family Regents Endowed Chair Professor at the University of Texas at Austin from September 2007. He earned his PhD

in Chemical Physics from the University of Illinois-Urbana in 1988, and he was a Fulbright Fellow in 1988–89 at the Max Planck Institute für Strömungsforschung in Göttingen, Germany. He was at Northwestern University from January 2000 to August 2007, where he was the John Evans Professor of Nanoengineering and director of NU's Biologically Inspired Materials Institute. He is a Fellow of the Materials Research Society, the American Physical Society, and the American Association for the Advancement of Science. He was recently awarded the 2014 MRS Turnbull Lectureship prize.



Hongwei Zhu

Hongwei Zhu is a Professor of School of Materials Science and Engineering, Tsinghua University, China. He received his BS degree in Mechanical Engineering (1998) and PhD degree in Materials Processing Engineering (2003) from Tsinghua University. After Post Doc. studies in Japan and USA, he began his independent career as a faculty member at Tsinghua University (2008 ~ present). His current research interests involve structural design

and engineering of nanomaterials for energy and environmental applications.

The combination of graphene with metals, semiconductors, ceramics, polymers, and biomaterials may have a great influence on the properties of graphene. The surface physics and chemistry of the substrates, interfacial structure and interaction, and interface impurities lead to changes in the morphology and electronic structure of graphene, and thus its properties. The integration of graphene may also bring about some new characteristics to the substrates and form intriguing graphene-on-surface systems. These graphene-on-surface systems greatly extend its application in various fields. The interface between graphene and its support plays a dominant role in effectively combining the merits of each component in these hybrid systems. Manipulation of the interfacial structure and interaction is crucial for designing and optimizing devices based on graphene and its derivatives. Interfaces also play an important role in obtaining high quality graphene. Graphene can be either exfoliated from a mother material or grown on selected substrates by various methods including epitaxial growth and chemical vapor deposition (CVD).^{15–17} CVD that uses a metal substrate as both a growth template and a catalyst offers an economical way to scale up the preparation of graphene. In a typical CVD process for graphene growth, the lattice of the substrate should match that of graphene, and the surface roughness, grain orientation, thickness and

surface impurities of the substrate can affect the quality and properties of graphene. In addition to the growth process, the transfer of graphene from its growth substrate to another target substrate also involves graphene-on-surface systems, such as graphene-on-polymers, graphene-on-liquids and graphene-on-semiconductors (depending on the target substrate). They can also deteriorate the quality of graphene.¹⁸ Defects and contamination introduced during the transfer can lead to discontinuities in the graphene, and thus decrease the performance of the devices using it. Great attention has been paid to the interface between graphene and its support substrate to maintain its properties.

The present review will focus on the physical and chemical properties of the surfaces and interfaces involved in hybrid graphene systems. As illustrated in Fig. 1, typical interfacial structures and interactions between graphene and metals, semiconductors, ceramics, polymers, biomaterials, and liquids, as well as their influence on the properties of graphene and the performance of devices using it are reviewed in detail. Interfaces involved in the growth and transfer of graphene are also discussed, followed by applications of graphene and its derivatives in optoelectronics, surface catalysis, anti-friction surfaces and coatings and composites. Finally, perspectives on the opportunities and challenges are discussed.

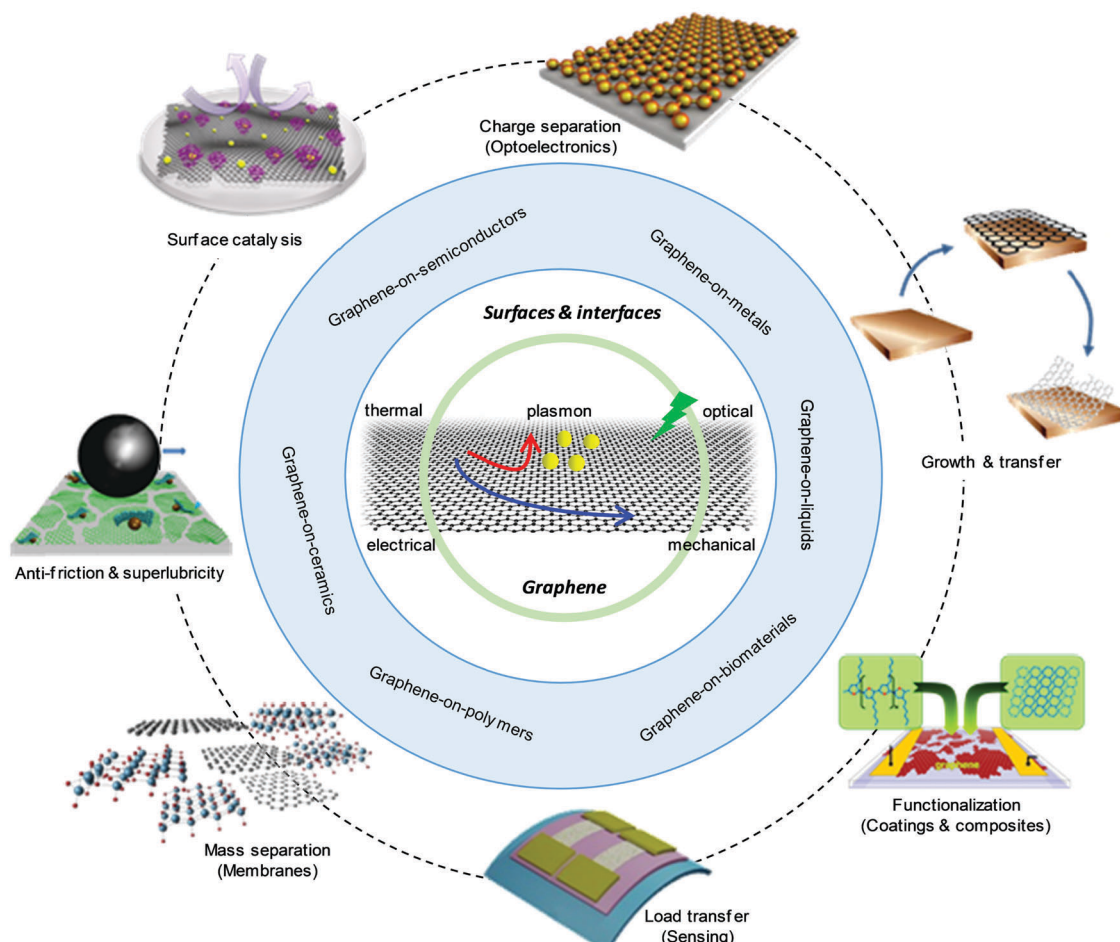


Fig. 1 Overview of "graphene-on-surface" systems showing the surface and interface influences and relevant applications.

2. Graphene on surfaces

The unique properties of graphene are mainly attributed to its single-atom thickness and 2D structure. Therefore, the manipulation and conservation of the chemical and physical stability of its 2D structure is critical. The single-atom thick nature of graphene means that it is unlikely to stand alone without a substrate in real applications and its interaction with the substrate has become the most critical research topic. In addition, the tunable electronic structure of graphene makes it highly sensitive to the environment, which can produce various functionalities. Metals, semiconductors, ceramics, polymers, biomaterials, and even liquids have been used as a support substrate for graphene. In the following sections, these interfacial interactions, their effects on the properties of graphene and the potential applications of graphene-on-surface systems are reviewed in detail.

2.1 Graphene-on-metals

The interactions between graphene and metals can be traced back to the first preparation of graphene on single crystal transition metals (TMs), such as Pt(111) and Ru(0001). The low energy electron diffraction patterns of these metals annealed at high temperatures indicate a crystalline graphitic layer, and this has become a common graphene preparation method. Later, CVD was introduced to use single or multi-crystal metal catalysts as substrates for the growth of high quality graphene.^{19–21} The interfacial structures and interaction strength have a significant influence on the morphology and electronic structure of CVD grown graphene. Understanding the interactions between graphene and metal surfaces is the key to manipulating the properties of CVD grown graphene. In all graphene research studies, the study of its interfaces with metals is one of the most important subjects. With the dramatically increased interest in graphene, comprehensive reviews on graphene appeared to summarize systematic theories.^{10,11,22,23} Besides, a corrugated surface of graphene can be obtained due to the lattice mismatch at the graphene/metal interface, which can be used as a template to form periodic metallic nanostructures. They can be applied in various fields, such as surface-enhanced Raman spectroscopy (SERS).

2.1.1 Structure of the graphene/metal interface. The direct growth of graphene on metals can be classified into two types: surface carbon segregation during the cooling process and migration of decomposed hydrocarbons. Traditional CVD for graphene synthesis usually produces polycrystalline graphene films that consist of disoriented grains. To understand the interactions at the graphene/metal interface, the effects of grain orientations are neglected in the present review. We only focus on the cases where single crystal graphene is epitaxially grown on perfectly ordered metal surfaces.

Table 1 summarizes the values of the distance between the graphene and the substrate metal surface and the binding energy of the d-band center relative to the Fermi energy.¹¹ These values suggest that graphene interacts with different metals quite differently. Such differences can be expressed by the linear relationship between the relative binding energy of

Table 1 Comparison of binding energy at the d-band center of transition metal surfaces with respect to the reported values for graphene–metal separation (for strongly corrugated moiré-structures, the area with the smallest separation was chosen as it represents the area with the strongest adsorption). Reproduced with permission from ref. 11. Copyright 2012, Elsevier B.V.

Element	Lattice plane	Graphene–metal separation	Binding energy of the d-band center relative to the Fermi level
Co	(0001)	0.21	−1.17
Ni	(111)	0.21	−1.29
Cu	(111)	0.33	−2.67
Ru	(0001)	0.21	−1.41
Rh	(111)	0.22	−1.73
Pd	(111)	0.25	−1.83
Ag	(111)	0.33	−4.3
Re	(0001)	0.21	−0.51
Ir	(111)	0.34	−2.11
Pt	(111)	0.33	−2.25
Au	(111)	0.33	−3.56

the d-band center and the separation distance because the d-band electrons are primarily responsible for the bonding between graphene and the metals.²⁴ An absolute binding energy less or greater than 2 eV is respectively considered as weak or strong interaction at the graphene/metal interface.¹¹

Apart from interacting with pure metals, graphene can also be formed on the surface of carbides of some metals with a strong reactivity with carbon, such as Ti, Hf, Ta and W. These different graphene/metal interactions can be distinguished by their binding energies as shown in Fig. 2a. Detailed mechanisms of such interactions are not yet very clear, but the separation distance at the graphene/metal interface is directly related to the changes in the electronic structure of graphene. Graphene with a large separation from the substrate should have little change in its electronic structure, whereas a very strong interaction occurs when the energy of the π-band is significantly altered.

Lattice matching also plays an important role in determining the interface structure. Local binding at the interface produces buckling that forces carbon atoms to move away from their most stable sites. Thus, a well ordered periodic crumpling is generated throughout the graphene, which is also denoted as a moiré structure. As shown in Fig. 2b, the basic absorption models of graphene on hexagonally arranged metal surfaces can be summarized into four types: (i) carbon atoms are absorbed on the triangular hollow sites of a metal surface (the blue ones in the upper left); (ii) carbon atoms occupy alternate sites immediately above metal atoms (metal-atop sites) and the ‘fcc’ hollow sites (the green ones in the upper right); (iii) carbon atoms alternately occupy metal-atop sites and the ‘hcp’ hollow sites (the purple ones in the bottom left); and (iv) the carbon bonds lie between the metal atom sites, known as a bridge structure (the black ones in the bottom right).¹¹

For most systems with a lattice mismatch, several models usually coexist as a result of the formation of a moiré structure. However, it has been found that there is only one single adsorption site for carbon atoms on Ni and Co substrates due to the good lattice match, yielding strong interactions. Similar separation distances were found in systems of graphene-on-Rh

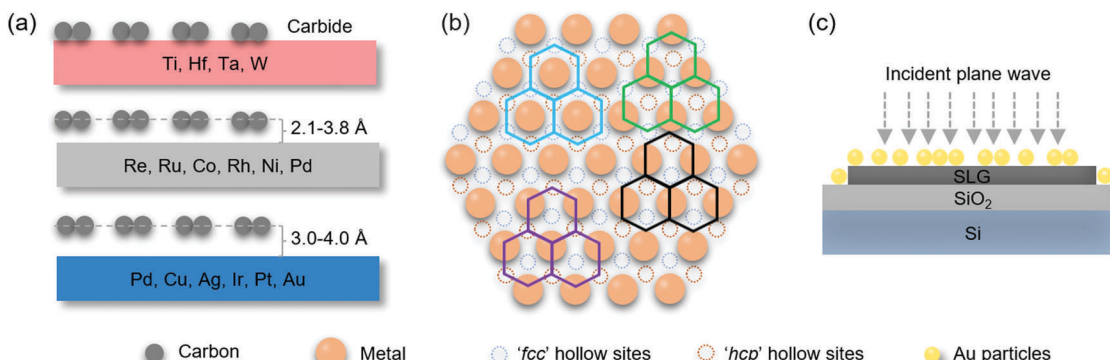


Fig. 2 (a) Three different graphene/metal interactions were suggested as a result of their different separations. (b) Four basic absorption models of graphene-on-metal surfaces. (i) Carbon atoms are absorbed on the triangular hollow sites of a metal surface (the blue ones in the upper left); (ii) carbon atoms occupy alternate sites immediately above metal atoms (metal-atop sites) and the 'fcc' hollow sites (the green ones in the upper right); (iii) carbon atoms alternately occupy metal-atop sites and the 'hcp' hollow sites (the purple ones in the bottom left); and (iv) the carbon bonds lie between the metal atom sites. (c) Illustration of the configuration in a SERS sample.

and graphene-on-Ru where a clear increase in binding energy was observed.²⁵ Although graphene-on-Re has the same separation distance as other systems, its binding energy is quite different. In general, graphene formed with the bridge structure has the strongest adsorption with the smallest separation (the black one in Fig. 2b). For type (ii) where carbon atoms alternately occupy metal-atop sites and the 'fcc' hollow sites, and type (iii) where carbon atoms are located on metal-atop sites and 'hcp' hollow sites, the interactions are weaker with separations in the range of 2.1–3.8 Å.²⁶ Carbon atoms located at the triangular hollow sites have the weakest interaction and the largest separation of 3.0–4.0 Å.

Graphene/metal interactions are relevant to factors such as the interface separation and binding energy, whether they form metal carbide and lattice mismatch, but the mechanisms are complex. Strong interactions at the graphene/metal interface occur due to (i) the chemical reaction of carbide formed during deposition, (ii) well matched lattices with the smallest graphene/substrate separations such as Ni and Co, (iii) an obvious increase in binding energy due to strong interactions with the π -band in graphene, and (iv) a large moiré pattern formed. A weak interaction usually occurs at an interface where carbon atoms are located on the triangular hollow sites of the substrate. It is worth noting that the separation distance is not always proportional to the interaction strength because a strong interaction may cause corrugation that eventually increases the separation at the interface. Such a moiré structure of graphene offers promising applications as a template for the synthesis of metallic nanostructures.

2.1.2 Metallic nanostructures on graphene. Although the lattice mismatch complicates the electronic configuration at the graphene/metal interface, the well ordered periodic structure of the interface provides a strong alternating interaction between graphene and its substrate, forming a corrugated surface. Such a surface is an excellent template for the preparation of nanostructures of metal clusters by vapor deposition techniques. The differences in the strength and depth of the sites can cause periodic nucleation that can grow into nanostructure unit cells of

metal clusters. It was found that metals including Ir, Pt, W, Re, Fe, Rh, Pd, Ru, and Ni formed atom clusters that produced moiré patterns with graphene sheets on many substrates, such as Ir(111), Ru(0001), and Rh(111).^{27–30} The structure of the deposited metal clusters strongly depends on the type of metal substrate. An immediate application of these clusters is in SERS (Fig. 2c). The Au particle arrays were deposited on a graphene sheet supported by a SiO₂/Si substrate with a certain size and separation.³¹ With well ordered nano arrays on the atomically smooth surface of graphene, the Raman signal was dramatically promoted due to the surface plasmon induced by the incident field in electromagnetic hot spots.^{32–34}

2.2 Graphene-on-semiconductors

Semiconductors have been widely used in electronic and optoelectronic devices, such as field-effect transistors (FETs), photodetectors, photovoltaics, lasers, and light-emitting diodes. The graphene/semiconductor heterostructure is an important research field in graphene based technology.¹² A Schottky junction can be formed when graphene has an intimate contact with semiconductors and the barrier height can be modified by tuning the Fermi level of graphene. The bandgap of semiconductors is affected because of their chemical bonding with graphene.^{35,36} Semiconductors with sizes in nanoscale exhibit different optical, electrical, and chemical reactivity properties from their bulk counterparts. When interacting with graphene, they can form mixed dimensional heterostructures through various interactions. Graphene can also act as a template for the controllable growth of various organic semiconductors. In the following section, we will discuss the interfaces between graphene and inorganic and organic semiconductors, as well as their nanoscale quantum dots (QDs) and those with other dimensions.

2.2.1 Graphene/inorganic semiconductors. Inorganic semiconductors consist of elemental semiconductors and compound semiconductors. Si and Ge are the typical group IV elemental semiconductors and group II–VI and III–V semiconductors are mainly compound semiconductors. These inorganic semiconductors can provide smooth surfaces onto which planar

graphene can be transferred with intimate contact. Due to the semimetal properties and high carrier mobility of graphene, a Schottky junction with rectifying effects can be formed as graphene contacts the semiconductors. Fig. 3a and b show the diagrams of ideal energy bands for the formation of a graphene/semiconductor (n-type) Schottky junction.¹² Graphene is usually obtained by mechanical exfoliation or CVD, and then transferred onto the cleaned surface of a semiconductor. Assuming that the work function of graphene is larger than that of the semiconductor ($\phi_G > \phi_S$), electrons flow from the semiconductor to the lower energy states of graphene until their Fermi levels align at equilibrium, forming a region called the depletion layer or space charge region at the interface. The Schottky barrier height (ϕ_B) and built-in potential (V_{bi}) are given by $\phi_B = \phi_G - \chi$ and $V_{bi} = \phi_G - \phi_S$, where χ is the electron affinity. For n-type semiconductors with work functions larger than that of graphene, i.e. $\phi_S > \phi_G$, electrons flow from graphene to the semiconductor during ideal contact.

A Schottky barrier between graphene and a semiconductor was first reported in 2009, when the Schottky barriers between SiC and epitaxially grown and mechanically exfoliated graphene were compared.³⁷ In the experiments, the Schottky barrier height of mechanically exfoliated graphene and that of epitaxially grown graphene deposited on SiC were measured to be 0.85 eV and 0.36 eV, respectively. The lower Schottky barrier of epitaxially grown graphene/SiC was mainly attributed to the pinning of the Fermi level raised by donor centers in an interfacial C-rich buffer layer that leads to n-doping in graphene. In 2010, a graphene/silicon Schottky junction was achieved (Fig. 3c).³⁸ And this work revealed the photovoltaic properties of the graphene/semiconductor Schottky junction. Since this pioneering study on

the graphene/semiconductor Schottky junction, more inorganic semiconductors, such as GaAs, GaN, CdS and perovskite, have been studied.^{39–42} In contrast to the traditional metal/semiconductor Schottky junction, the barrier height of a graphene/semiconductor Schottky junction can be adjusted by gate bias or doping due to the tunable Fermi level of graphene.^{43,44} The tunability of the Schottky barrier height was demonstrated by a junction of CVD grown graphene on hydrogen passivated Si that yielded a current on/off ratio of $\sim 10^5$.⁴⁴ Also, for a graphene/GaN Schottky junction, the shift and 2D/G peak ratio in the Raman spectrum decreased as a high reverse bias was applied, which confirmed that the change of the Fermi level of graphene changed the Schottky barrier height.³⁹ The temperature dependence of the current-voltage ($I-V$) characteristics of a graphene/GaAs Schottky junction suggests that the current increases with temperature due to the increased probability of conduction electrons at high temperature that can overcome the barrier (Fig. 3d and e).³⁹ What calls for special attention is the quality of the interface in a graphene/semiconductor Schottky junction. A clean and passivated surface is crucial for achieving ideal Schottky diodes.⁴⁵

2.2.2 Mixed-dimensional heterostructures. Downsizing semiconductors to the nanometer scale with 0D, 1D and 2D structures can give them new optical and electronic properties. The single (C) atom nature of graphene gives it the ability to combine with mixed-dimensional inorganic semiconductors to form various heterostructures (Fig. 4). In most cases, these heterostructures interact through van der Waals (vdW) forces, such as the integration of graphene with black phosphorus QDs,⁴⁶ ZnO nanowires (NWs),⁴⁷ and transition metal dichalcogenide (TMD) layered materials.^{48–57} There are some good reviews on these vdW heterostructures.^{58–60} Compared with other interactions at the interface, vdW forces usually introduce fewer defects, and thus result in less damage to the structure of graphene, which is favorable for maintaining its properties.

There also exist other interactions, such as $\pi-\pi$ stacking and electrostatic interactions. For these interactions, we take QDs for a detailed discussion. QDs with diameters of 2–20 nm have been receiving widespread interest because their electronic and optical properties can be manipulated by their size, shape, and composition, as well as the benefits arising from their solution phase manufacturing. However, they tend to aggregate due to their large surface-to-volume ratio, leading to significant

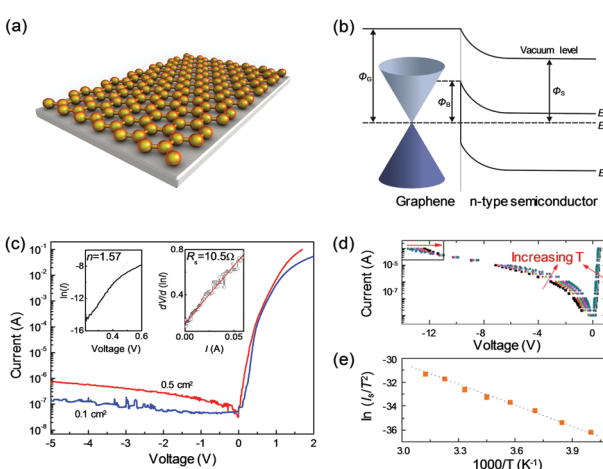


Fig. 3 (a) Schematic and (b) energy band diagrams of a graphene/semiconductor Schottky junction. Reproduced with permission from ref. 12. Copyright 2016, AIP Publishing LLC. (c) $I-V$ characteristics for a graphene/silicon Schottky junction with two different junction areas. Reproduced with permission from ref. 38. Copyright 2010, John Wiley & Sons, Inc. (d) $I-V$ characteristics for a graphene/GaAs Schottky junction for temperatures from 250 to 320 K. (e) Extracted saturation current plotted in terms of $\ln(I_s/T^2)$ vs. $1000/T$. Reproduced with permission from ref. 39. Copyright 2012, American Physical Society.

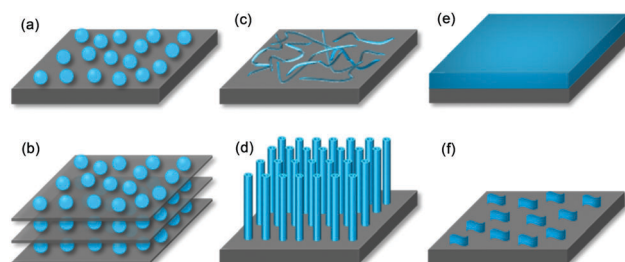


Fig. 4 Schematic diagrams of graphene integrated with (a and b) 0D structures (e.g. nanoparticles and quantum dots), (c and d) 1D structures (e.g. nanotubes, nanobelts and nanowires) and (e and f) 2D structures (e.g. nanoplates and layered materials).

surface and electron–hole recombination. The flexible 2D thin film nature of graphene, together with its superior electrical conductivity, rich surface chemistry, and excellent electrochemical properties, makes it a promising candidate as a platform for the loading of QDs to prevent undesired aggregation, and/or as a carrier extractor and transporter to retard electron–hole recombination.

The binding of QDs with graphene can form various structures, depending on their relative sizes. Graphene sheets of nanometer size that are denoted as graphene QDs are likely to wrap around other QDs. It has been reported that the Zn²⁺ on ZnO QDs' surface reacts with functional groups on GO to detach sections of graphene layers that then partially surround the ZnO QDs to form a quasi-core/shell structure.⁶¹ A more commonly investigated structure is QDs anchored on the graphene with edges of hundreds of nanometers to several micrometers as illustrated in Fig. 4a. This structure can be achieved by two methods. The first is to prepare graphene sheets and colloidal QDs separately, functionalize them with chemical groups, and then combine them by π - π stacking^{62,63} or electrostatic interactions.⁶⁴ The second is to synthesize the QDs *in situ* on the graphene. In such preparation processes, GO usually acts as a precursor of graphene and the growth matrix of the target QDs. The reduction of GO and the formation of QDs occur simultaneously during the reaction process. Studies aiming to combine QDs and graphene nanosheets in this way have been mostly focused on the *in situ* growth of metal sulfides.^{65–69} To further improve the loading rate of QDs and achieve better dispersity, poly(acrylic acid)⁶⁸ and PSS⁷⁰ were introduced into the reaction systems to provide more nucleation sites. Large area graphene sheets can also be modified by loading QDs to form layered structures (Fig. 4b). The QDs on the graphene are often prepared by solution processing and electrochemical techniques.^{71,72} To achieve intimate interfacial contact between the QDs and the graphene layers, various methods have been developed. The graphene layer can be deposited using electrophoretic deposition, and then immersed in QD precursor solutions for QD layer growth.⁷³ The introduction of electrostatic interaction at the interface of graphene and the QD layer also achieved a better contact.⁷⁴

2.2.3 Graphene/organic semiconductors. Organic semiconductors have been demonstrated to be a potential candidate for light-absorbing materials and their band gap can be tuned chemically to cover the entire spectral range from near infrared to ultraviolet (UV).⁷⁵ However, the excitons generated in organic semiconductors usually have a short diffusion length and low mobility, which present severe obstacles in achieving high efficiency devices. Combining graphene with organic semiconductors provides hybrid materials offering more adaptable functions with unique physical properties than the individual components. Similar to the interfaces of graphene/inorganic semiconductors, a built-in electric field is formed when they contact each other. When light is absorbed by the organic semiconductor, some of the light-induced excitons migrate to the interface and the electron–hole pairs are separated by the built-in electric field at the interface. If non-equilibrium doping of graphene occurs, it changes the conductivity.^{76,77} In such

structures, graphene provides not only a heterointerface constituent element, but also an efficient channel for charge transport due to its high carrier mobility, which reduces the recombination rate of electrons and holes produced from the irradiated organic semiconductor. Therefore, the overall optoelectronic properties can be greatly improved.

Graphene can also act as a vdW epitaxial growth template for various organic semiconductors.^{78,79} The epitaxial approach is advantageous in terms of controlling the interface quality and microstructure of the organic semiconductors near the interface and improving the performance of the graphene based optoelectronic device. For example, pentacene, a typical organic semiconductor, was quasi-epitaxially grown in the lying-down orientation on graphene templates.⁸⁰ This controlled molecular orientation improved the optoelectronic properties of pentacene, especially the carrier lifetime and exciton diffusion length, which allowed the optimum thickness of the photoactive layer to be doubled, generating significantly greater light absorption.⁸⁰ These results indicate that the photon harvesting and conversion of the hybrid materials can be effectively adjusted by tuning the heterointerface of the graphene/organic semiconductor.

2.3 Graphene-on-ceramics

When graphene is CVD grown on or transferred to ceramic substrates, their properties would be greatly affected by the chemical and physical conditions of the interface. The hydrophilicity/hydrophobicity properties, impurities, photon scattering, and adsorbents cause significant changes in the properties of graphene as illustrated in Fig. 5. They may affect the atomic arrangement, result in doping effects or lead to anisotropic transport properties of graphene. A better understanding of their interactions guides us in modifying the properties of graphene through interface engineering. Functional ceramics would undergo a polarization change under the stimulus of an external force or temperature variation, leading to doping

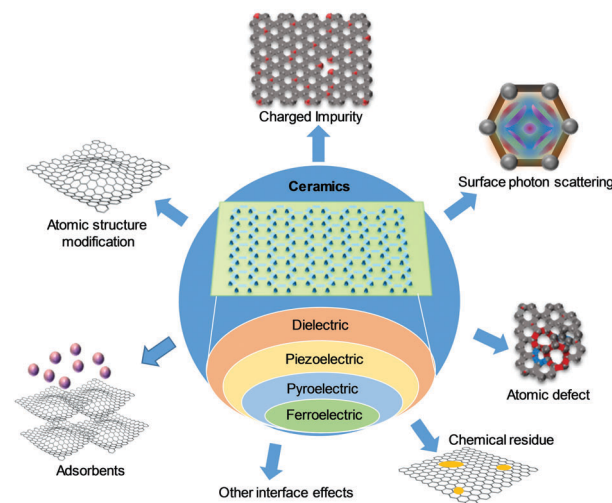


Fig. 5 Interface effects that may affect the properties of graphene in graphene-on-ceramic systems.

effects or changes in the carrier densities of graphene when it forms contacts with them. The interfaces in these hybrid systems affect the properties of graphene and their combination may generate some new functional devices.

2.3.1 Graphene/dielectric ceramics. A dielectric material is an electrical insulator that can be polarized by an electric field. Theoretically the intrinsic limit of electron mobility of $2 \times 10^5 \text{ cm}^2 \text{ V}^{-1} \text{ s}^{-1}$ can be realized by suspending graphene at room temperature. However, dielectric substrates limit the room temperature mobility of graphene due to charged impurity scattering in dielectric layers and surface photon scattering, as well as chemical residues and adsorbed atmospheric species. Therefore, the substrate surface chemistry is significantly important for the electrical transport properties of graphene.⁸¹

The graphene/substrate interaction changes the atomic arrangement of the carbon atoms in graphene on dielectric ceramics, which in turn affects its electrical transport properties. It has been reported that the surface corrugation of graphene lowers its carrier mobility and suppresses weak localization in graphene based devices.⁸² Therefore, reducing the magnitude of the corrugation is favorable for electrical performance. In fact, the corrugation of graphene on ceramics is quite different from the intrinsic ripples of freestanding graphene due to the interface effects. For example, it was observed that monolayer graphene partially conformed to the morphology of a substrate that had been cleaned to an atomic scale.⁸³ Flat graphene prepared by depositing it onto a mica support provided atomically flat terraces over large areas.⁸⁴ Both discoveries indicate that the substrate plays an important role in determining the morphology of the supported graphene monolayer and the use of a corrugated substrate might be a useful approach to change the transport properties of graphene. In addition, fewer wrinkles are generated on graphene grown by CVD and transferred onto a hydrophobic substrate rather than one that is hydrophilic.⁸⁵ Graphene with a terraced morphology can be formed on the C face of the SiC substrate, different from that with a flat morphology on the Si face. This may be ascribed to the different interface structures in these two cases.⁸⁶ In addition, a drastic improvement of carrier mobility up to $40\,000 \text{ cm}^2 \text{ V}^{-1} \text{ s}^{-1}$ was achieved at room temperature in air using ultra-flat hexagonal boron nitride (h-BN) as the dielectric substrate.⁸⁷

Substrate induced charged impurities, the atomic structures at the steps and edges, and phonon scattering can significantly change the transport properties of graphene. For example, the hole mobility of graphene on an HfO₂ substrate showed close dependence on the impurity concentration in the HfO₂. A thicker HfO₂ film lowered the hole mobility of graphene due to more impurities introduced during atomic layer deposition.⁸⁸ According to first-principles calculations by density functional theory (DFT), H-passivated SiO₂ surfaces do not affect the electronic properties of graphene. However, the oxygen defects on a SiO₂ surface can interact chemically with the graphene layer and disturb the band structure of π electrons, resulting in hole-doping effects in the graphene adsorbed on the SiO₂ surface.⁸⁹ In addition, the surface treatment of SiO₂ may cause scattering centers at the graphene/SiO₂ interface, such as silanol groups (Si-OH) with strong polarization and siloxane groups

(Si-O-Si) with weak polarization.⁹⁰ It was revealed that negatively charged Si-OH groups decreased the carrier mobility and shifted the Dirac point of graphene due to the doping effect. In contrast, high carrier mobility of graphene was obtained as the Si-O-Si groups became dominant because their polarization was very weak and they could not function as Coulomb scattering centers. Besides, high carrier mobility of graphene was obtained when SiO₂ was passivated with highly aligned -CH₃ end-group molecules.^{91–96} In addition, the dielectric constant of the underlying substrate also significantly affects the properties of micro-mechanically exfoliated graphene on different oxide dielectrics, such as SiO₂, Al₂O₃, and HfO₂. It has been suggested that a stronger doping effect would be expected with higher-dielectric-constant oxide substrates because stronger polarization would induce a larger interface dipole density.⁹⁷ In some cases, the interaction between graphene and the underlying dielectric can even produce anisotropic conductivity in graphene. This phenomenon was observed in graphene/SiC hybrid materials where trapped Si atoms at the graphene/SiC interface tended to aggregate at step edges and promoted local scattering. Since graphene grown on the Si face of the SiC substrate has clearly defined parallel steps, this conduction anisotropy can be explained by a synergistic effect of geometric anisotropy and residual Si.⁹⁸ Surface phonon scattering that depends on the thermal excitation of the contact surface is another dominant source of scattering in high quality graphene. It was reported that the addition of a low- κ polymer buffer layer between graphene and conventional gate dielectrics suppresses the extrinsic surface phonon scattering, offering a new strategy to inhibit carrier mobility degradation in graphene based electronic devices.⁹⁹

Water adsorbents, as well as chemical residues, may affect the hybridization between a dielectric substrate and graphene. The impact of a dielectric SiO₂ substrate on the electronic properties of graphene after water adsorption was investigated using DFT calculations. It was found that the doping of graphene could be obtained with much lower H₂O concentrations as a SiO₂ substrate was introduced.¹⁰⁰ It was believed that the hydrophobically modified substrate minimized the amount of H₂O trapped at the graphene/SiO₂ interface. Bidirectional *I*-V measurements indicated that such a modification reduced the resistance-voltage hysteresis because the hysteresis was often caused by the oriented polarization of water molecules.⁹⁰ Chemical residues, such as PMMA originating from transferred CVD grown graphene, might generate more scattering sources. The carrier mobility of transferred graphene doubled after the PMMA residue was removed.¹⁰¹

2.3.2 Graphene/functional ceramics. Piezoelectric materials have both dielectric and piezoelectric properties. Piezoelectric effects occur only in non-centrosymmetric crystals where a deformation can generate a voltage, and an external voltage produces a deformation of the solid. Lead magnesium niobate-lead titanate (PMN-PT) and lead zirconate titanate (PZT) are typical piezoelectric ceramics. Similar to dielectric ceramics, piezoelectric ceramics can be exploited to tune the electrical properties of graphene due to their polarization. For example, graphene deposited on a piezoelectric PZT substrate was used

as a photodetector, and showed an order of magnitude more sensitive photoconduction response than that of graphene on a SiO_2 substrate. The polarization of the piezoelectric substrate produces an electric field that facilitates the spatial separation of photogenerated carriers and promotes the hole doping of graphene.¹⁰² The polarization of a piezoelectric substrate can be controlled by the external mechanical load, which causes graphene doping and scattering at the stressed substrate interface. A sensor with graphene/piezoelectric nanowire heterostructures can be used for static pressure measurements because of the synergistic mechanisms between strain-induced polarization charges in piezoelectric nanowires and the change of carrier scattering in graphene.¹⁰³ Piezoelectric ceramics also provide a platform to study tunable strain effects in graphene. For example, a biaxial strain was induced in a graphene sheet by applying a perpendicular electric field to the piezoelectric PMN-PT substrate. The electrical properties of graphene subjected to this strain were then characterized by Raman spectroscopy. The D, G, 2D, and 2D_0 peaks blue-shifted under compressive strain and red-shifted under tensile strain.¹⁰⁴ Such a controllable biaxial strain effect is desirable for the study of the basic vibrational properties of graphene, such as the calculation of Grüneisen parameters. Similar Raman shifts were also observed in CVD grown graphene. However, grain boundaries might have a different strain distribution from that inside the grain. As a result, an unexpected trend in the Raman peak positions with strain was also observed.¹⁰⁵ Pyroelectric materials undergo a polarization change when heated or cooled, generating a temporary voltage or current in an external circuit. The piezoelectric effect and dielectric properties inherent in all pyroelectric materials allow flexible and controllable modification of the spontaneous polarization by an external force (piezo-active) or temperature variation (pyro-active), which further affects the electrical properties of graphene supported on such a substrate. Mechanical stimulus changes the properties of graphene on pyroelectric ceramics in a similar way to that on piezoelectric ceramics as discussed above. As for the impacts of temperature variation, a CVD grown graphene/pyroelectric PZT ceramic system was investigated.¹⁰⁶ It was shown that the carrier type in the graphene changed from electrons to holes when the device temperature was changed by adjusting the power of an incident laser beam. The carrier density also exhibited dependence on temperature due to the polarization orientation of the PZT layer. The carrier density is increased or decreased when the polarization orientation in PZT is in up or down direction, respectively. It suggests the key role of PZT polarization in the investigated system.

Ferroelectrics have a spontaneous electric polarization that can be switched by an electric field. Combining the non-volatile memory behavior of ferroelectric thin films with graphene in a FET provides a platform to study the electrical behavior of this atomic layer material. The polarization field can either increase or decrease charge carriers, as a ferroelectric thin film was used as the gate dielectric in the graphene based FET, which makes this integrated device potentially useful in non-volatile memory applications.

2.4 Graphene-on-polymers

Combining polymers with graphene and its derivatives offers a way to widen their potential applications. They can be combined by noncovalent and covalent interactions (Fig. 6). Noncovalent interactions cause fewer interruptions to the structure of graphene, and thus less damage to its properties, whereas the interaction strength is limited in this case. For cases that require a stronger interaction at the graphene/polymer interface, GO is preferred because the functional groups tend to form chemical bonding with polymers. Strategies have also been proposed to functionalize graphene or GO with chemical groups, aiming at a designed interface interaction with polymers. These interactions significantly influence the properties of the graphene-on-polymer systems.

2.4.1 Graphene/polymers. Pristine graphene consists of sp^2 -hybridized carbon atoms in a honeycomb like structure with few functional groups, so its combination with polymers is usually by vdW forces. In general, vdW forces have little effect on the atomic arrangement in the graphene sheet which therefore retains the excellent physical properties of graphene.¹⁰⁷ A graphene film has been transferred to PE, forming a flexible and transparent electrode that could be used as an alternative to traditional indium tin oxide (ITO) electrodes.¹⁰⁸ Recently, graphene-on-polymer sensors have been developed. Graphene woven fabrics (GWF) on stretchable and highly sensitive PDMS were fabricated and used as a strain sensor.¹⁰⁹ The combination of network and tiling structures of GWF is so sensitive to deformation yet with enhanced material integrity. The adjacent graphene sheets slide as the PDMS is deformed, which changes the interfacial resistance, and thus affects the resistance of the GWF.^{110,111} By combining artificial intelligence with digital signal processing, it is expected that, in the future, the graphene based sensing system will represent a new smart tool to classify and analyze signals in various fields.

Polymers with a π bond and correct geometrical configurations can bind with graphene through $\pi-\pi$ interactions.¹¹² In graphene/polymer composites, the effectiveness of its reinforcement in the electrical, thermal and mechanical properties is strongly related to the quality of its dispersion in the polymer matrix.¹¹³ Noncovalent functionalization using molecules or polymers that can form $\pi-\pi$ interactions with graphene offers an effective way to prevent its agglomeration, and meanwhile maintain its excellent properties.^{114–116} Kevlar has been widely used as a high

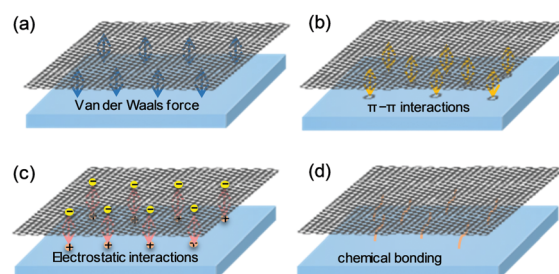


Fig. 6 Noncovalent interactions between polymers and graphene: (a) vdW force, (b) $\pi-\pi$ interactions, (c) electrostatic interactions and (d) chemical bonding.

performance reinforcement in composites. Its aromatic ring structure exhibits effective $\pi-\pi$ interactions with graphene, and taking advantage of this, Lian *et al.*¹¹⁷ fabricated Kevlar functionalized graphene nanoribbons (GNRs) and used them to reinforce PVA and PMMA to improve their tensile strength, Young's modulus, and thermal stability. However, the organic functionalization molecules at the interface between graphene and the matrix deteriorate the electrical and thermal properties of the composites. Considering this, CNTs were employed to achieve dispersable graphene sheets and the electrical properties were well maintained.¹¹⁸ Exfoliated montmorillonite nanoplatelets were introduced to stabilize graphene sheets through hydrogen bonding and the good mechanical properties from these two components contribute to the overall performance of the composites.¹¹⁹

2.4.2 Graphene oxide/polymers. Different from graphene, the rich functional groups on the GO surface make it dispersable in aqueous solutions and water-soluble polymers. The hydrogen and chemical bonding at the interface render them a stronger contact, leading to good reinforcement in GO/polymer composites.^{120,121} When GO is designed to be integrated into non water-soluble polymers, surface functionalization is also required to make it compatible with the polymer matrix and thus well dispersed.^{122,123} Besides, negatively or positively charged GO can be prepared and then combined with conversely charged polymers through electrostatic interactions. It was reported that the charged GO can self-assemble onto polymers with a network structure.¹²⁴ The dispersity of GO in the polymer matrix and the interface interaction determine whether they can be effectively used as reinforcement fillers in composites. Targeting at this, other methods to combine GO with polymers, such as *in situ* polymerization, have been developed.^{125,126}

Currently, membrane technology is considered to be the most effective approach for wastewater treatment and water purification. In the past few years, derivatives of graphene including nanoporous graphene and GO membranes have been demonstrated to have novel mass transport properties and plenty of applications in filtration and separation.^{127–131} GO nanosheets have been assembled on various polymer membranes, such as polyamide thin film composites (TFC), polyvinylidene fluoride (PVDF) microfiltration and ultrafiltration membranes, a poly-acrylonitrile (PAN) porous membrane, and a polysulfone (PSF) porous support, using various assembly processes including layer-by-layer (LbL), electric field assisted assembly, and covalent grafting. Functionalized GO¹³² and GOQDs¹³³ have also been combined with polymers for various potential applications. As reported by Zeng *et al.*, GO-QDs were covalently bound to amino-modified PVDF membranes to achieve desirable long term stability and durability in aqueous environments.¹³⁴ GO can affect the surface of the polymer matrix, including morphology, wetting, charged state, and roughness, which further changes the properties of the hybrid membrane.

2.5 Graphene-on-biomaterials

2.5.1 Graphene/biomacromolecule interfaces. Biomacromolecules, such as nucleic acids and proteins, are the elementary

units used to construct a living organism. Combining graphene with these biomacromolecules can generate intriguing hybrid systems to be applied in fields such as DNA sequencing, protein purification, biomolecule sensing, biomedicine, and bioimaging.^{135–139} Theoretical and experimental studies on the interplay between graphene and biomacromolecules are of great significance.

Graphene and its derivatives are combined with nucleic acids mainly through $\pi-\pi$ interactions, hydrophobic effects, hydrogen bonding, vdW forces, and electrostatic interactions. DFT calculations and molecular dynamics (MD) simulations were used to investigate the interfaces of $\pi-\pi$ interactions. It was found that the polarizability of nucleobases greatly influences their binding energy with graphene at the interface.¹⁴⁰ The curvature of carbon materials also influences their interaction strength with nucleobases, which was confirmed by quantum chemical calculations. The properties of nucleobases upon binding to graphene experienced great changes. It was demonstrated with nucleus-independent chemical shift calculations that aromaticity for all nucleobases is enhanced after they form interfaces with graphene.¹⁴¹ The combination of nucleic acids and graphene can cause conformational changes of nucleic acids that protect them from nuclease digestion.¹⁴² Hydrogen bond-like interactions at the interface between guanine and graphene were also reported.¹⁴³ As for the combination of DNA and GO, theoretical calculations revealed that the strand of DNA determines whether it can constantly adhere to GO via $\pi-\pi$ interactions.¹⁴⁴ It was further confirmed by experimental results that the interface interaction strength is not only determined by the DNA strand but also affected by its secondary and tertiary structures.¹³⁷ A partial deformation of the DNA double helix was demonstrated to increase its interactions with GO.¹⁴⁵ Apart from these factors, NaCl concentration and DNA length also have effects on their binding rate and intensity.^{146,147} The binding interactions of graphene and its derivatives with proteins are similar to the case of nucleic acids. It was found that proteins lost most of their native secondary and tertiary structures after being adsorbed on graphene.¹⁴⁸ Functionalized graphene causes less damage to the protein structure due to the hindrance effects of the functional groups that weaken the interactions.

2.5.2 Graphene/cell interfaces. Functionalized graphene has shown great promise in biomedical applications. The transmembrane translocation mechanisms of graphene and its interactions with cells are critical issues to be solved for its expanded applications in biosystems. Cell membranes are the main subjects of graphene-cell interface investigations since they are the protective layers of cells. Understanding how graphene interacts with cell membranes is crucial for investigating the fundamental biological responses and cytotoxicity to cells. The relative sizes of graphene and cells determine how they interact. Graphene of a large size can provide a stable and continuous platform for cells, which is an advantage over 1D NWs and 0D nanoparticles (NPs).¹⁴⁹ Small graphene sheets can adhere to the cell surface or enter the cell by internalization, which was confirmed through theoretical calculations.¹⁵⁰ The size of graphene affects the way of penetration and its shape decides the penetration rate.

Interactions including hydrophobic effects, electrostatic interactions, and vdW forces have been demonstrated between graphene and cells. Functionalized graphene has different interactions with cell membranes compared to pristine graphene. It was found that pristine graphene accumulates on the monkey renal cell membrane through a strong hydrophobic interaction, causing high toxicity to the cells. In contrast, the functionalized graphene can be internalized by the cells.¹⁵¹ The hydrophobicity/hydrophilicity of graphene could be modulated by changing the O/C ratio, which in turn changes its potential biological interactions.¹⁵² It was proposed that a system would reach its minimum Gibbs energy when the graphene sheets were present in the hydrophobic interior of the biological membrane.¹⁵³ Besides, graphene can also be combined with cells by electrostatic interactions.^{154–156}

The interface between a cell and graphene provides unique thermal, mechanical, and electrical properties, which has great potential for various applications including biosensors, drug delivery, energy harvesting, and biomedical applications, such as thermotherapies. MD simulation was used to quantify the thermal transfer across the graphene/cell membrane interface. It was found that graphene interacted with the lipid bilayer on the cell by vdW forces and the intercalated water layers could modulate the interfacial thermal coupling and promote the interfacial thermal conductance.¹⁵⁷ This research group also explored the mechanical response of the interface and found that the graphene coated lipid bilayer provided remarkable resistance to loads and the intercalated water layer offered additional protection.¹⁵⁸ The electrical properties of graphene can be modified by its interactions with cells. The strong adhesion of a rod-shaped *Bacillus subtilis* cell wall on graphene generated wrinkles in the graphene, induced a dipole moment and orbital rehybridization, and thus modified its electrical properties and caused transport anisotropy.¹⁵⁹ The electro-mechanical coupling of a cell with graphene can also change the properties of graphene.¹⁶⁰ Various graphene/lipid membrane based hybrid transistors have been investigated for their potential applications in biorecognition and biosensing. Detection by a graphene/cell hybrid is based on carrier doping that occurs as a result of the electronegativity or dipole moment of the cell in which graphene provides sensitive detection due to its quantum capacitance.^{161–165}

2.6 Graphene-on-liquids

2.6.1 Graphene growth on liquid metals. Among all the graphene fabrication methods, CVD is the least expensive and is industry friendly. It can be used to prepare graphene films on a variety of substrates. Large area uniform polycrystalline and even single crystal graphene films have been grown by CVD on metal substrates using various carbon precursors. However, the graphene fabricated by CVD is known to contain various defects, vacancies, and wrinkles. The surface morphology is of great importance for the CVD process because any contaminant or surface roughness can affect the properties of the graphene films produced. A liquid can provide a clean and atomically flat surface to avoid the above defects (Fig. 7). In addition, the growth

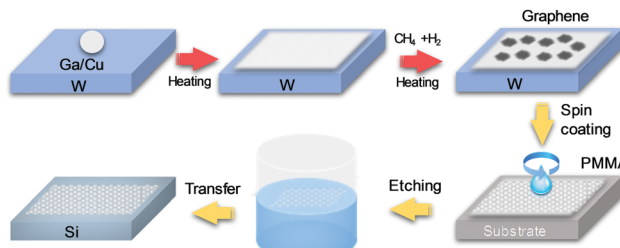


Fig. 7 Graphene films grown over liquid Ga or Cu supported on a W substrate.

of graphene on a liquid metal is usually a self-terminating process caused by the high surface energy of the liquid metal. Carbon atoms are blocked from contacting the liquid surface once full coverage of graphene is obtained.

Molten Cu was the first liquid catalyst reported for the synthesis of single-crystal monolayer hexagonal graphene flakes. Later, continuous graphene films were obtained by stitching the graphene flakes together.^{166–168} One advantage of such a process is the elimination of the effects of the heterogeneous surface of solid Cu on the nucleation of graphene because carbon prefers to nucleate at defects, steps, and boundaries. In addition, the homogeneous high quality hexagonal graphene flakes can be assembled into films consisting of a single grain. Weak interactions at disoriented heterogeneous grain boundaries of polycrystalline graphene lead to its inferior electrical properties compared to single crystal graphene. Scanning electron microscopy (SEM) characterization and its extraordinary electron mobility in comparison with the graphene synthesized on solid Cu substrates confirmed the advantages of using liquid metals as growth substrates.¹⁶⁹

Other liquid metals, such as Ga, have also been demonstrated to be decent catalysts for the synthesis of graphene films. Ga is not only a carbon-insoluble metal, similar to Cu, but also a highly active metal catalyst. The atomically flat and homogeneous surface of Ga at elevated temperatures can reduce the nucleation density to as low as $10^{-3} \mu\text{m}^{-2}$, which is favorable for the growth of uniform monolayer graphene films.^{170,171} Silicided polycrystalline platinum has also been used for graphene growth.¹⁷² A liquid surface was obtained by coating a silicon-containing film onto a polycrystalline Pt foil, followed by heating. The reaction of Pt foil with the coating at high temperature resulted in a liquid platinum silicide layer that was atomically flat and homogeneous. In all, liquid metals provide a defect-free surface with atomic flatness, homogeneity, for the synthesis of high-quality graphene films and the process is self-terminating.

2.6.2 Graphene–water interaction. The water wetting of graphene is very common during its transfer. Its effects on the properties of graphene should be taken into consideration in surface studies under ambient conditions because water, as an acceptor, introduces a shift of the Fermi level in graphene and can significantly alter its electrical properties.^{14,173} In addition, the flow of ionic and non-ionic liquids on graphene can generate a voltage due to an electrochemical charge/discharge mechanism and the “phonon drag effect”.^{174–176} In general, the

intrinsic hydrophobicity of graphene gives rise to a contact angle with water varying from $\sim 45^\circ$ to as high as 93° .^{177–179} The hydrophobic behavior of free-standing graphene is mostly attributed to the vdW forces at the graphene/water interface. However, the contact angle of water on single layer graphene can be altered by varying the supporting substrate. Besides, the number of layers of graphene also affects its interactions with water. It was found that few-layer graphene acted significantly differently from monolayer graphene due to vdW forces dominating the graphene–water interfaces.¹⁸⁰ In addition, the morphology of the graphene surface also has an effect on its interaction with water. Wrinkles, defects, and dislocations have been demonstrated to dramatically change the contact angle of water by providing multiform geometric sites for water adsorption.^{181–183}

As mentioned in Section 2.4.2, an effective way for water purification is to use membranes. Discussions there are centered on the interactions between GO and polymers in composite membranes. It was also reported that GO membranes fabricated by vacuum filtration on the surface of the PVDF substrate possess ultrafast liquid water transportation. Due to the narrow dimension of nanocapillaries and the co-existence of sp^2 aromatic channels with various oxygen functionalities, GO membranes can afford excellent selectivity towards various ions based on the molecular sieving effect and diverse chemical interactions, showing promise in filtration and separation. The transportation is carried out by the millimeter-long nanocapillaries in these GO membranes (Fig. 8).^{184,185} Due to the interactions between GO and ions, the selective penetration properties of GO membranes were investigated.¹⁸⁵ Hydrated ions with different diameters, qualities and charges may have different electrostatic and chemical interactions with the functional groups on the GO surface, leading to great changes in the penetration abilities of GO membranes. The functional groups make GO negatively charged; therefore, negative ions tend to be rejected but some

are still allowed to permeate to meet the electric neutrality. For positively charged ions, alkali metals (*e.g.* Na^+ , K^+ , Mg^{2+}) cannot form coordination compounds with GO due to the lack of d or f electron orbits. They can only interact with GO through $\pi-\pi$ interactions and the interaction strength is dependent on the properties of the ions. Conversely, the hydration shell outside these positive ions can weaken the interface interaction between GO and alkali metal ions. The penetration abilities of heavy-metal (*e.g.* Mn^{2+} , Cd^{2+} , Cu^{2+}) salt solutions are obviously lower than those of alkali salts, which can be attributed to the tight interactions between these heavy-metal ions and the functional groups on the GO surface. In addition, GO membranes are able to interact with organic contaminants in solutions *via* $\pi-\pi$ interactions or even chemical bonding, which is significant for water purification. Based on this, it is further expected that other nanosheets will be designed to intercalate into GO sheets to form hybrid membranes to realize precise control in inter-spacings and high efficiency ion rejection while preserving the high water permeation simultaneously, for possible applications in water desalination.

3. Graphene growth and transfer

Graphene can be grown by CVD, mechanical exfoliation, epitaxial synthesis, and an oxidation–reduction reaction. In general, high-quality graphene with controllable properties is grown on a metal substrate that acts as the catalyst for CVD, and is then transferred to a support substrate. It can also be grown on the surface of a dielectric material by CVD. The interface between these catalyst substrates and graphene has a significant influence on the quality and properties of the as-obtained graphene. To have a better understanding of the influence of the surface of the substrate on the growth mechanism and to manipulate and optimize the properties of graphene, we will discuss the growth substrates and growth mechanisms of graphene in the following section. The effects of the properties of the substrate on the properties of CVD grown graphene will be reviewed in detail.

3.1 Graphene growth

3.1.1 Graphene growth on metals. CVD uses a mixture of methane and hydrogen in argon under low pressure to deposit graphene on a substrate at high temperature. For most CVD processes, a metal substrate acts as a catalyst to promote the decomposition of the carbon source for graphene growth.¹⁸⁶ The process is illustrated in Fig. 9a. Metal catalysts can also assist the growth of graphene on dielectrics, which is a new development. Some researchers coated $Ni^{187,188}$ or Cu^{189} catalysts to prepare graphene on the top of metal surfaces and at the interfaces between metals and semiconductor substrates. It was also reported that graphene on a ceramic substrate can be obtained by covering SiO_2 with a layer of Cu as the growth catalyst and then removing it by dewetting and evaporating.¹⁹⁰

Graphene-on-metals are usually prepared by the decomposition of hydrocarbons and the surface diffusion of carbon atoms. The growth of graphene on metal substrates with different carbon

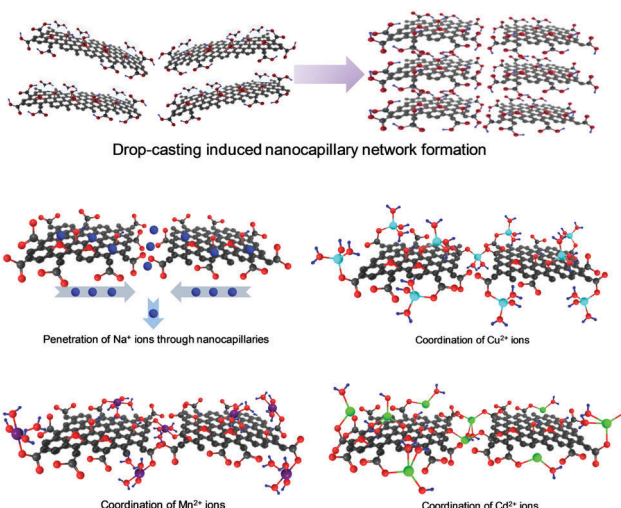


Fig. 8 Schematic diagrams of the GO membrane and the interaction with different ions in water. Reproduced with permission from ref. 185. Copyright 2012, American Chemical Society.

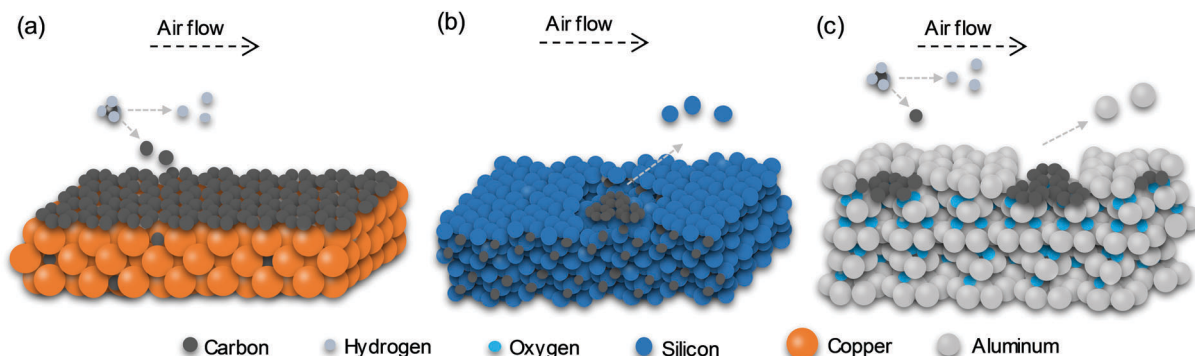


Fig. 9 CVD graphene growth on surfaces: (a) a metal catalyst substrate, (b) epitaxial growth on SiC, (c) an oxide substrate.

solubility follows different growth mechanisms. For a metal substrate with high carbon solubility, such as Ni,¹⁹¹ carbon atoms dissolve in the substrate at high temperature and then precipitate as a multilayer graphene film. Carbon is barely soluble in Cu¹⁹² and is insoluble in some dielectric substrates. For these substrates, carbon radicals are usually directly deposited on the substrate surface where their diffusion determines the growth mechanism and the morphology of the graphene obtained.^{193,194} There are some obstacles to be overcome during the graphene growth process. The H-terminated graphene edges on Cu are energetically stable¹⁹⁵ and carbon atoms have to break bonds with the substrates.¹⁹⁶ Both are energy barriers for carbon atoms to join the growing graphene sheet. Small graphene islands are formed when such barriers control the growth mechanism. Otherwise, growth is limited by carbon diffusion and dendritic grains are formed. Oxygen can promote the dehydrogenation of graphene edges, and thus facilitate the attachment of carbon atoms. Therefore, oxygen can change the growth mechanism of CVD graphene from edge-attachment-limited to diffusion-limited.¹⁹⁵ The orientation of the metal substrate also influences the growth kinetics. Graphene growth on Cu(111) is diffusion-limited, while that on Cu(100) is attachment-limited, even though the diffusion rate of carbon atoms on Cu(100) is lower.¹⁹⁶

The physical profile of the growth substrate also affects the morphology, surface coverage, homogeneity, nucleation density, and crystal domain size of the graphene produced. Electrochemical polishing is a useful technique to obtain perfectly planar Cu substrates. Graphene prefers to nucleate at surface grooves or grain boundaries, so making the substrate surface smoother reduces the number of nucleation sites,¹⁹⁷ thus forming larger graphene grains. Polycrystalline graphene is formed in rotational domains in the nucleation or growth processes, depending on the orientation of the Cu substrate. Steps on a Cu substrate reduce the graphene growth rate and rotate its grain boundaries.^{196,198} However, graphene can grow across misoriented boundaries and different grain orientations in Ru¹⁹⁹ and Ni²⁰⁰ substrates. Graphene growth is easier on surfaces with a uniform coverage,²⁰¹ fewer defects, and a bilayer formed on the smoother catalyst surface.²⁰² Valleys on a rough Cu substrate trap more carbon radicals than a flat surface, resulting in the

aggregation of amorphous graphene fragments.²⁰³ The single layer coverage of graphene grown on a smooth substrate can be over 95%.²⁰³ In addition, an ultra smooth growth surface can prevent the formation of cracks and wrinkles during graphene transfer.²⁰² In summary, high quality graphene can be obtained on a smooth Cu substrate due to its higher single layer coverage, fewer defects, and grain orientations. It was reported that the sheet resistance of graphene grown on smooth Cu substrates decreased from 647 to 120 $\Omega \text{ sq}^{-1}$ and its fracture strength was improved over 76%.²⁷

The purity and thickness of some metal substrates can also affect the number of graphene layers formed and their coverage. Monolayer graphene can be obtained on 99.999% Cu foil, while the same growth process on 99.8% Cu foil produces only bilayer graphene.¹⁸⁶ In addition to pure metals, alloys, such as Cu–Ni,²⁰⁴ Au–Ni,²⁰⁵ and Ni–Mo,²⁰⁵ have been used as graphene growth substrates. The thickness of graphene can be tuned by adjusting the thickness of the metal substrate. It has been shown that fewer graphene layers were formed on thicker Fe²⁰⁶ and thinner Co film produced a graphene monolayer.²⁰⁷

Crystal facets of the metal substrate also cause great differences in the graphene obtained. Under the same growth conditions, a graphene film grown on a Cu(111) surface has a single orientation, while that grown on a Cu(100) surface exhibits rotational disorder due to the multiple rotational domains arising from the nucleation.¹⁹⁵ It has also been shown that a higher percentage of monolayer graphene grew on the (111) surface of Au than on other surfaces.²⁰⁸ A wrinkle-free single-crystal monolayer graphene was synthesized on a H-terminated Ge substrate.²⁰⁹ On the Ge(110) face, many nucleated graphene islands merged into a single-crystal layer, while graphene grown on Ge(111) was a monolayer but polycrystalline.

3.1.2 Graphene growth on dielectrics. Graphene growth on dielectric substrates, called remote metal-assisted growth, has also been reported.^{210,211} Graphene grown on SiC and sapphire (Al_2O_3) by CVD is illustrated in Fig. 9b and c, respectively. A layer of SiC was generated on the surface of a SiO_2 substrate by carbothermal reduction and this acted as a catalyst for graphene growth.²¹² It was found that the SiO_2 surface decomposed at high temperature and Si atoms with dangling bonds remained, where the carbon source tended to decompose. The decomposition of

the carbon source and the accumulation of carbon atoms produced graphene.²¹³ Pretreatment of the SiC substrate surface has a great influence on the morphology of CVD grown graphene. Si atoms are evaporated from the SiC crystal during high temperature annealing, leaving a carbon-rich surface for graphene growth.²¹⁴ The decomposition energies of different terraces on the surface are different and Si-C bonds near step edges are weaker so that Si sublimation is faster here than in other places. As a result, epitaxial graphene formation is not uniform on SiC surfaces with many steps.²¹⁵

The correct crystal orientation of the growth substrate is crucial for achieving high quality graphene. For example, the quality of graphene grown on SiC is strongly affected by the terminations, polytypes, and orientations of the substrate. There are more than 200 SiC polytypes with different crystal lattices and stacking sequences. 3C-SiC, 4H-SiC, and 6H-SiC (C represents cubic, H represents hexagonal, and the numbers refer to the number of layers) are the three major types.²¹⁴ Both 4H-SiC and 6H-SiC have a hexagonal structure, and thus are suitable templates for graphene growth. 3C-SiC is also a compatible template due to its six-fold symmetry on the (111) facet.¹⁹⁶ SiC is polar and possesses two different terminating faces, a Si(0001) face and a C(0001̄) face. A buffer layer can be formed on the Si face after the Si sublimation where sp^3 bonds occur between C and Si²¹⁶ and graphene with sp^2 bonds grows.²¹⁷ Therefore, the buffer layer can significantly influence the carrier mobility of graphene. Hydrogen intercalation has been proposed to resolve this issue.²¹⁸ The surface energy of the C face is lower than that of the Si face, leading to faster, but less controllable, graphene growth.¹⁹⁶ However, unlike the Si face, no buffer layer can be formed on the C-face. The electrical properties of graphene on the C-face are similar to those of freestanding graphene.²¹⁹ Some other nonpolar faces can also affect the morphology and properties of graphene.²²⁰ The mismatch in the thermal expansion coefficient between graphene and SiC can cause wrinkles in the graphene obtained.²²¹ For example, graphene grown on 8° off-axis SiC exhibited bunches of steps, while that grown on the on-axis substrate was flat.²²²

Graphene has also been grown on Al₂O₃ by vdW epitaxy and CVD.^{223,224} In both cases, the quality and morphology of graphene are determined by the Al₂O₃ crystal orientation. Similar to what happens on a SiO₂ substrate, oxygen is desorbed and some pits are formed on the surface as the Al₂O₃ substrate is heated. Graphene is then nucleated in these pits. Since the pits tend to be formed around steps, the nucleation density of graphene is significantly affected by the orientation and morphology of the substrate.²²⁴ Song *et al.* preheated an Al₂O₃ substrate and found that it increased graphene nucleation during CVD. In addition, it was demonstrated that the presence of oxygen during heating could promote the capture of CH₄.²²⁵

Besides, h-BN is considered to be a graphene growth substrate, because the hexagonal lattice structure provides a flat surface with less than 2% lattice mismatch between graphene and h-BN. Because of the weak vdW interaction between carbon atoms and the h-BN substrate, the carbon atoms move quickly on the h-BN surface. Thus graphene grown on h-BN by molecular beam epitaxy is dominated by the surface morphology of the h-BN substrate.²²⁶ Further, large-area single crystalline graphene

was successfully grown on h-BN by a plasma-assisted deposition method and a 2D superlattice of trigonal moiré pattern was observed.²²⁷

3.2 Graphene transfer

As mentioned above, CVD graphene grown on a metallic substrate that serves as the catalyst needs to be transferred to other substrates for device preparation and applications.²²⁸ During transfer, graphene would form interfaces with protective polymers and transfer liquid media. The interaction strength and wettability of the interface have significant effects on the properties of the transferred graphene. Polymer and solvent residues lead to impurity doping of graphene and cracks and wrinkles are generated during the transfer process. The electrical properties of CVD grown graphene may experience a significant decrease during the transfer process because of these complex interface interactions. Various interface engineering methods have been proposed aiming to maintain the continuity of the transferred graphene, and thus result in less damage to its properties.

3.2.1 Surface protected transfer. Various organic polymers, such as polymethyl-methacrylate (PMMA), polydimethylsiloxane (PDMS), polystyrene (PS), poly(bisphenol A carbonate) (PC), ethylene vinyl acetate (EVA), and polycyclic aromatic hydrocarbons, have been used as the support layer to protect graphene during transfer.^{108,191,192,229–233} Some supporting layers are then removed by dissolving in an organic solvent or by annealing, leaving only the graphene on the target substrate. Fig. 10 is an illustration of polymer-protected graphene transfer.

3.2.1.1 Catalyst etching transfer. For catalyst etching transfer, the graphene grown on a catalyst substrate is usually covered with a polymer film by drop coating. The metal catalyst is etched away and the graphene sheet protected by the polymer floats on the etching solution (Fig. 10a). The graphene/polymer hybrid film is rinsed with deionized water, and transferred onto the target dielectric substrate to complete the transfer. For some applications, the polymer is finally removed, leaving only

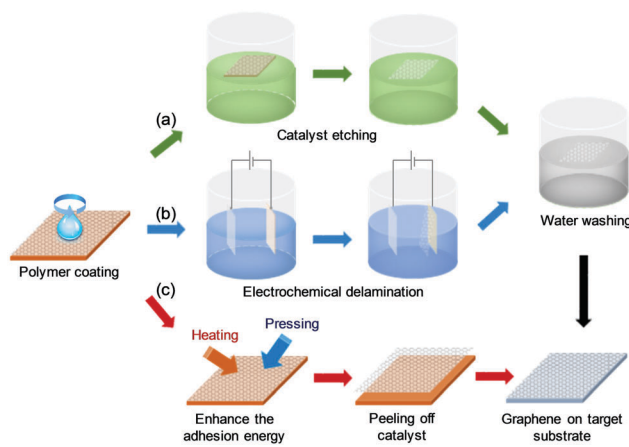


Fig. 10 Illustration of the protected transfer process for graphene. (a) Etching away the catalyst substrate. (b and c) Without etching away the catalyst, electrochemical transfer and peeling off the graphene/polymer layer with other assistance, respectively.

graphene on the substrate, and this is the toughest step. Residual polymers and solvent can cause impurity doping, and thus affect the electrical properties of the transferred graphene.^{234,235} To resolve this problem, the so-called “dry” transfer method was developed, which used an elastomeric stamp or frame to remove the polymer from graphene without trapping liquid between graphene and the target substrate.^{230,236} However, transferring the whole original graphene film without any polymer residue is still a great challenge. Annealing at high temperature can remove the residue, but may affect the electrical properties of graphene. Studies suggest that $-\text{CH}_2$ tends to adsorb on graphene.^{237,238} Tian *et al.* showed that long-chain alkanes or polyethylene (PE)-like molecules were likely to adsorb on the surface of graphene due to their high adsorption energies.²³⁹ Polymers free of PE-like structures, such as pentacene (a polycyclic aromatic hydrocarbon), were then used for the transfer of graphene to minimize contamination, which resulted in clean graphene with a homogeneous surface.²³¹ New two-phase configurations, such as the interface between an organic solvent and an aqueous solution, have been used to support monolayer graphene, which avoids the use of polymeric materials that cause contamination problems.^{240,241}

In addition to polymer residues, defects such as folds/cracks and wrinkles are also inevitable during graphene transfer. Experiments suggest that the defects in the transferred graphene are mainly caused by high contact angles with the transfer liquid media.²⁴² Cho *et al.* substituted water with a low surface tension solution as the transfer medium and obtained high quality graphene with fewer folds and cracks, due to the better contact of the graphene/polymer film with the target substrate.²⁴² Hong *et al.* achieved a clean graphene surface with fewer ripples and tears using a pressure sensitive adhesive film.²⁴³ The employment of a novel protective polymer to successfully transfer graphene from rough substrates onto uneven substrates without damaging its continuity is a great step forward in the polymer protected transfer process.²³³

3.2.1.2 Delamination transfer. Catalyst etching transfer is effective, but generates metal catalyst waste, and transfer strategies without etching are competitive in terms of economic and eco-friendly production of graphene. Since the adhesion energy of monolayer graphene to metals is higher than that of the transferred graphene on dielectric substrates,²⁴⁴ extra assistance, such as heating/pressing or electrochemistry, is needed to overcome the energy barrier (Fig. 10b and c).

In a typical electrochemical delamination transfer, the polymer/graphene/catalyst acts as an electrode to supply direct current and voltage in an electrolytic cell.^{245–247} H_2 bubbles are generated at the edges of the catalyst, providing a force to separate the graphene/polymer layer from the catalyst substrate. However, the transfer usually breaks the continuity of the graphene and partially etches the catalyst substrate.²⁴⁵ A bubble-free delamination process was realized using an optimal supply voltage to transfer the graphene, resulting in a better surface structure.²⁴⁸ Cho *et al.* developed a repeatable mechanical delamination method for the transfer of graphene onto epoxy with definitive adhesive and exfoliated force based on the accurate adhesion energy value of graphene synthesized on copper.²⁴⁴ Rapid separation was also able to improve the graphene transfer from a copper foil seed to Si strips with an epoxy.²⁴⁹ Plasma treatment, chemical functionalization combined with pressure and heating at 150 °C were used to enhance the adhesion between graphene and the protective polymer, and then successfully detach graphene from Cu used as a growth substrate.²⁵⁰ Liu *et al.* achieved etching-free roll-to-roll transfer of graphene onto a plastic substrate by hot water delamination based on the different hydrophobic/hydrophilic properties of graphene and the native copper oxide layer.²²⁹

3.2.2 Direct transfer. Direct transfer without polymer protection is more desirable because it maintains the cleanliness of the transferred graphene. However, it is more challenging because the atom thin graphene layer is more likely to be affected during

Table 2 A summary of transfer methods and the performance of the transferred graphene

Ref.	Original substrate	Transfer method	Target substrate	Performance ($\text{cm}^2 \text{V}^{-1} \text{s}^{-1}$)
220	Cu foil	Catalyst etching	Almost any surface	$4000 \Omega \text{ sq}^{-1}$
221	Cu foil	Catalyst etching	Si/SiO_2	8050 for hole 9940 for electron
228	Cu foil	Catalyst etching	SiO_2	3500
229	Cu foil	Catalyst etching	Arbitrary substrate	$980 \Omega \text{ sq}^{-1}$
233	Cu foil	Catalyst etching	Si/SiO_2	None
235	Cu foil	Catalyst etching	Si/SiO_2	8881 ± 1729 for hole 3549 ± 982 for electron
236	Cu foil	Catalyst etching	Si/SiO_2	17 700
208	Rough Cu	Catalyst etching	Uneven substrates	2912.5 ± 206.4
238	Cu foil	Electrochemical delamination	Si/SiO_2	2400–4046
239	Platinum	Electrochemical delamination	Arbitrary substrate	7100
240	Cu foil	Electrochemical delamination	Si/SiO_2	2000
241	Cu foil	Electrochemical delamination	Si/SiO_2	$773 \pm 241 \Omega \text{ h}^{-1}$
237	Cu foil	Peeling off delamination	Polymer on Si/SiO_2	~1000
242	Cu foil	Peeling off delamination	Polymer on Si	None
243	Cu foil	Peeling off delamination	Polymer	1140
219	Cu foil	Peeling off delamination	Polymer	$5200 \Omega \text{ sq}^{-1}$
244	Cu foil	Direct transfer	TEM grids	None
245	Cu foil	Direct transfer	Any substrate	63 000
246	Cu foil	Direct transfer	PET, glass, Si/SiO_2	5602 for hole 4535 for electron

the transfer. Zettl *et al.* transferred graphene onto amorphous carbon TEM grids with the assistance of a low surface tension organic liquid. Graphene was bound to the top of the TEM grid as the organic liquid evaporated.²⁵¹ Wu *et al.* transferred large area graphene onto a target substrate using a graphite holder and an isopropyl alcohol–water mixture to minimize the external force around the graphene on the surface of the solution.²⁵² Chen *et al.* took advantage of the electrostatic attraction between graphene/copper and the target substrate to load a monolayer graphene film directly onto the target substrate after the catalyst copper foil was etched away.²⁵³

The properties of CVD grown graphene on different substrates are similar, but are changed differently due to the formation of defects and contamination induced by the transfer. The electrical properties of graphene are closely related to its continuity and doping state and these may undergo significant changes during its transfer. Table 2 summarizes the carrier mobilities of graphene transferred using different transfer methods. It can be seen that transfer methods that can reuse the catalyst substrate produce graphene with a worse quality than catalyst etching transfer methods. Therefore, more research studies are needed to optimize graphene transfer that maintains its original properties.

4. Applications of graphene-on-surfaces

4.1 Optoelectronics

In view of the important features mentioned in Section 2.2, graphene-on-semiconductor systems can be exploited for optoelectronic^{38,254,255} and sensing applications.^{256–258} In these devices, the interface always plays an important role in the overall performance. Thus, various engineering methods, such as doping, surface passivation and adding an interfacial layer, have been developed for designing the interface and optimizing the device performance. As for the mixed-dimensional heterostructures, the control and optimization of interfacial interactions are also of great significance for achieving good device performance with synergistic effect from separate components.²⁵⁹

A graphene-on-semiconductor Schottky junction operated under forward bias can be used as a solar cell. The first graphene-on-semiconductor solar cell was fabricated with an efficiency of 1.7% by assembling graphene with Si in 2010 (Fig. 11a).³⁸ In this solar cell, graphene functions as a transparent window layer and a carrier transporting layer, and Si absorbs light. Several changes to the electrical and optical designs were introduced to improve the solar cell performance.²⁶⁰ Chemical doping was used to tune the work function of graphene, which led to an increase in the open circuit voltage of the solar cell.^{261–268} In addition, an interfacial layer and surface passivation were introduced and designed to minimize the interfacial charge recombination and improve the conversion efficiency.^{269–273} Antireflective coatings and electrical design improved the power conversion efficiency to 15.6% (Fig. 11b).^{274,275} This graphene-on-semiconductor Schottky junction can also be used as a photodetector when operated in the reverse bias mode (Fig. 11c).¹²

Photodiodes are common types of graphene-on-semiconductor photodetectors. Their spectral responses usually depend on the band gap of the semiconductors in the Schottky junction (Fig. 11d).²⁵⁴ For example, spectral sensitivity in a broad range from visible to near-infrared has been demonstrated by combining graphene with many semiconductors, such as Si,^{254,276,277,278} Ge,²⁷⁹ GaAs,^{280,281} GaN,^{282,283} and ZnO.²⁸⁴ Graphene itself can also be used as a light absorbing material, and its photoresponse extends to the infrared region.^{285–287} In such photodetector devices, a built-in field is used to trap photoinduced electrons, which prolongs the lifetime of the photoinduced carrier. Meanwhile, a perfect surface of the semiconductor can overcome the trapping effect across the interface to achieve a faster photoresponse (Fig. 11e).²⁸⁵ For example, plasmonic effects increased the responsivity of a graphene-on-Si photodetector to as high as 83 A/W with a fast rise time of less than 600 ns at a wavelength of 1.55 μm (Fig. 11f).²⁸⁵ Graphene with a highly sensitive surface can absorb molecules and the corresponding charge transfer can modulate its Fermi level and Schottky barrier height.²⁵⁷ It was found that the ideality factor decreased with the increase of the Schottky barrier height as the bare surface of a graphene-on-Si Schottky junction was exposed to aromatic molecules (Fig. 11g).

Mixed-dimensional heterostructures of graphene and inorganic semiconductors have been demonstrated with desirable performance in electronic and optoelectronic devices by combining the merits of each component. For example, graphene barristors with high current on/off ratios were achieved by using MoS₂ or WS₂ as the atomically thin vertical ultra short channel layer (Fig. 12a).^{48,49} Phototransistors based on these heterostructures can overcome the limitation of the weak optical absorption property of graphene. PbS QDs were used as an additional medium to generate photo-induced carriers with holes transferred to the graphene layer (Fig. 12b).⁷² The spectral selectivity and photoresponse of the graphene based heterostructure can be controlled by tuning the type and size of the additional media.^{50–52} Similar to graphene/bulk semiconductor Schottky diodes, graphene combined with other mixed-dimensional semiconductors can also be used as photodiodes and photovoltaic devices.^{47,53–57,288–291} In particular, the efficient separation of photoinduced carriers and ultrafast response were achieved with a unique sandwich heterostructure of graphene and 2D semiconductors to produce a light absorber as the work function of graphene was modified (Fig. 12c and d).^{55–57} Based on these results, graphene shows great potential for creating thin film devices, owing to its two-dimensionality and structural flatness. Graphene serves multiple functions as a transparent electrode, active junction layer, hole collector and even anti-reflection layer in graphene-on-semiconductor heterojunction photodevices, such as solar cells and photodetectors, and could be extended to other electronics.

4.2 Surface catalysis

Catalysis plays a critical role in the fields of energy conversion and storage, environmental science, and organic chemistry. Graphene and its derivatives have unique physical and chemical properties, including a tunable electronic structure, high electrical

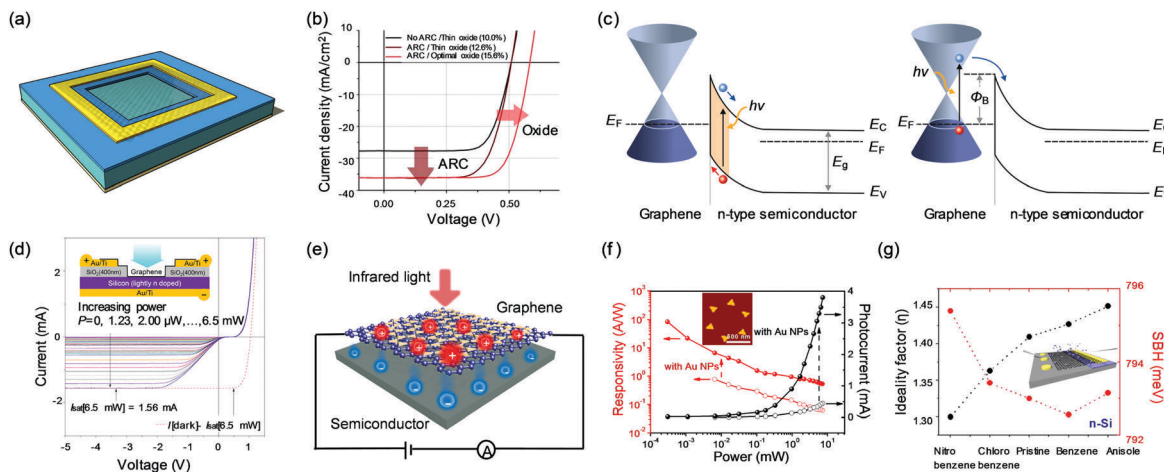


Fig. 11 (a) Diagram of the graphene-on-Si Schottky junction solar cell. Reproduced with permission from ref. 38. Copyright 2010, John Wiley & Sons, Inc. (b) I - V characteristics of the graphene-on-silicon Schottky junction solar cell with native oxide and antireflective coatings after doping. Reproduced with permission from ref. 274. Copyright 2013, American Chemical Society. (c) Energy band diagrams of a graphene-on-semiconductor photodetector in the reverse bias mode. When the incident photon energy exceeds the semiconductor band gap, electron–hole pairs are generated in the semiconductor region, while when the incident photon energy is less than the semiconductor band gap, electron–hole pairs are generated in graphene. Reproduced with permission from ref. 12. Copyright 2016, AIP Publishing LLC. (d) I - V characteristics of a graphene-on-Si Schottky photodiode for incident light power up to 6.5 mW. The inset shows a diagram of the photodiode. Reproduced with permission from ref. 254. Copyright 2013, American Chemical Society. (e) Concept diagram and (f) photoresponse of a graphene infrared photodetector. The vertical built-in field is used for trapping the photoinduced electrons and a plasmonic effect can realize photon trapping in the graphene. The inset of (f) shows the morphology of triangle-like Au NPs. Reproduced with permission from ref. 285. Copyright 2017, American Chemical Society. (g) Variation of the ideality factor and Schottky barrier height of the graphene-on-Si Schottky junction exposed to liquid aromatic molecules. The inset shows a diagram of the graphene diode chemical sensor. Reproduced with permission from ref. 257. Copyright 2013, American Chemical Society.

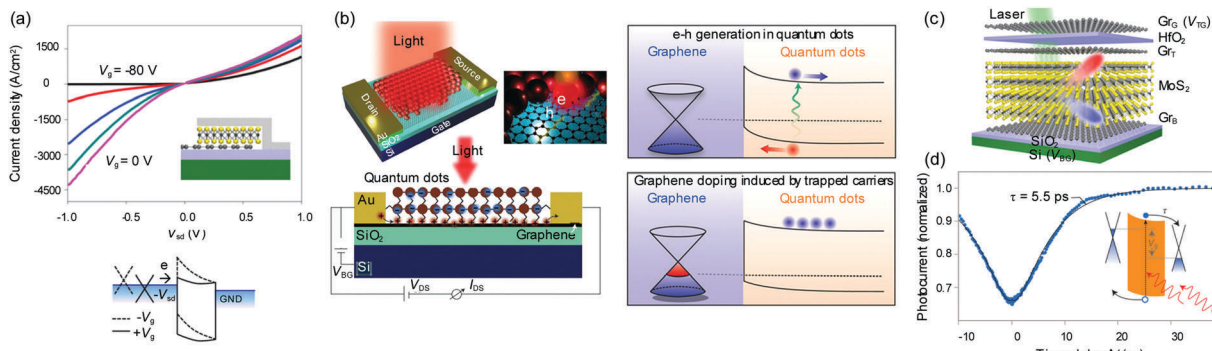


Fig. 12 (a) I - V characteristics of graphene/ MoS_2 /metal FETs. The energy band diagram under positive or negative V_g shows that the gate voltage can effectively modulate the charge transport. The inset shows a schematic diagram of vertical graphene/ MoS_2 /metal FETs. Reproduced with permission from ref. 48. Copyright 2013, Macmillan Publishers Limited. (b) Device schematic and energy band diagrams of graphene/PbS QDs phototransistors. A built-in field is formed across the interface of the graphene/PbS QDs heterostructure, and holes can be transferred to the graphene layer from PbS QDs under illumination. Reproduced with permission from ref. 72. Copyright 2012, Macmillan Publishers Limited. (c) Schematic diagram of the vertical graphene/ MoS_2 /graphene heterostructure in which MoS_2 is used as the light absorber. Reproduced with permission from ref. 56. Copyright 2013, Macmillan Publishers Limited. (d) Photoresponse as a function of the time delay of a graphene/WSe₂/graphene heterostructure. The inset shows the energy band diagram of this heterostructure. Reproduced with permission from ref. 57. Copyright 2016, Macmillan Publishers Limited.

conductivity and carrier mobility, large surface area, and high tolerance to strong acids and alkalis. Defective and/or heteroatom-doped graphene electrocatalysts and photocatalysts have attracted significant attention.^{292–295} Graphene itself can work as a catalyst because defects and edges are catalytically active. Surface modification of graphene by introducing heteroatoms helps to increase the number of active sites, thus improving its catalytic activity. Besides, it can serve as an effective support for NPs with high catalytic activities. A well designed interface

is crucial for the good dispersity of these NPs and their interplay with the supporting graphene, thus achieving a good catalytic performance.

4.2.1 Graphene-based electrocatalysts

4.2.1.1 Catalytic properties of graphene. Pristine graphene is not active in chemical reactions due to its low density of states at the Fermi level. However, the defects or edges (Fig. 13) in graphene provide electrochemically active sites for catalytic reactions.^{296,297} Nakada *et al.* found that for finite graphite

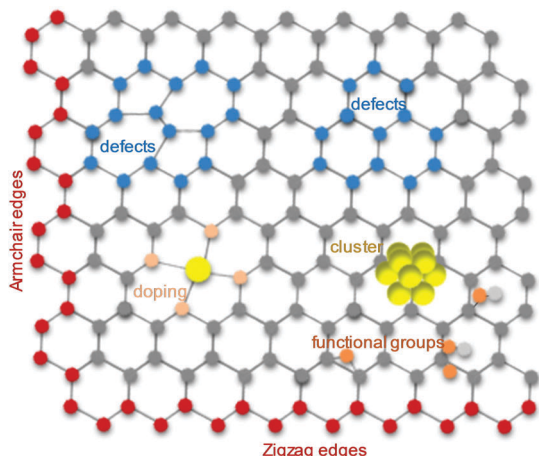


Fig. 13 Schematic representation of electrochemically active sites, defects, edges, doping, and functional groups in graphene.

there was a special atomic zigzag edge state that had a high charge density.²⁹⁶ Jiang *et al.* investigated the chemical reactivity of the zigzag edges on a GNR by DFT calculations and found that the C–H bond dissociation energy of the zigzag edges was higher than those of graphene sheets, nanotubes, and armchair edges due to the presence of zigzag edge states near the Fermi level.²⁹⁷ Deng *et al.* found that the zigzag edges of graphene are chemically active in the oxygen reduction reaction (ORR), whereas the armchair edges and an in-plane network of graphene are inert.²⁹⁸ Shen *et al.* proposed a more straightforward method to compare the catalytic activities of the edges and the basal plane in graphite.²⁹⁹

By investigating the ORR in an air-saturated micro-droplet at a specified location either on the edge or on the basal plane of a highly oriented pyrolytic graphite (HOPG) using an electrochemical micromanipulator-microinjection system (Fig. 14a and b), Shen *et al.* demonstrated that the edges of the carbon material were more active than its basal plane for ORR (Fig. 14c) and such a conclusion was applicable to other carbon materials.²⁹⁹ Jin *et al.* developed a graphene quantum dot (GQD-GNR) structure as a catalyst of ORR and found that the numerous surface/edge defects on the GQD-GNR surface and at their interfaces were the active sites. These defects along with efficient charge transfer between the intimately contacting GQDs and GNRs account for the high activity and stability of graphene in ORR.³⁰⁰ Jia *et al.* prepared defects in graphene intentionally by removing heteroatoms from graphene. Fig. 14d illustrates the removal of N from an N-doped graphene matrix. The defective graphene was demonstrated to be effective for all three basic electrochemical reactions, *e.g.*, ORR, oxygen evolution reaction (OER), and hydrogen evolution reaction (HER) (Fig. 14e–g), and the defect formation mechanism was useful for the design of next generation catalysts for electrocatalysis.³⁰¹

4.2.1.2 Catalytic properties of doped graphene. The introduction of heteroatoms into graphene has also been demonstrated to be an effective way to increase its number of active sites and improve its catalytic activity.^{302,303} The charge distribution and electronic

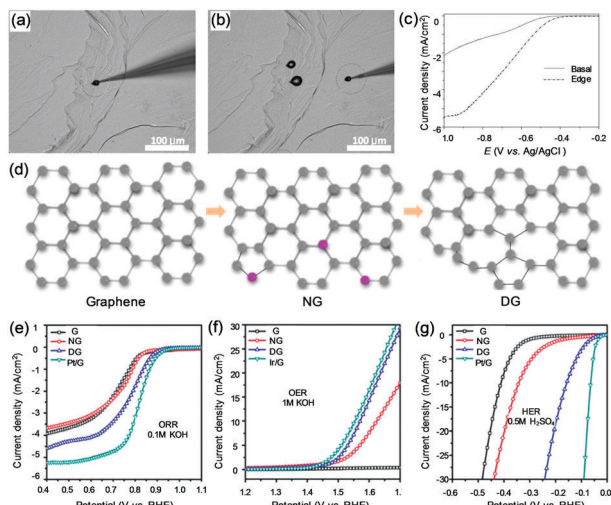


Fig. 14 (a and b) Optical photographs of highly oriented pyrolytic graphite as the working electrode with an air-saturated droplet deposited on its edge and basal plane. (c) Linear sweep voltammetry (LSV) curves of the ORR tested for a droplet located either on the edge or on the basal plane of the highly oriented pyrolytic graphite. Reproduced with permission from ref. 299. Copyright 2014, John Wiley & Sons, Inc. (d) Schematic representation of the formation of defective graphene. (e–g) Linear sweeping voltammetry curves of the pristine graphene, N-doped graphene, and defective graphene for oxygen reduction, oxygen evolution, and hydrogen evolution reactions, respectively. They demonstrate that defective graphene is effective for electrochemical reactions. Reproduced with permission from ref. 301. Copyright 2016, John Wiley & Sons, Inc.

properties of graphene can be tuned by using heteroatoms of different size and electronegativity. Heteroatoms, such as nitrogen,³⁰⁴ sulfur,³⁰⁵ boron,³⁰⁶ phosphorus,³⁰⁷ and iodine,³⁰⁸ have been demonstrated to be excellent catalysts for the ORR without CO poisoning and the methanol crossover effect on alkaline electrolytes. Okamoto found by DFT calculations that oxygen adsorption became energetically favorable for N-doped graphene as the number of N atoms around the C=C bond increased and both 4e[−] and 2e[−] reduction became feasible.³⁰⁹ Zhang *et al.* concluded that the ORR on N-doped graphene was by a direct 4e[−] pathway, and the nitrogen doping and defects provided a high positive spin and/or charge density that facilitated the ORR on the graphene surface.^{310,311} Based on experimental and theoretical results, other researchers argued that the active sites of N-doped graphene originated from the carbon atoms adjacent to the nitrogen-dopants.^{312–314} Therefore, although extensive work has been conducted, the catalytic mechanism of the doped-graphene still remains unclear.

There are three major nitrogen configurations in an N-doped graphene plane: graphitic, pyrrolic, and pyridinic states.^{315,316} Great effort has been made to identify the active sites in N-doped graphene, but controversy still exists. Due to the difficulties in producing specific N-doping species and the effects from the intrinsic defects and residual metal in the doped graphene,^{316–318} more experimental and theoretical works are needed to comprehensively understand heteroatom-doped graphene. In addition to single-atom-doped graphene, co-doped graphene can provide further possibilities of the electronic

properties for improving its catalytic activity.^{319,320} Boron and nitrogen co-doped graphene,^{321,322} sulfur and nitrogen co-doped graphene,^{323,324} and phosphorus and nitrogen co-doped graphene³²⁵ have been reported as efficient catalysts for the ORR and supercapacitors. In addition to non-metal dopants, TMs, such as Fe and Co, have been confined in N-doped graphene matrices to form TM-N_x centers, which exhibit high catalytic performance for the ORR and direct catalytic oxidation of benzene to phenol at room temperature.^{326–329} Based on DFT calculations, Calle-Vallejo *et al.* concluded that a TM site could be stabilized by four pyridinic nitrogen atoms in graphene, creating a TM-N_x active center for the ORR.³³⁰

4.2.1.3 Graphene-supported catalysts. Due to its high electrical conductivity and excellent mechanical properties, graphene meets the requirements of an ideal electrocatalyst support (Fig. 13). DFT calculations suggest that the defects in a graphene substrate can act as strong trapping sites for metal clusters and inhibit catalyst sintering.^{331–337} This interfacial interaction is favorable for the stability and can further tailor the averaged-band center of the deposited metal/alloy clusters, leading to a strong interference with oxygen adsorption and increased charge transfer from the clusters to the substrate (Fig. 13).^{333–336} These studies provide possible strategies for promoting the activity and stability of CO oxidation/oxygen reduction reactions over metal NP/graphene structures by defect engineering (Fig. 13).^{333–337}

The synergistic effect of graphene and metal-based NPs with high electrocatalytic activities can result in superior catalytic performance.^{338–341} Noble metals including Pt, Ir, and Pd and their alloys are considered to be the most efficient catalysts for energy conversion and storage;^{342–345} however, their high cost and limited availability on Earth make them less competitive for large-scale commercial applications. Therefore, non-precious metal-based catalysts have attracted increasing interest. TM-based NPs including Fe₃O₄,³⁴⁶ Fe₃C,³⁴⁷ and Co₃O₄³⁴⁸ in combination with graphene are efficient catalysts. Furthermore, hybridizing sulfides of TMs, such as MoS₂, MoSe₂, WS₂ and so on, with graphene sheets can create perfect HER catalysts featuring high activity, favorable kinetics, and excellent durability.^{349–353}

To protect the TM-based electrocatalysts from corrosion and maintain their high activity and stability in acidic solid polymer electrolytes, a new strategy has been proposed to encapsulate TM NPs in carbon nanotubes or graphitic layers.^{354–360} However, most of the carbon shells used for catalyst protection are too thick and usually consist of multilayer graphitic carbon or composites, which may obstruct the electron transfer from the metal catalysts to the carbon layer, and significantly reduce the catalytic activity.^{354,355} Tavakkoli *et al.* constructed single-shell carbon-encapsulated iron nanoparticles (SCEINs) on single-wall carbon nanotubes and used the material as a highly active and durable non-noble-metal catalyst for the HER in an acidic electrolyte. The single carbon layer exhibited no inhibition of the desired access of reactants to the vicinity of the iron NPs, but protected the active metallic core from oxidation.³⁶¹ Deng *et al.* reported a hierarchical structure with a homogeneous CoNi nanoalloy encapsulated by ultrathin graphene shells (1–3 layers)

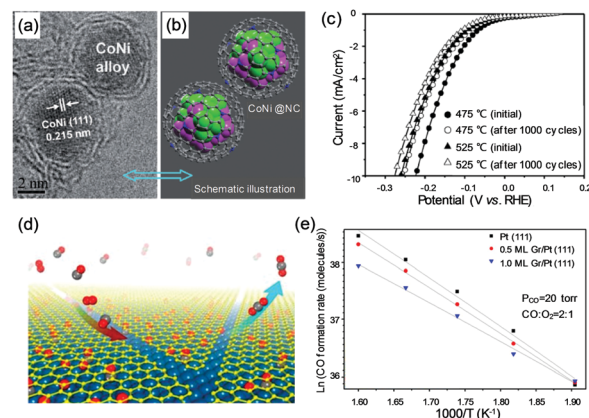


Fig. 15 (a) HRTEM image of CoNi@NC, showing graphene shells and encapsulated metal nanoparticles. (b) Schematic representation of the CoNi@NC structure. (c) Durability measurements with CoNi@NC prepared at 475 and 525 °C. Polarization curves were recorded before the first and after 1000 CV sweeps between –142 mV and +108 mV (vs. RHE) at 100 mV s^{–1}. Reproduced with permission from ref. 362, Copyright 2015, John Wiley & Sons, Inc. (d) Schematic representation of the simultaneous intercalation of CO and O₂ molecules underneath graphene flakes through the domain boundaries and the release of CO₂ from the interface. (e) Arrhenius plots of the CO₂ formation rate on the Pt(111) and the Gr/Pt(111) surfaces in the temperature range 525–625 K. Reproduced with permission from ref. 364. Copyright 2014, National Academy of Sciences.

to improve its HER performance in acidic media (Fig. 15a and b). The high HER activity of the CoNi@NC was confirmed by electrochemical measurements (Fig. 15c).³⁶² DFT calculations indicated that the ultrathin graphene shells could dramatically promote electron penetration from the CoNi to the graphene surface. Reducing the number of layers in the graphene sheet and increasing the amount of the nitrogen dopant significantly increased the electron density in the graphene shells, which further improved the HER activity.³⁶² Encapsulation provides an efficient way for the rational design of high-performance and low-cost electrocatalysts for energy-related applications.³⁶³ Catalytic reactions occurring in the nano-space between a graphene layer and the metal by tuning the interfacial reactions is another promising way to achieve high-performance catalysis (Fig. 15d).³⁶⁴ Mu *et al.* visualized the penetration of CO into a graphene/Pt(111) interface at room temperature and found that the oxidation of CO was confined to the graphene/Pt interface.³⁶⁵ Further study revealed that the reaction barrier for CO oxidation over the Pt(111) surface covered by graphene was lower than that over a bare Pt(111) surface. The electronic interaction between the top graphene layer and CO molecules underneath could weaken the C–O bond in CO, promoting the formation of O–CO bonds, and thus alleviating the CO poisoning effects on Pt catalysts (Fig. 15e).³⁶⁴ The 2D confinement effect can be extended to other graphene-like covering materials, such as BN, 2D chalcogenides, and 2D oxides.

4.2.2 Graphene-based photocatalysts. Unlike electrocatalysis where graphene itself can act as the catalyst, it is used as a loading platform for photocatalysts to avoid undesired aggregation and as a conductive network to improve the separation and transportation of photogenerated excitons in photocatalysis.

Considering this, a good contact between the catalyst and graphene is necessary to maximize charge separation, minimize carrier recombination, and thus improve the photocatalytic performance. In addition to providing strong electronic interactions, the incorporated graphene can also absorb reactants by physical absorption and π - π conjugation (for aromatic contaminants), which is favorable for the photocatalyzed degradation of organics.^{366–382}

Many anchoring methods have been used to *in situ* grow NPs on the surface of pristine or functionalized graphene nanosheets or combine the pre-synthesized NPs with graphene nanosheets.^{366,371,372,376,381,383–387} To date, various nanostructures including NWs,^{369,388} nanorods,^{373–375,378,382} nanotubes,^{379,389} and nanosheets^{377,380,390} have been introduced on the surface of graphene nanosheets. Semiconductor particles have also been wrapped by graphene nanosheets to form core–shell structures^{391–393} by mechanical mixing, *in situ* growth, and electrostatic adsorption. The enlarged contact area between the catalysts and graphene facilitates effective photoinduced carrier separation and charge transport to the reactants. Several three-dimensional hierarchical structures with increased light absorption have been fabricated, such as intercalated,³⁹⁴ foam,^{395–397} sandwich-like,^{398,399} forest-like,⁴⁰⁰ flower-like,^{367,368,401} and hollow core–shell structures.^{402,403} Multilaminate, multihole and hollow structures can significantly increase the optical path length as a result of the high multilayer scattering of incident light, which promotes photon absorption in the semiconductor catalysts, and thus increases the number of photogenerated charge carriers that are then separated by the graphene/semiconductor heterojunction and transferred to the interface with the solution to accelerate photocatalytic reactions.

4.3 Anti-friction and superlubricity

2D materials possess outstanding lubrication properties with their thickness down to a few atomic layers.⁴⁰⁴ Graphene offers distinctive properties as a solid lubricant and can be potentially used as an ultrathin coating on surfaces to reduce energy consumption in mechanical components.^{405,406} A typical tribology system always involves various surfaces and interfaces, such as solid/solid, solid/liquid/solid, and so on. The properties derived from the “graphene-on-surface” make it an ideal protective surface coating and friction modifier. Therefore, understanding the friction between two pieces of graphene, or between graphene and another material, is important for achieving good electrical, thermal, and mechanical connections.

4.3.1 Tribology of graphene. The high chemical inertness, extreme strength, and easy shear ability of graphene and atomically smooth surface are the major favorable attributes contributing to its extraordinary tribological behavior. The fact that it is ultrathin, even with multilayers, makes it suitable for nano-scale or micro-scale systems with oscillating, rotating, and sliding contacts to reduce friction and wear. It has been found that the mechanism of a graphene friction modifier is affected by a variety of factors including the thickness of graphene, the surface morphology and chemistry, and the fabrication process.⁴⁰⁵ The behaviors of monolayer graphene and multilayer graphene (or graphite) are

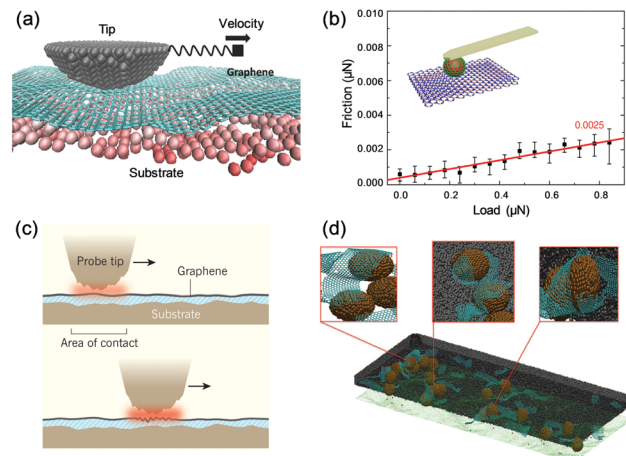


Fig. 16 Tribology of graphene. (a) Schematic representation of a probe tip sliding against a graphene coating on a substrate. Reproduced with permission from ref. 408. Copyright 2014, IOP Publishing. (b) Friction force as a function of load for a graphene/h-BN tribo-pair. Reproduced with permission from ref. 409. Copyright 2017, Macmillan Publishers Limited. (c) Flexible graphene increases friction. Reproduced with permission from ref. 411. Copyright 2016, Macmillan Publishers Limited. (d) Scroll formation in an ensemble of graphene patches on nano-diamonds when subjected to sliding. Reproduced with permission from ref. 421. Copyright 2015, American Association for the Advancement of Science.

quite different, even though both materials have the same surface morphology and chemical structure. Experiments suggest that monolayer graphene can exhibit higher friction than multi-layer graphene and graphite, and the friction increases with continued sliding.⁴⁰⁷ Based on the force–distance relationship, it has been proven that the difference between graphene and graphite is related to vdW forces. The frictional force between a probe tip and graphene (Fig. 16a)⁴⁰⁸ does not rely on the presence of a substrate, but decreases with the thickness of graphene going from 1 to 4 layers. The decrease of friction with the increase in the number of layers is affected by the adhesion force between graphene and the substrate. The mechanical confinement to the substrate plays an important role in the frictional behavior of graphene. Loosely bound or suspended graphene sheets can pucker due to tip–graphene adhesion and this can increase the contact area and allow further deformation of graphene during sliding, leading to more friction. Because thinner graphene has a lower bending stiffness, the puckering effect and frictional resistance are greater for thin graphene layers.

The sliding friction between graphene and graphite, and graphene and h-BN under high contact pressures can be directly measured using a graphene-coated microsphere probe.⁴⁰⁹ An exceptionally low friction coefficient (0.0025) has been measured with local asperity contact pressures up to 1 GPa (Fig. 16b), which is attributed to the sustainable overall incommensurability caused by the multi-asperity contact covered with randomly oriented graphene nanograins. Such microscale superlubricity can be extended to sliding between a variety of surfaces. However, if the graphene is strongly bound to a substrate, the puckering effect will be suppressed and no thickness dependence should be observed. The substrate roughness can significantly enhance the

friction of graphene, making it orders of magnitude larger than that on a smooth substrate due to the puckering effect. The adhesive force between graphene and the substrate plays opposite roles in the puckering effects on smooth and rough substrates. On a smooth substrate, a larger adhesion hinders wrinkle formation in graphene, resulting in lower friction. In contrast, the adhesion to a rough substrate induces roughness in the graphene and increases the friction.⁴⁰⁸ The friction of graphene on an atomically flat substrate, such as h-BN, is low and comparable to that of bulk graphene.⁴⁰⁹ The friction of graphene folded onto bulk-like graphene is indistinguishable from that of monolayer graphene on SiO₂, despite the ultra-smoothness of bulk-like graphene.

For few-layer 2D materials adhered to a substrate, the static friction force gradually changes as the number of layers increases before reaching a constant value. Recently, this layer-dependent transition phenomenon has been explained with atomistic simulations.⁴¹⁰ Atomic force analysis revealed that static friction is a manifestation of the natural tendency of thinner and less-constrained graphene to change its configuration as a direct consequence of its greater flexibility. That is, the tip atoms become more strongly pinned (Fig. 16c),⁴¹¹ and show greater synchrony in their stick-slip behavior. As the number of atom contacts, *e.g.* the true contact area, increases, the quality, in this case, the local pinning state of individual atoms and the overall commensurability, also evolves in frictional sliding on graphene. The evolving contact quality is the critical reason for the time-dependent friction of configurationally flexible interfaces.

4.3.2 Graphene lubricants. Graphene can be used as a solid or colloidal liquid lubricant for macroscale metallic sliding components and high-pressure contacts. In addition to a dramatic reduction of friction caused by the graphene present at the sliding interfaces as a solid lubricant, a significant decrease in the corrosion-induced wear (tribo-corrosion) was achieved with a graphene passivation layer.⁴⁰⁵ Therefore, graphene layers can significantly suppress the friction and wear of sliding steel interfaces.^{412,413} For example, the friction of steel was decreased by nearly one order of magnitude in dry nitrogen and humid air environments by the presence of a graphene coating, and the corresponding wear volume and rate were reduced by 3–4 orders of magnitude.

In addition to being used as a solid lubricant, graphene has been used as an additive in conventional lubricants,^{414–417} such as oils and solvents. Even the addition of a minimal amount of graphene platelets to oil is capable of causing a noticeable reduction in the friction and wear of steel. Organic solvent lubricants may also benefit from graphene additives. For example, alkylated graphene with various alkyl chain lengths was prepared by the coupling of alkylamine with carboxylic groups and was then dispersed in different organic solvents, and this significantly reduced the friction and wear of steel.⁴¹⁷ These enhanced lubrication properties were attributed to graphene sheets between the rubbing surfaces that prevented a direct contact with the steel and provided low resistance to shearing.

4.3.3 Superlubricity. Superlubricity, or more precisely structural superlubricity, involves the relative motion of two

incommensurate crystalline surfaces with super low dry friction. The superlubricity of graphite and graphene has aroused increasing interest in recent years.^{409,418–420} Interfaces capable of relative motion at speeds in the range of meters-per-second with very low energy dissipation are of crucial importance for a broad spectrum of applications. The dependence of frictional forces on normal load in incommensurate micrometer-size contacts between atomically smooth single-crystal graphite surfaces was investigated under ambient conditions.⁴¹⁸ The contacts exhibited superlubricity under a normal (perpendicular) load. The measured friction coefficients were essentially zero and independent of the load up to 1.67 MPa. These observations of load-independent superlubricity in microscale contacts are a promising result for numerous practical applications. The interpretation of such superlubrication behavior is based on the premise that (i) the high lateral stiffness of graphene makes a commensurable contact with most solid surfaces nearly impossible, and (ii) combined with the weak interaction with most materials, incommensurability leads to a state of ultralow friction when graphene slides over a different material. How to obtain long-lasting superlubricity between graphene layers under high normal load in an ambient atmosphere still remains a challenge.

Superlubricity at the engineering scale has been achieved by combining graphene with nanodiamond particles and diamond-like carbon (DLC) (Fig. 16d).⁴²¹ Macroscopic superlubricity originates because graphene patches on a sliding interface wrap around nanodiamonds to form nanoscrolls with reduced contact area that slide against the DLC surface, achieving incommensurate contact and a substantially reduced coefficient of friction (~ 0.004). The tribological evolution of a single graphene patch at the nanoscale resembles that of a single asperity contact, whereas the mesoscopic behavior resembles a multiple asperity contact. The superlubricity of GNR on gold has also been observed.⁴²² A GNR-Au(111) contact exhibited superlubricity under static and kinetic friction forces of 100 pN. The detailed dynamics of the sliding motion are nevertheless influenced by local surface properties, such as various degrees of commensurability caused by the surface reconstruction. By suitable alignment of graphene on a Ge(111) substrate, the friction of graphene remained low even after fluorination or oxidation.⁴²³ This behavior is closely related to the suppression of the molecular-level deformation of graphene within the moiré superlattice structure. The formation of an interconnected meshwork with an increased interfacial charge density imposes a strong anchoring effect on graphene.

4.4 Coatings and composites

Coating offers an economical way to change and improve the surface properties of various devices. Composites with well designed and manufactured structures can combine the properties of reinforcement and the matrix, generating improved performance or even some new characteristics. Owing to its excellent electrical and thermal conductivity, heat dissipating capability, mechanical properties, *etc.*, graphene has received great attention as a coating material and filler in various composites. For both cases, the interfaces strongly affect whether the excellent properties of

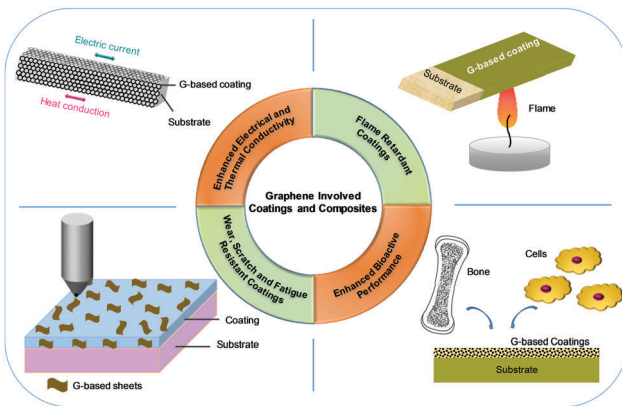


Fig. 17 Typical uses of graphene in coatings and composites.

graphene can be effectively exploited to achieve desirable overall performance. Understanding of the interface interactions guides us in interface engineering for optimizing the properties of graphene-involved coatings and composites. We will discuss the contributions of graphene based coatings and composites to improve electrical and thermal conductivity, flame and fire resistance, mechanical strength, and bioactive performance of bare substrates or matrices as illustrated in Fig. 17.

4.4.1 Graphene integration for enhanced electrical and thermal conductivity. Graphene has excellent electrical and thermal conductivity,^{5–8} which makes it a good candidate to act as a coating material for enhancing the electrical and thermal conductivity of the substrates. It has been demonstrated that graphene deposited on conductive Cu NWs can enhance the elastic surface scattering of electrons and decrease inelastic surface scattering by preventing the oxidation of graphene/Cu NWs, and thus significantly improve their electrical and thermal conductivity.⁴²⁴ In another study, Kim *et al.* coated eosin Y and eosin B functionalized rGO and bare GO onto cotton yarns. The electrical conductivity of the fiber was increased by approximately four orders of magnitude after five dip-coating and reduction cycles, which could make it useful in smart electronic textiles.⁴²⁵ Pretreatment of the to-be-coated substrates has been developed to improve the electrostatic interactions between substrates and graphene based materials.^{425,426} Compared with a pure resin coating, the graphene/resin composite coating with a high graphene content of 50 wt% resulted in a significant improvement in the thermal conductivity by as much as 842%.⁴²⁷ In some cases, the graphene surface was pretreated to improve the dispersion of graphene in a polymeric matrix. For example, Jiang *et al.* coated exfoliated graphene nanoplates with a low molecular weight paraffin wax to improve its dispersion.⁴²⁸

Graphene can serve as a conducting filler for polymer and ceramic composites. An electrically conductive graphene filler can form an interpenetrating and continuous network as the percolation threshold is reached, resulting in a sudden increase in the electrical conductivity of the composite.⁴²⁹ For thermal conductivity, the planar structure of graphene offers a 2D path for phonon transport. In addition, the good coupling between

the rGO sheets and polymeric matrices due to the epoxy groups remaining after reduction can reduce the Kapitza effect and enhance the thermal conductivity of the composite.⁴³⁰ Simulations combined with experiments show that the thermal conductivity of these nanocomposites is influenced by graphene size, interfacial bonding strength, and polymer density. Increased polymer density and graphene size and chemical bonding formation at their interface are significant for improving the overall thermal properties.⁴³¹

4.4.2 Graphene integration for flame retardants. Polymers are extensively used in modern life, but they easily burn with a high rate of heat release. In recent years, flame retardant coatings have become attractive due to their easy fabrication. Graphene has a high thermal conductivity and heat dissipating ability and many studies have shown its remarkable performance in reducing the flammability of polymer composites.

The combustion of graphene/polymer composites results in the formation of a dense char layer.⁴³² Graphene, as well as these dense char layers, can effectively keep the thermal decomposition products from approaching the flame zone and prevent oxygen from reaching the underlying polymer matrix, leading to a significant reduction of the peak heat release rate (PHRR) and a much longer time to ignition (TTI).^{432,433} An intumescent flame retardant polyacrylamide and GO (IFR-PAM/GO) composite was prepared by LbL deposition and used to coat cotton fabrics. The IFR-PAM/GO-coated fabrics became less flammable with lower PHRR and longer TTI and improved thermal stability.⁴³⁴ With the same method, a chitosan/GO/alginate composite was deposited on the surface of flexible polyurethane foams *via* alternatively submerging the foam into the GO filled solutions. High mass char residue and reduced PHRR were achieved and the barrier effect of the GO-filled coating was considered to be the main reason for the enhancement. This graphene based coating layer can not only slowdown the diffusion of degradation products, but also hinder the propagation of oxygen and heat into the interior of the polymer matrix.⁴³⁵ Graphene can also be combined with many other flame retardant additives, such as CuO,⁴³³ ZnS,⁴³⁶ and MoS₂,⁴³⁷ to improve the PHRR and TTI of various polymers.

4.4.3 Graphene integration for scratch and fatigue resistance. In many industries, such as automobile, aviation, and shipping, solid surface wear and fatigue usually occur due to the cyclic stress. Improving the surface of the material while retaining its structural integrity is of great importance in such applications. Graphene possesses incredible mechanical strength due to the strong covalent bonds between the carbon atoms in its hexagonal arrangement. The elastic modulus and intrinsic strength of defect free graphene are 1 TPa and 130 GPa, respectively,⁹ which make it an excellent 2D robust filler material to improve the surface mechanical properties or to improve the overall mechanical performance of composites.

The enhancement of mechanical properties brought by the incorporation of moderate levels of graphene into substrates can be attributed to the pull-out, crack bridging, crack deflection and crack tip shielding of graphene or the graphene/matrix interface.⁴³⁸ The strength of interface interactions determines whether stress can be effectively transferred from the matrix to

graphene. As a result, the interface between graphene and the matrix should be well optimized to retard crack propagation. In addition, the dispersion of graphene also plays an important role. The use of single- or few-layer graphene with reasonable lateral dimensions and graphene oxide without imparting damage upon the flakes as fillers, and construction of a strong interface with the matrix *via* chemical bonding result in a good mechanical performance of the composite.¹¹³ It was found that incorporation of only a small amount of graphene would lead to obvious improvements in the mechanical performance of the composite. A graphene reinforced waterborne polyurethane composite coating was prepared by a sol-gel method, which doubled the tensile strength of polyurethane with 2 wt% graphene incorporation.⁴³⁹ Incorporation of 10 wt% graphene into polytetrafluoroethylene (PTFE) was able to decrease its wear rate ~4000 fold.⁴⁴⁰ To improve the interactions between graphene and the matrix, chemical functionalization has been introduced. GO sheets were attached to the surface of a Ti substrate using a silane agent, 3-aminopropyltriethoxysilane (APTES), and then reduced by a hydrothermal method.⁴⁴¹ The obtained top layer graphene (G-APTES) showed good adhesion, low friction, and excellent anti-friction properties, making G-APTES a promising protective coating.

4.4.4 Graphene integration for improving bioactivity. In recent decades we have witnessed tremendous improvements in biomedical implants. It is tremendously important to find a suitable coating to provide or improve the bioactivity of the implant surface. GO has attracted great attention due to its biocompatibility, surface functionalizability and promising antimicrobial activity, leading to good biocompatibility and antibacterial activities of GO based coatings.

GO can interact with proteins through hydrogen bonds and hydrophobic interactions leading to structural rearrangements of these protein molecules and cell adhesion. There is an increased cell proliferation of the graphene coated substrate instead of exerting any cytotoxic effects on the cells.⁴⁴² Recently, numerous studies have been conducted on the fabrication of composite coatings containing graphene or its derivatives to reinforce hydroxyapatite (HA). Researchers found that a GO coating on an AZ91 Mg alloy surface significantly promoted the nucleation and crystallization of HA during the biomineralization of a modified simulated body fluid (SBF). Meanwhile, the as-synthesized GO/HA coating could dramatically improve the corrosion resistance of the Mg alloy.⁴⁴³ A HA/graphene nanosheet composite coating was deposited on a Ti substrate by a vacuum cold spray method.^{444,445} Due to the fast adsorption of key serum proteins, such as fibronectin, on the graphene, the coating exhibited excellent attachment to a proliferation of osteoblast cells. A HA/GO composite coating prepared by electrophoretic deposition on a Ti substrate improved the mechanical properties and *in vitro* biocompatibility of the composite and provided ~95% cell viability at 2 wt% GO content.⁴⁴⁶ Graphene based composite coatings were also demonstrated to have a high bioactivity in SBF, as well as exhibit antibacterial and noncytotoxic activity.^{447,448} Other graphene derivatives, such as gelatin-functionalized GO, were reported to be highly bioactive coatings by themselves or when combined with HA.^{442,449}

5. Summary and outlook

This article provides an overview of the interface physics and chemistry of graphene-on-surface systems. The interfaces between graphene and its growth substrates, transfer media, support substrates, and even the environment may significantly affect the properties of graphene. Driven by the excellent properties and promising applications of graphene and graphene based materials,⁴⁵⁰ a tremendous amount of research concerning interfacial interactions and their influence has been conducted, with the aim of being better able to manipulate the properties of graphene and optimize the performance of graphene based devices. However, there are still major challenges to overcome.

One of the key challenges is the scalable synthesis of high quality graphene with the desired properties. Because the growth substrate can significantly affect the growth mechanism and exhibit doping effects on the graphene obtained, a thorough understanding of their interface would contribute to the efficient control over the number of layers, morphology, size, electronic structure, and doping of CVD grown graphene. Considering the effects of the interface, methods including pretreatment of the growth substrate and growing graphene on liquid metal catalysts have been explored and graphene with the desired properties has been obtained. However, further work is needed to develop methods for the scaled-up preparation of high quality graphene.

The interface interactions between graphene and polymers, the transfer medium and the target substrate may have detrimental effects on its properties. Polymer and water residues during the transfer process also have a negative influence on the electrical properties of graphene. Methods aiming at reducing contaminations such as employing novel protective polymers and eliminating the use of transfer liquid have been proposed to decrease the damage to graphene. Novel strategies that maintain the structural integrity and properties of graphene are highly desired. The ideal solution is to grow graphene directly on the target substrate without the complex transfer process and introduction of undesired negative effects.

A rational design of the interfacial interactions between graphene and its support layers is also of great importance. For example, in some cases, the interaction should be strong enough to achieve better contact so that more functional groups can be introduced. However, a strong interaction often causes unwanted effects on the properties of pristine graphene. The interfacial microstructure needs to be optimized based on the systematic control of performance. Advanced techniques and analytical equipment can be used to facilitate the manipulation and more precise characterization and analysis of graphene and graphene based materials.

Acknowledgements

This work was supported by the National Natural Science Foundation of China (51372133, 51672150, 51402060, and 61229401). J.-B. Xu would like to thank the Research Grants Council of Hong Kong for its support, particularly, *via* grant no. AoE/P-03/08, 14204616, 14207515, and the CUHK Group

Research Scheme. We thank Prof. Peter Thrower for helpful discussions.

Notes and references

- 1 K. S. Novoselov, A. K. Geim, S. V. Morozov, D. Jiang, Y. Zhang, S. V. Dubonos, I. V. Grigorieva and A. A. Firsov, *Science*, 2004, **306**, 666–669.
- 2 H. P. Boehm, A. Clauss, G. O. Fischer and U. Hofmann, *Z. Naturforsch., B: Anorg. Chem., Org. Chem., Biochem., Biophys., Biol.*, 1962, **17**, 150.
- 3 E. Fitzer, K. H. Kochling, H. P. Boehm and H. Marsh, *Pure Appl. Chem.*, 1995, **67**, 473–506.
- 4 A. K. Geim and K. S. Novoselov, *Nat. Mater.*, 2007, **6**, 183–191.
- 5 A. K. Geim, *Science*, 2009, **324**, 1530–1534.
- 6 X. Li, L. Tao, Z. Chen, H. Fang, X. Li, X. Wang, J.-B. Xu and H. Zhu, *Appl. Phys. Rev.*, 2017, **4**, 021306.
- 7 F. Bonaccorso, Z. Sun, T. Hasan and A. C. Ferrari, *Nat. Photonics*, 2010, **4**, 611–622.
- 8 A. A. Balandin, *Nat. Mater.*, 2011, **10**, 569–581.
- 9 C. Lee, X. Wei, J. W. Kysar and J. Hone, *Science*, 2008, **321**, 385–388.
- 10 J. Winterlin and M. L. Bocquet, *Surf. Sci.*, 2009, **603**, 1841–1852.
- 11 M. Batzill, *Surf. Sci. Rep.*, 2012, **67**, 83–115.
- 12 X. Li and H. Zhu, *Phys. Today*, 2016, **69**, 46–51.
- 13 K. Yang, Y. Li, X. Tan, R. Peng and Z. Liu, *Small*, 2013, **9**, 1492–1503.
- 14 Y. Yang, K. Brenner and R. Murali, *Carbon*, 2012, **50**, 1727–1733.
- 15 S. Park and R. S. Ruoff, *Nat. Nano*, 2009, **4**, 217–224.
- 16 O. V. Yazyev and Y. P. Chen, *Nat. Nano*, 2014, **9**, 755–767.
- 17 X. Li, L. Colombo and R. S. Ruoff, *Adv. Mater.*, 2016, **28**, 6247–6252.
- 18 J. Kang, D. Shin, S. Bae and B. H. Hong, *Nanoscale*, 2012, **4**, 5527–5537.
- 19 A. E. Morgan and G. A. Somarjai, *Surf. Sci.*, 1968, **12**, 405–425.
- 20 J. W. May, *Surf. Sci.*, 1969, **17**, 267–270.
- 21 T. A. Land, T. Michely, R. J. Behm, J. C. Hemminger and G. Comsa, *Surf. Sci.*, 1992, **264**, 261–270.
- 22 O. Chuhei and N. Ayato, *J. Phys.: Condens. Matter*, 1997, **9**, 1–20.
- 23 N. R. Gall, E. V. Rut'kov and A. Y. Tontegode, *Int. J. Mod. Phys. B*, 1997, **11**, 1865–1911.
- 24 A. T. N'Diaye, S. Bleikamp, P. J. Feibelman and T. Michely, *Phys. Rev. Lett.*, 2006, **97**, 215501.
- 25 A. B. Preobrajenski, M. L. Ng, A. S. Vinogradov and N. Mårtensson, *Phys. Rev. B: Condens. Matter Mater. Phys.*, 2008, **78**, 073401.
- 26 E. Miniussi, M. Pozzo, A. Baraldi, E. Vesselli, R. R. Zhan, G. Comelli, T. O. Menteş, M. A. Niño, A. Locatelli, S. Lizzit and D. Alfè, *Phys. Rev. Lett.*, 2011, **106**, 216101.
- 27 T. N. D. Alpha, G. Timm, B. Carsten, M. Josef, C. Johann and M. Thomas, *New J. Phys.*, 2009, **11**, 103045.
- 28 Y. Pan, M. Gao, L. Huang, F. Liu and H.-J. Gao, *Appl. Phys. Lett.*, 2009, **95**, 093106.
- 29 E. Sutter, P. Albrecht, B. Wang, M. L. Bocquet, L. Wu, Y. Zhu and P. Sutter, *Surf. Sci.*, 2011, **605**, 1676–1684.
- 30 M. Sicot, S. Bouvron, O. Zander, U. Rüdiger, Y. S. Dedkov and M. Fonin, *Appl. Phys. Lett.*, 2010, **96**, 093115.
- 31 F. Schedin, E. Lidorikis, A. Lombardo, V. G. Kravets, A. K. Geim, A. N. Grigorenko, K. S. Novoselov and A. C. Ferrari, *ACS Nano*, 2010, **4**, 5617–5626.
- 32 W. Xu, X. Ling, J. Xiao, M. S. Dresselhaus, J. Kong, H. Xu, Z. Liu and J. Zhang, *Proc. Natl. Acad. Sci. U. S. A.*, 2012, **109**, 9281–9286.
- 33 W. Chen, X. Gui, Y. Zheng, B. Liang, Z. Lin, C. Zhao, H. Chen, Z. Chen, X. Li and Z. Tang, *Adv. Opt. Mater.*, 2017, **5**, 1600715.
- 34 J. Wu, Y. Xu, P. Xu, Z. Pan, S. Chen, Q. Shen, L. Zhan, Y. Zhang and W. Ni, *Nanoscale*, 2015, **7**, 17529–17537.
- 35 J. S. Lee, K. H. You and C. B. Park, *Adv. Mater.*, 2012, **24**, 1084–1088.
- 36 A. Tayyebi, M. Outokesh, M. Tayyebi, A. Shafikhani and S. S. Sngör, *J. Alloys Compd.*, 2016, **663**, 738–749.
- 37 S. Sonde, F. Giannazzo, V. Rainieri, R. Yakimova, J. R. Huntzinger, A. Tiberj and J. Camassel, *Phys. Rev. B: Condens. Matter Mater. Phys.*, 2009, **80**, 241406.
- 38 X. Li, H. Zhu, K. Wang, A. Cao, J. Wei, C. Li, Y. Jia, Z. Li, X. Li and D. Wu, *Adv. Mater.*, 2010, **22**, 2743–2748.
- 39 S. Tongay, M. Lemaitre, X. Miao, B. Gila, B. R. Appleton and A. F. Hebard, *Phys. Rev. X*, 2012, **2**, 011002.
- 40 K. Yan, Z. Wei, J. Li, H. Chen, Y. Yi, X. Zheng, X. Long, Z. Wang, J. Wang, J. Xu and S. Yang, *Small*, 2015, **11**, 2269–2274.
- 41 S. Tongay, M. Lemaitre, T. Schumann, K. Berke, B. R. Appleton, B. Gila and A. F. Hebard, *Appl. Phys. Lett.*, 2011, **99**, 102102.
- 42 S. Kim, T. H. Seo, M. J. Kim, K. M. Song, E. K. Suh and H. Kim, *Nano Res.*, 2015, **8**, 1327–1338.
- 43 C. C. Chen, M. Aykol, C. C. Chang, A. F. J. Levi and S. B. Cronin, *Nano Lett.*, 2011, **11**, 1863–1867.
- 44 H. Yang, J. Heo, S. Park, H. J. Song, D. H. Seo, K. E. Byun, P. Kim, I. Yoo, H. J. Chung and K. Kim, *Science*, 2012, **336**, 1140–1143.
- 45 D. Sinha and J. U. Lee, *Nano Lett.*, 2014, **14**, 4660–4664.
- 46 L. Pan, X. D. Zhu, K. N. Sun, Y.-T. Liu, X. M. Xie and X. Y. Ye, *Nano Energy*, 2016, **30**, 347–354.
- 47 R. Liu, X. C. You, X. W. Fu, F. Lin, J. Meng, D. P. Yu and Z. M. Liao, *Sci. Rep.*, 2015, **5**, 10125.
- 48 W. J. Yu, Z. Li, H. Zhou, Y. Chen, Y. Wang, Y. Huang and X. Duan, *Nat. Mater.*, 2013, **12**, 246–252.
- 49 T. Georgiou, R. Jalil, B. D. Belle, L. Britnell, R. V. Gorbachev, S. V. Morozov, Y. J. Kim, A. Gholinia, S. J. Haigh, O. Makarovskiy, L. Eaves, L. A. Ponomarenko, A. K. Geim, K. S. Novoselov and A. Mishchenko, *Nat. Nano*, 2013, **8**, 100–103.
- 50 W. Zhang, C. P. Chuu, J. K. Huang, C. H. Chen, M. L. Tsai, Y. H. Chang, C. T. Liang, Y. Z. Chen, Y. L. Chueh, J. H. He, M. Y. Chou and L. J. Li, *Sci. Rep.*, 2014, **4**, 3826.

- 51 D. De Fazio, I. Goykhman, D. Yoon, M. Bruna, A. Eiden, S. Milana, U. Sassi, M. Barbone, D. Dumcenco, K. Marinov, A. Kis and A. C. Ferrari, *ACS Nano*, 2016, **10**, 8252–8262.
- 52 K. Roy, M. Padmanabhan, S. Goswami, T. P. Sai, G. Ramalingam, S. Raghavan and A. Ghosh, *Nat. Nano*, 2013, **8**, 826–830.
- 53 L. Zhang, L. Fan, Z. Li, E. Shi, X. Li, H. Li, C. Ji, Y. Jia, J. Wei, K. Wang, H. Zhu, D. Wu and A. Cao, *Nano Res.*, 2011, **4**, 891–900.
- 54 M. Bernardi, M. Palummo and J. C. Grossman, *Nano Lett.*, 2013, **13**, 3664–3670.
- 55 L. Britnell, R. M. Ribeiro, A. Eckmann, R. Jalil, B. D. Belle, A. Mishchenko, Y. J. Kim, R. V. Gorbachev, T. Georgiou, S. V. Morozov, A. N. Grigorenko, A. K. Geim, C. Casiraghi, A. H. C. Neto and K. S. Novoselov, *Science*, 2013, **340**, 1311–1314.
- 56 W. J. Yu, Y. Liu, H. Zhou, A. Yin, Z. Li, Y. Huang and X. Duan, *Nat. Nano*, 2013, **8**, 952–958.
- 57 M. Massicotte, P. Schmidt, F. Vialla, K. G. Schädler, A. R. Planete, K. Watanabe, T. Taniguchi, K. J. Tielrooij and F. H. L. Koppens, *Nat. Nano*, 2016, **11**, 42–46.
- 58 D. Jariwala, T. J. Marks and M. C. Hersam, *Nat. Mater.*, 2017, **16**, 170–181.
- 59 Y. Liu, N. O. Weiss, X. Duan, H. C. Cheng, Y. Huang and X. Duan, *Nat. Rev. Mater.*, 2016, **1**, 16042.
- 60 A. K. Geim and I. V. Grigorieva, *Nature*, 2013, **499**, 419–425.
- 61 D. I. Son, B. W. Kwon, D. H. Park, W. S. Seo, Y. Yi, B. Angadi, C. L. Lee and W. K. Choi, *Nat. Nano*, 2012, **7**, 465–471.
- 62 X. Geng, L. Niu, Z. Xing, R. Song, G. Liu, M. Sun, G. Cheng, H. Zhong, Z. Liu, Z. Zhang, L. Sun, H. Xu, L. Lu and L. Liu, *Adv. Mater.*, 2010, **22**, 638–642.
- 63 F. Miao, S. Ruiqing, Z. Hongbing and C. Yu, *Nanotechnology*, 2010, **21**, 075601.
- 64 L. L. Li, K. P. Liu, G. H. Yang, C. M. Wang, J. R. Zhang and J. J. Zhu, *Adv. Funct. Mater.*, 2011, **21**, 869–878.
- 65 A. Cao, Z. Liu, S. Chu, M. Wu, Z. Ye, Z. Cai, Y. Chang, S. Wang, Q. Gong and Y. Liu, *Adv. Mater.*, 2010, **22**, 103–106.
- 66 C. Nethravathi, T. Nisha, N. Ravishankar, C. Shivakumara and M. Rajamathi, *Carbon*, 2009, **47**, 2054–2059.
- 67 L. Xue, C. Shen, M. Zheng, H. Lu, N. Li, G. Ji, L. Pan and J. Cao, *Mater. Lett.*, 2011, **65**, 198–200.
- 68 P. Wang, T. Jiang, C. Zhu, Y. Zhai, D. Wang and S. Dong, *Nano Res.*, 2010, **3**, 794–799.
- 69 F. Liu, X. Shao, J. Wang, S. Yang, X. Meng, X. Liu and M. Wang, *Mater. Sci. Semicond. Process.*, 2013, **16**, 429–434.
- 70 C. Zhou, Z. Wang, J. Xia, B. K. Via, F. Zhang, Y. Xia and Y. Li, *C. R. Chim.*, 2012, **15**, 714–718.
- 71 Y. T. Kim, J. H. Han, B. H. Hong and Y. U. Kwon, *Adv. Mater.*, 2010, **22**, 515–518.
- 72 G. Konstantatos, M. Badioli, L. Gaudreau, J. Osmond, M. Bernechea, F. P. G. de Arquer, F. Gatti and F. H. L. Koppens, *Nat. Nano*, 2012, **7**, 363–368.
- 73 C. X. Guo, H. B. Yang, Z. M. Sheng, Z. S. Lu, Q. L. Song and C. M. Li, *Angew. Chem., Int. Ed.*, 2010, **49**, 3014–3017.
- 74 F. X. Xiao, J. Miao and B. Liu, *J. Am. Chem. Soc.*, 2014, **136**, 1559–1569.
- 75 S. R. Forrest and M. E. Thompson, *Chem. Rev.*, 2007, **107**, 923–925.
- 76 E. H. Huisman, A. G. Shulga, P. J. Zomer, N. Tombros, D. Bartesaghi, S. Z. Bisri, M. A. Loi, L. J. A. Koster and B. J. van Wees, *ACS Appl. Mater. Interfaces*, 2015, **7**, 11083–11088.
- 77 C. J. Shih, R. Pfattner, Y. C. Chiu, N. Liu, T. Lei, D. Kong, Y. Kim, H. H. Chou, W. G. Bae and Z. Bao, *Nano Lett.*, 2015, **15**, 7587–7595.
- 78 D. He, Y. Zhang, Q. Wu, R. Xu, H. Nan, J. Liu, J. Yao, Z. Wang, S. Yuan, Y. Li, Y. Shi, J. Wang, Z. Ni, L. He, F. Miao, F. Song, H. Xu, K. Watanabe, T. Taniguchi, J.-B. Xu and X. Wang, *Nat. Commun.*, 2014, **5**, 5162.
- 79 K. Xiao, W. Deng, J. K. Keum, M. Yoon, I. V. Vlassiouk, K. W. Clark, A. P. Li, I. I. Kravchenko, G. Gu, E. A. Payzant, B. G. Sumpter, S. C. Smith, J. F. Browning and D. B. Geohegan, *J. Am. Chem. Soc.*, 2013, **135**, 3680–3687.
- 80 S. B. Jo, H. H. Kim, H. Lee, B. Kang, S. Lee, M. Sim, M. Kim, W. H. Lee and K. Cho, *ACS Nano*, 2015, **9**, 8206–8219.
- 81 J. H. Chen, C. Jang, S. Xiao, M. Ishigami and M. S. Fuhrer, *Nat. Nano*, 2008, **3**, 206–209.
- 82 S. V. Morozov, K. S. Novoselov, M. I. Katsnelson, F. Schedin, L. A. Ponomarenko, D. Jiang and A. K. Geim, *Phys. Rev. Lett.*, 2006, **97**, 016801.
- 83 M. Ishigami, J. H. Chen, W. G. Cullen, M. S. Fuhrer and E. D. Williams, *Nano Lett.*, 2007, **7**, 1643–1648.
- 84 C. H. Lui, L. Liu, K. F. Mak, G. W. Flynn and T. F. Heinz, *Nature*, 2009, **462**, 339–341.
- 85 V. E. Calado, G. F. Schneider, A. M. M. G. Theulings, C. Dekker and L. M. K. Vandersypen, *Appl. Phys. Lett.*, 2012, **101**, 103116.
- 86 P. Luxmi, J. Fisher, N. Srivastava, R. M. Feenstra, Y. Sun, J. Kedzierski, P. Healey and G. Gu, *Appl. Phys. Lett.*, 2009, **95**, 073101.
- 87 C. R. Dean, A. F. Young, I. Meric, C. Lee, L. Wang, S. Sorgenfrei, K. Watanabe, T. Taniguchi, P. Kim, K. L. Shepard and J. Hone, *Nat. Nano*, 2010, **5**, 722–726.
- 88 C. Zhang, D. Xie, J.-L. Xu, X.-M. Li, Y.-L. Sun, R.-X. Dai, X. Li and H.-W. Zhu, *J. Appl. Phys.*, 2015, **118**, 144301.
- 89 X. F. Fan, W. T. Zheng, C. Viorel, Z. X. Shen and K. Jer-Lai, *J. Phys.: Condens. Matter*, 2012, **24**, 305004.
- 90 K. Nagashio, T. Yamashita, T. Nishimura, K. Kita and A. Toriumi, *J. Appl. Phys.*, 2011, **110**, 024513.
- 91 X. Wang, J.-B. Xu, C. Wang, J. Du and W. Xie, *Adv. Mater.*, 2011, **23**, 2464–2468.
- 92 K. Chen, X. Wang, J.-B. Xu, L. Pan, X. Wang and Y. Shi, *J. Phys. Chem. C*, 2012, **116**, 6259–6267.
- 93 X. Wan, K. Chen, J. Du, D. Q. Liu, J. Chen, X. Lai, W. Xie and J.-B. Xu, *J. Phys. Chem. C*, 2013, **117**, 4800–4807.
- 94 K. Chen, X. Wan, D. Liu, Z. Kang, W. Xie, J. Chen, Q. Miao and J.-B. Xu, *Nanoscale*, 2013, **5**, 5784–5793.
- 95 X. Wan, K. Chen and J.-B. Xu, *Small*, 2014, **10**, 4443–4454.
- 96 X. Wang, J.-B. Xu, W. Xie and J. Du, *J. Phys. Chem. C*, 2011, **115**, 7596–7602.
- 97 S. Seung Min and C. Byung Jin, *Nanotechnology*, 2010, **21**, 335706.

- 98 M. K. Yakes, D. Gunlycke, J. L. Tedesco, P. M. Campbell, R. L. Myers-Ward, C. R. Eddy, D. K. Gaskill, P. E. Sheehan and A. R. Laracuente, *Nano Lett.*, 2010, **10**, 1559–1562.
- 99 D. B. Farmer, H. Y. Chiu, Y. M. Lin, K. A. Jenkins, F. Xia and P. Avouris, *Nano Lett.*, 2009, **9**, 4474–4478.
- 100 T. O. Wehling, A. I. Lichtenstein and M. I. Katsnelson, *Appl. Phys. Lett.*, 2008, **93**, 202110.
- 101 A. Pirkle, J. Chan, A. Venugopal, D. Hinojos, C. W. Magnuson, S. McDonnell, L. Colombo, E. M. Vogel, R. S. Ruoff and R. M. Wallace, *Appl. Phys. Lett.*, 2011, **99**, 122108.
- 102 W. C. Tan, W. H. Shih and Y. F. Chen, *Adv. Funct. Mater.*, 2014, **24**, 6818–6825.
- 103 Z. Chen, Z. Wang, X. Li, Y. Lin, N. Luo, M. Long, N. Zhao and J.-B. Xu, *ACS Nano*, 2017, **11**, 4507–4513.
- 104 F. Ding, H. Ji, Y. Chen, A. Herklotz, K. Dörr, Y. Mei, A. Rastelli and O. G. Schmidt, *Nano Lett.*, 2010, **10**, 3453–3458.
- 105 W. Jie, Y. Y. Hui, Y. Zhang, S. P. Lau and J. Hao, *Appl. Phys. Lett.*, 2013, **102**, 223112.
- 106 C. Y. Hsieh, Y. T. Chen, W. J. Tan, Y. F. Chen, W. Y. Shih and W. H. Shih, *Appl. Phys. Lett.*, 2012, **100**, 113507.
- 107 H. Y. Mao, Y. H. Lu, J. D. Lin, S. Zhong, A. T. S. Wee and W. Chen, *Prog. Surf. Sci.*, 2013, **88**, 132–159.
- 108 S. Bae, H. Kim, Y. Lee, X. Xu, J. S. Park, Y. Zheng, J. Balakrishnan, T. Lei, H. Ri Kim, Y. I. Song, Y. J. Kim, K. S. Kim, B. Ozilmez, J. H. Ahn, B. H. Hong and S. Iijima, *Nat. Nano*, 2010, **5**, 574–578.
- 109 X. Li, R. Zhang, W. Yu, K. Wang, J. Wei, D. Wu, A. Cao, Z. Li, Y. Cheng, Q. Zheng, R. S. Ruoff and H. Zhu, *Sci. Rep.*, 2012, **2**, 870.
- 110 T. Yang, W. Wang, H. Zhang, X. Li, J. Shi, Y. He, Q.-s. Zheng, Z. Li and H. Zhu, *ACS Nano*, 2015, **9**, 10867–10875.
- 111 T. Yang, Y. Wang, X. Li, Y. Zhang, X. Li, K. Wang, D. Wu, H. Jin, Z. Li and H. Zhu, *Nanoscale*, 2014, **6**, 13053–13059.
- 112 V. Georgakilas, J. N. Tiwari, K. C. Kemp, J. A. Perman, A. B. Bourlinos, K. S. Kim and R. Zboril, *Chem. Rev.*, 2016, **116**, 5464–5519.
- 113 R. J. Young, I. A. Kinloch, L. Gong and K. S. Novoselov, *Compos. Sci. Technol.*, 2012, **72**, 1459–1476.
- 114 S. Stankovich, R. D. Piner, X. Chen, N. Wu, S. T. Nguyen and R. S. Ruoff, *J. Mater. Chem.*, 2006, **16**, 155–158.
- 115 Y. Xu, H. Bai, G. Lu, C. Li and G. Shi, *J. Am. Chem. Soc.*, 2008, **130**, 5856–5857.
- 116 B. Q. Su, S. Pang, V. Aljani, C. Li, X. Feng and K. Müllen, *Adv. Mater.*, 2009, **21**, 3191–3195.
- 117 M. Lian, J. Fan, Z. Shi, H. Li and J. Yin, *Polymer*, 2014, **55**, 2578–2587.
- 118 C. Zhang, S. Huang, W. W. Tjiu, W. Fan and T. Liu, *J. Mater. Chem.*, 2012, **22**, 2427–2434.
- 119 C. Zhang, W. W. Tjiu, W. Fan, Z. Yang, S. Huang and T. Liu, *J. Mater. Chem.*, 2011, **21**, 18011–18017.
- 120 B. J. Liang, Y. Huang, L. Zhang, Y. Wang, Y. Ma, T. Guo and Y. Chen, *Adv. Funct. Mater.*, 2009, **19**, 2297–2302.
- 121 B. K. W. Putz, O. C. Compton, M. J. Palmeri, S. T. Nguyen and L. C. Brinson, *Adv. Funct. Mater.*, 2010, **20**, 3322–3329.
- 122 S. Stankovich, D. A. Dikin, G. H. B. Domke, K. M. Kohlhaas, E. J. Zimney, E. A. Stach, R. D. Piner, S. T. Nguyen and R. S. Ruoff, *Nature*, 2006, **442**, 282–286.
- 123 W. Li, X. Z. Tang, H. B. Zhang, H. B. Zhang, Z. G. Jiang, Z. Z. Yu, X. S. Du and Y. W. Mai, *Carbon*, 2011, **49**, 4724–4730.
- 124 W. Fan and C. Zhang, *J. Mater. Res.*, 2013, **28**, 611–619.
- 125 Y. Huang, W. Qin, Y. Zhou, H. Niu, Z. Z. Yu and J. Y. Dong, *Chem. Mater.*, 2010, **22**, 4096–4102.
- 126 M. Fang, K. Wang, H. Lu, Y. Yang and S. Nutt, *J. Mater. Chem.*, 2009, **19**, 7098–7105.
- 127 P. Sun, K. Wang and H. Zhu, *Adv. Mater.*, 2016, **28**, 2287–2310.
- 128 B. Radha, A. Esfandiar, F. C. Wang, A. P. Rooney, K. Gopinadhan, A. Keerthi, A. Mishchenko, A. Janardanan, P. Blake, L. Fumagalli, M. Lozada-Hidalgo, S. Garaj, S. J. Haigh, I. V. Grigorieva, H. A. Wu and A. K. Geim, *Nature*, 2016, **538**, 222–225.
- 129 K. Celebi, J. Buchheim, R. M. Wyss, A. Drouadian, P. Gasser, I. Shorubalko, J. I. Kye, C. Lee and H. G. Park, *Science*, 2014, **344**, 289–292.
- 130 R. R. Nair, H. A. Wu, P. N. Jayaram, I. V. Grigorieva and A. K. Geim, *Science*, 2012, **335**, 442–444.
- 131 W. Gu, W. Zhang, X. Li, H. Zhu, J. Wei, Z. Li, Q. Shu, C. Wang, K. Wang, W. Shen, F. Kang and D. Wu, *J. Mater. Chem.*, 2009, **19**, 3367–3369.
- 132 H. M. Hegab, Y. Wimalasiri, M. Ginic-Markovic and L. Zou, *Desalination*, 2015, **365**, 99–107.
- 133 M. A. Shannon, P. W. Bohn, M. Elimelech, J. G. Georgiadis, B. J. Marinas and A. M. Mayes, *Nature*, 2008, **452**, 301–310.
- 134 Z. Zeng, D. Yu, Z. He, J. Liu, F. X. Xiao, Y. Zhang, R. Wang, D. Bhattacharya and T. T. Y. Tan, *Sci. Rep.*, 2016, **6**, 20142.
- 135 S. K. Min, W. Y. Kim, Y. Cho and K. S. Kim, *Nat. Nano*, 2011, **6**, 162–165.
- 136 S. Gräslund, P. Nordlund, J. Weigelt, B. M. Hallberg, J. Bray, O. Gileadi, S. Knapp, U. Oppermann, C. Arrowsmith, R. Hui, J. Ming, S. dhe-Paganon, H. W. Park, A. Savchenko, A. Yee, A. Edwards, R. Vincentelli, C. Cambillau, R. Kim, S. H. Kim, Z. Rao, Y. Shi, T. C. Terwilliger, C. Y. Kim, L. W. Hung, G. S. Waldo, Y. Peleg, S. Albeck, T. Unger, O. Dym, J. Prilusky, J. L. Sussman, R. C. Stevens, S. A. Lesley, I. A. Wilson, A. Joachimiak, F. Collart, I. Dementieva, M. I. Donnelly, W. H. Eschenfeldt, Y. Kim, L. Stols, R. Wu, M. Zhou, S. K. Burley, J. S. Emtage, J. M. Sauder, D. Thompson, K. Bain, J. Luz, T. Gheyi, F. Zhang, S. Atwell, S. C. Almo, J. B. Bonanno, A. Fiser, S. Swaminathan, F. W. Studier, M. R. Chance, A. Sali, T. B. Acton, R. Xiao, L. Zhao, L. C. Ma, J. F. Hunt, L. Tong, K. Cunningham, M. Inouye, S. Anderson, H. Janjua, R. Shastry, C. K. Ho, D. Wang, H. Wang, M. Jiang, G. T. Montelione, D. I. Stuart, R. J. Owens, S. Daenke, A. Schütz, U. Heinemann, S. Yokoyama, K. Büßow and K. C. Gunsalus, *Nat. Meth.*, 2008, **5**, 135–146.
- 137 C. H. Lu, H. H. Yang, C. L. Zhu, X. Chen and G. N. Chen, *Angew. Chem., Int. Ed.*, 2009, **48**, 4785–4787.
- 138 M. Yan, G. Sun, F. Liu, J. Lu, J. Yu and X. Song, *Anal. Chim. Acta*, 2013, **798**, 33–39.
- 139 H. Li, F. Liu, S. Sun, J. Wang, Z. Li, D. Mu, B. Qiao and X. Peng, *J. Mater. Chem. B*, 2013, **1**, 4146–4151.

- 140 S. Gowtham, R. H. Scheicher, R. Ahuja, R. Pandey and S. P. Karna, *Phys. Rev. B: Condens. Matter Mater. Phys.*, 2007, **76**, 033401.
- 141 D. Umadevi and G. N. Sastry, *J. Phys. Chem. Lett.*, 2011, **2**, 1572–1576.
- 142 L. Cui, Z. Chen, Z. Zhu, X. Lin, X. Chen and C. J. Yang, *Anal. Chem.*, 2013, **85**, 2269–2275.
- 143 S. Panigrahi, A. Bhattacharya, S. Banerjee and D. Bhattacharyya, *J. Phys. Chem. C*, 2012, **116**, 4374–4379.
- 144 S. He, B. Song, D. Li, C. Zhu, W. Qi, Y. Wen, L. Wang, S. Song, H. Fang and C. Fan, *Adv. Funct. Mater.*, 2010, **20**, 453–459.
- 145 L. Tang, H. Chang, Y. Liu and J. Li, *Adv. Funct. Mater.*, 2012, **22**, 3083–3088.
- 146 M. Wu, R. Kempaiah, P. J. J. Huang, V. Maheshwari and J. Liu, *Langmuir*, 2011, **27**, 2731–2738.
- 147 H. Lei, L. Mi, X. Zhou, J. Chen, J. Hu, S. Guo and Y. Zhang, *Nanoscale*, 2011, **3**, 3888–3892.
- 148 G. Zuo, X. Zhou, Q. Huang, H. Fang and R. Zhou, *J. Phys. Chem. C*, 2011, **115**, 23323–23328.
- 149 P. Nguyen and V. Berry, *J. Phys. Chem. Lett.*, 2012, **3**, 1024–1029.
- 150 R. Guo, J. Mao and L. T. Yan, *Biomaterials*, 2013, **34**, 4296–4301.
- 151 A. Sasidharan, L. S. Panchakarla, P. Chandran, D. Menon, S. Nair, C. N. R. Rao and M. Koyakutty, *Nanoscale*, 2011, **3**, 2461–2464.
- 152 N. Chatterjee, H. J. Eom and J. Choi, *Biomaterials*, 2014, **35**, 1109–1127.
- 153 A. V. Titov, P. Král and R. Pearson, *ACS Nano*, 2010, **4**, 229–234.
- 154 T. S. Sreeprasad, P. Nguyen, A. Alshogeathri, L. Hibbeler, F. Martinez, N. McNeil and V. Berry, *Sci. Rep.*, 2015, **5**, 9138.
- 155 N. Mohanty and V. Berry, *Nano Lett.*, 2008, **8**, 4469–4476.
- 156 R. Frost, G. E. Jönsson, D. Chakarov, S. Svedhem and B. Kasemo, *Nano Lett.*, 2012, **12**, 3356–3362.
- 157 Y. Wang, Z. Qin, M. J. Buehler and Z. Xu, *Nat. Commun.*, 2016, **7**, 12854.
- 158 Z. Song, Y. Wang and Z. Xu, *Theor. Appl. Mech. Lett.*, 2015, **5**, 231–235.
- 159 S. Deng, E. Gao, Y. Wang, S. Sen, S. T. Sreenivasan, S. Behura, P. Král, Z. Xu and V. Berry, *ACS Nano*, 2016, **10**, 8403–8412.
- 160 R. Kempaiah, A. Chung and V. Maheshwari, *ACS Nano*, 2011, **5**, 6025–6031.
- 161 T. Cohen-Karni, Q. Qing, Q. Li, Y. Fang and C. M. Lieber, *Nano Lett.*, 2010, **10**, 1098–1102.
- 162 Q. He, H. G. Sudibya, Z. Yin, S. Wu, H. Li, F. Boey, W. Huang, P. Chen and H. Zhang, *ACS Nano*, 2010, **4**, 3201–3208.
- 163 P. K. Ang, M. Jaiswal, C. H. Y. X. Lim, Y. Wang, J. Sankaran, A. Li, C. T. Lim, T. Wohland, Ö. Barbaros and K. P. Loh, *ACS Nano*, 2010, **4**, 7387–7394.
- 164 L. H. Hess, M. Jansen, V. Maybeck, M. V. Hauf, M. Seifert, M. Stutzmann, I. D. Sharp, A. Offenhäusser and J. A. Garrido, *Adv. Mater.*, 2011, **23**, 5045–5049.
- 165 L. Yang, Y. Zhao, W. Xu, E. Shi, W. Wei, X. Li, A. Cao, Y. Cao and Y. Fang, *Nano Lett.*, 2017, **17**, 71–77.
- 166 D. Geng, B. Luo, J. Xu, Y. Guo, B. Wu, W. Hu, Y. Liu and G. Yu, *Adv. Funct. Mater.*, 2014, **24**, 1664–1670.
- 167 B. Wu, D. Geng, Z. Xu, Y. Guo, L. Huang, Y. Xue, J. Chen, G. Yu and Y. Liu, *NPG Asia Mater.*, 2013, **5**, e36.
- 168 D. Geng, L. Meng, B. Chen, E. Gao, W. Yan, H. Yan, B. Luo, J. Xu, H. Wang, Z. Mao, Z. Xu, L. He, Z. Zhang, L. Peng and G. Yu, *Adv. Mater.*, 2014, **26**, 6423–6429.
- 169 S. Y. Cho, M. S. Kim, M. Kim, K. J. Kim, H. M. Kim, D. J. Lee, S. H. Lee and K. B. Kim, *Nanoscale*, 2015, **7**, 12820–12827.
- 170 M. Zeng, L. Tan, J. Wang, L. Chen, M. H. Rümmeli and L. Fu, *Chem. Mater.*, 2014, **26**, 3637–3643.
- 171 G. Ding, Y. Zhu, S. Wang, Q. Gong, L. Sun, T. Wu, X. Xie and M. Jiang, *Carbon*, 2013, **53**, 321–326.
- 172 V. Babenko, A. T. Murdock, A. A. Koós, J. Britton, A. Crossley, P. Holdway, J. Moffat, J. Huang, J. A. Alexander-Webber, R. J. Nicholas and N. Grobert, *Nat. Commun.*, 2015, **6**, 7536.
- 173 G. Kalon, Y. J. Shin and H. Yang, *Appl. Phys. Lett.*, 2011, **98**, 233108.
- 174 J. Yin, X. Li, J. Yu, Z. Zhang, J. Zhou and W. Guo, *Nat. Nano*, 2014, **9**, 378–383.
- 175 Y. He, J. Lao, T. Yang, X. Li, X. Zang, X. Li, M. Zhu, Q. Chen, M. Zhong and H. Zhu, *Appl. Phys. Lett.*, 2015, **107**, 081605.
- 176 G. Xue, Y. Xu, T. Ding, J. Li, J. Yin, W. Fei, Y. Cao, J. Yu, L. Yuan, L. Gong, J. Chen, S. Deng, J. Zhou and W. Guo, *Nat. Nano*, 2017, **12**, 317–321.
- 177 Y. J. Shin, Y. Wang, H. Huang, G. Kalon, A. T. S. Wee, Z. Shen, C. S. Bhatia and H. Yang, *Langmuir*, 2010, **26**, 3798–3802.
- 178 S. Wang, Y. Zhang, N. Abidi and L. Cabrales, *Langmuir*, 2009, **25**, 11078–11081.
- 179 H. Zhou, P. Ganesh, V. Presser, M. C. F. Wander, P. Fenter, P. R. C. Kent, D. E. Jiang, A. A. Chialvo, J. McDonough, K. L. Shuford and Y. Gogotsi, *Phys. Rev. B: Condens. Matter Mater. Phys.*, 2012, **85**, 035406.
- 180 J. Rafiee, X. Mi, H. Gullapalli, A. V. Thomas, F. Yavari, Y. Shi, P. M. Ajayan and N. A. Koratkar, *Nat. Mater.*, 2012, **11**, 217–222.
- 181 K. Xu, P. Cao and J. R. Heath, *Science*, 2010, **329**, 1188–1191.
- 182 P. Cao, K. Xu, J. O. Varghese and J. R. Heath, *Nano Lett.*, 2011, **11**, 5581–5586.
- 183 J. Shim, C. H. Lui, T. Y. Ko, Y. J. Yu, P. Kim, T. F. Heinz and S. Ryu, *Nano Lett.*, 2012, **12**, 648–654.
- 184 P. Sun, H. Liu, K. Wang, M. Zhong, D. Wu and H. Zhu, *Chem. Commun.*, 2015, **51**, 3251–3254.
- 185 P. Sun, M. Zhu, K. Wang, M. Zhong, J. Wei, D. Wu, Z. Xu and H. Zhu, *ACS Nano*, 2013, **7**, 428–437.
- 186 R. S. Edwards and K. S. Coleman, *Acc. Chem. Res.*, 2013, **46**, 23–30.
- 187 Z. Yan, Z. Peng, Z. Sun, J. Yao, Y. Zhu, Z. Liu, P. M. Ajayan and J. M. Tour, *ACS Nano*, 2011, **5**, 8187–8192.
- 188 Z. Peng, Z. Yan, Z. Sun and J. M. Tour, *ACS Nano*, 2011, **5**, 8241–8247.
- 189 C. Y. Su, A. Y. Lu, C. Y. Wu, Y. T. Li, K. K. Liu, W. Zhang, S. Y. Lin, Z. Y. Juang, Y. L. Zhong, F. R. Chen and L. J. Li, *Nano Lett.*, 2011, **11**, 3612–3616.

- 190 A. Ismach, C. Druzgalski, S. Penwell, A. Schwartzberg, M. Zheng, A. Javey, J. Bokor and Y. Zhang, *Nano Lett.*, 2010, **10**, 1542–1548.
- 191 K. S. Kim, Y. Zhao, H. Jang, S. Y. Lee, J. M. Kim, K. S. Kim, J. H. Ahn, P. Kim, J. Y. Choi and B. H. Hong, *Nature*, 2009, **457**, 706–710.
- 192 X. Li, W. Cai, J. An, S. Kim, J. Nah, D. Yang, R. Piner, A. Velamakanni, I. Jung, E. Tutuc, S. K. Banerjee, L. Colombo and R. S. Ruoff, *Science*, 2009, **324**, 1312–1314.
- 193 L. Li, X. Li, M. Du, Y. Guo, Y. Li, H. Li, Y. Yang, F. E. Alam, C.-T. Lin and Y. Fang, *Chem. Mater.*, 2016, **28**, 3360–3366.
- 194 X. Wan, K. Chen, D. Liu, J. Chen, Q. Miao and J.-B. Xu, *Chem. Mater.*, 2012, **24**, 3906–3915.
- 195 Y. Hao, M. S. Bharathi, L. Wang, Y. Liu, H. Chen, S. Nie, X. Wang, H. Chou, C. Tan, B. Fallahazad, H. Ramanarayanan, C. W. Magnuson, E. Tutuc, B. I. Yakobson, K. F. McCarty, Y.-W. Zhang, P. Kim, J. Hone, L. Colombo and R. S. Ruoff, *Science*, 2013, **342**, 720–723.
- 196 S. Nie, J. M. Wofford, N. C. Bartelt, O. D. Dubon and K. F. McCarty, *Phys. Rev. B: Condens. Matter Mater. Phys.*, 2011, **84**, 155425.
- 197 Z. Luo, S. Kim, N. Kawamoto, A. M. Rappe and A. T. C. Johnson, *ACS Nano*, 2011, **5**, 9154–9160.
- 198 L. Zhao, K. T. Rim, H. Zhou, R. He, T. F. Heinz, A. Pinczuk, G. W. Flynn and A. N. Pasupathy, *Solid State Commun.*, 2011, **151**, 509–513.
- 199 E. Sutter, P. Albrecht and P. Sutter, *Appl. Phys. Lett.*, 2009, **95**, 133109.
- 200 Y. Murata, V. Petrova, B. B. Kappes, A. Ebnonnasir, I. Petrov, Y. H. Xie, C. V. Ciobanu and S. Kodambaka, *ACS Nano*, 2010, **4**, 6509–6514.
- 201 B. Zhang, W. H. Lee, R. Piner, I. Kholmanov, Y. Wu, H. Li, H. Ji and R. S. Ruoff, *ACS Nano*, 2012, **6**, 2471–2476.
- 202 M. H. Griep, E. Sandoz-Rosado, T. M. Tumlin and E. Wetzel, *Nano Lett.*, 2016, **16**, 1657–1662.
- 203 Z. Luo, Y. Lu, D. W. Singer, M. E. Berck, L. A. Somers, B. R. Goldsmith and A. T. C. Johnson, *Chem. Mater.*, 2011, **23**, 1441–1447.
- 204 X. Liu, L. Fu, N. Liu, T. Gao, Y. Zhang, L. Liao and Z. Liu, *J. Phys. Chem. C*, 2011, **115**, 11976–11982.
- 205 B. Dai, L. Fu, Z. Zou, M. Wang, H. Xu, S. Wang and Z. Liu, *Nat. Commun.*, 2011, **2**, 522.
- 206 D. Kondo, K. Yagi, M. Sato, M. Nihei, Y. Awano, S. Sato and N. Yokoyama, *Chem. Phys. Lett.*, 2011, **514**, 294–300.
- 207 M. E. Ramón, A. Gupta, C. Corbet, D. A. Ferrer, H. C. P. Mowva, G. Carpenter, L. Colombo, G. Bourianoff, M. Doczy, D. Akinwande, E. Tutuc and S. K. Banerjee, *ACS Nano*, 2011, **5**, 7198–7204.
- 208 T. Oznuluer, E. Pince, E. O. Polat, O. Balci, O. Salihoglu and C. Kocabas, *Appl. Phys. Lett.*, 2011, **98**, 183101.
- 209 J. H. Lee, E. K. Lee, W. J. Joo, Y. Jang, B. S. Kim, J. Y. Lim, S. H. Choi, S. J. Ahn, J. R. Ahn, M. H. Park, C. W. Yang, B. L. Choi, S. W. Hwang and D. Whang, *Science*, 2014, **344**, 286–289.
- 210 P. Y. Teng, C. C. Lu, K. Akiyama-Hasegawa, Y. C. Lin, C. H. Yeh, K. Suenaga and P. W. Chiu, *Nano Lett.*, 2012, **12**, 1379–1384.
- 211 H. Kim, I. Song, C. Park, M. Son, M. Hong, Y. Kim, J. S. Kim, H. J. Shin, J. Baik and H. C. Choi, *ACS Nano*, 2013, **7**, 6575–6582.
- 212 A. Bachmatiuk, F. Börrnert, M. Grobosch, F. Schäffel, U. Wolff, A. Scott, M. Zaka, J. H. Warner, R. Klingeler, M. Knupfer, B. Büchner and M. H. Rümmeli, *ACS Nano*, 2009, **3**, 4098–4104.
- 213 G. Hong, Q. H. Wu, J. Ren and S. T. Lee, *Appl. Phys. Lett.*, 2012, **100**, 231604.
- 214 G. Yazdi, T. Iakimov and R. Yakimova, *Crystals*, 2016, **6**, 53.
- 215 G. R. Yazdi, R. Vasiliauskas, T. Iakimov, A. Zakharov, M. Syväjärvi and R. Yakimova, *Carbon*, 2013, **57**, 477–484.
- 216 A. Mattausch and O. Pankratov, *Phys. Rev. Lett.*, 2007, **99**, 076802.
- 217 J. B. Hannon, M. Copel and R. M. Tromp, *Phys. Rev. Lett.*, 2011, **107**, 166101.
- 218 C. Virojanadara, A. A. Zakharov, R. Yakimova and L. I. Johansson, *Surf. Sci.*, 2010, **604**, L4–L7.
- 219 J. Borysiuk, R. Bożek, K. Grodecki, A. Wysmolek, W. Strupiński, R. Stępniewski and J. M. Baranowski, *J. Appl. Phys.*, 2010, **108**, 013518.
- 220 B. K. Daas, S. U. Omar, S. Shetu, K. M. Daniels, S. Ma, T. S. Sudarshan and M. V. S. Chandrashekhar, *Cryst. Growth Des.*, 2012, **12**, 3379–3387.
- 221 G. F. Sun, J. F. Jia, Q. K. Xue and L. Li, *Nanotechnology*, 2009, **20**, 355701.
- 222 C. Virojanadara, R. Yakimova, J. R. Osiecki, M. Syväjärvi, R. I. G. Uhrberg, L. I. Johansson and A. A. Zakharov, *Surf. Sci.*, 2009, **603**, L87–L90.
- 223 J. Hwang, M. Kim, D. Campbell, H. A. Alsalman, J. Y. Kwak, S. Shivaraman, A. R. Woll, A. K. Singh, R. G. Hennig, S. Gorantla, M. H. Rümmeli and M. G. Spencer, *ACS Nano*, 2013, **7**, 385–395.
- 224 K. Saito and T. Ogino, *J. Phys. Chem. C*, 2014, **118**, 5523–5529.
- 225 H. J. Song, M. Son, C. Park, H. Lim, M. P. Levendorf, A. W. Tsen, J. Park and H. C. Choi, *Nanoscale*, 2012, **4**, 3050–3054.
- 226 J. M. Garcia, et al., *Solid State Commun.*, 2012, **152**, 975–978.
- 227 W. Yang, et al., *Nat. Mater.*, 2013, **12**, 792–797.
- 228 X. Chen, B. Wu and Y. Liu, *Chem. Soc. Rev.*, 2016, **45**, 2057–2074.
- 229 B. N. Chandrashekhar, B. Deng, A. S. Smitha, Y. Chen, C. Tan, H. Zhang, H. Peng and Z. Liu, *Adv. Mater.*, 2015, **27**, 5210–5216.
- 230 J. Song, F. Y. Kam, R. Q. Png, W. L. Seah, J. M. Zhuo, G. K. Lim, P. K. H. Ho and L. L. Chua, *Nat. Nano*, 2013, **8**, 356–362.
- 231 H. H. Kim, B. Kang, J. W. Suk, N. Li, K. S. Kim, R. S. Ruoff, W. H. Lee and K. Cho, *ACS Nano*, 2015, **9**, 4726–4733.
- 232 Y. C. Lin, C. Jin, J. C. Lee, S. F. Jen, K. Suenaga and P. W. Chiu, *ACS Nano*, 2011, **5**, 2362–2368.
- 233 J. Y. Hong, Y. C. Shin, A. Zubair, Y. Mao, T. Palacios, M. S. Dresselhaus, S. H. Kim and J. Kong, *Adv. Mater.*, 2016, **28**, 2382–2392.

- 234 J. W. Suk, W. H. Lee, J. Lee, H. Chou, R. D. Piner, Y. Hao, D. Akinwande and R. S. Ruoff, *Nano Lett.*, 2013, **13**, 1462–1467.
- 235 H. H. Kim, J. W. Yang, S. B. Jo, B. Kang, S. K. Lee, H. Bong, G. Lee, K. S. Kim and K. Cho, *ACS Nano*, 2013, **7**, 1155–1162.
- 236 J. W. Suk, A. Kitt, C. W. Magnuson, Y. Hao, S. Ahmed, J. An, A. K. Swan, B. B. Goldberg and R. S. Ruoff, *ACS Nano*, 2011, **5**, 6916–6924.
- 237 S. A. Svatek, O. R. Scott, J. P. H. Rivett, K. Wright, M. Baldoni, E. Bichoutskaia, T. Taniguchi, K. Watanabe, A. J. Marsden, N. R. Wilson and P. H. Beton, *Nano Lett.*, 2015, **15**, 159–164.
- 238 Z. Li, Y. Wang, A. Kozbial, G. Shenoy, F. Zhou, R. McGinley, P. Ireland, B. Morganstein, A. Kunkel, S. P. Surwade, L. Li and H. Liu, *Nat. Mater.*, 2013, **12**, 925–931.
- 239 Y. Su, H. L. Han, Q. Cai, Q. Wu, M. Xie, D. Chen, B. Geng, Y. Zhang, F. Wang, Y. R. Shen and C. Tian, *Nano Lett.*, 2015, **15**, 6501–6505.
- 240 G. Zhang, A. G. Güell, P. M. Kirkman, R. A. Lazenby, T. S. Miller and P. R. Unwin, *ACS Appl. Mater. Interfaces*, 2016, **8**, 8008–8016.
- 241 P. S. Toth, Q. M. Ramasse, M. Velicky and R. A. W. Dryfe, *Chem. Sci.*, 2015, **6**, 1316–1323.
- 242 H. H. Kim, S. K. Lee, S. G. Lee, E. Lee and K. Cho, *Adv. Funct. Mater.*, 2016, **26**, 2070–2077.
- 243 S. J. Kim, T. Choi, B. Lee, S. Lee, K. Choi, J. B. Park, J. M. Yoo, Y. S. Choi, J. Ryu, P. Kim, J. Hone and B. H. Hong, *Nano Lett.*, 2015, **15**, 3236–3240.
- 244 T. Yoon, W. C. Shin, T. Y. Kim, J. H. Mun, T.-S. Kim and B. J. Cho, *Nano Lett.*, 2012, **12**, 1448–1452.
- 245 Y. Wang, Y. Zheng, X. Xu, E. Dubuisson, Q. Bao, J. Lu and K. P. Loh, *ACS Nano*, 2011, **5**, 9927–9933.
- 246 L. Gao, W. Ren, H. Xu, L. Jin, Z. Wang, T. Ma, L. P. Ma, Z. Zhang, Q. Fu, L. M. Peng, X. Bao and H. M. Cheng, *Nat. Commun.*, 2012, **3**, 699.
- 247 C. J. L. d. I. Rosa, N. Lindvall, M. T. Cole, Y. Nam, M. Löfller, E. Olsson and A. Yurgens, *Appl. Phys. Lett.*, 2013, **102**, 022101.
- 248 C. T. Cherian, F. Giustiniano, I. Martin-Fernandez, H. Andersen, J. Balakrishnan and B. Özilmez, *Small*, 2015, **11**, 189–194.
- 249 S. R. Na, J. W. Suk, L. Tao, D. Akinwande, R. S. Ruoff, R. Huang and K. M. Liechti, *ACS Nano*, 2015, **9**, 1325–1335.
- 250 E. H. Lock, M. Baraket, M. Laskoski, S. P. Mulvaney, W. K. Lee, P. E. Sheehan, D. R. Hines, J. T. Robinson, J. Tosado, M. S. Fuhrer, S. C. Hernández and S. G. Walton, *Nano Lett.*, 2012, **12**, 102–107.
- 251 W. Regan, N. Alem, B. Alemán, B. Geng, Ç. Girit, L. Maserati, F. Wang, M. Crommie and A. Zettl, *Appl. Phys. Lett.*, 2010, **96**, 113102.
- 252 W. H. Lin, T. H. Chen, J. K. Chang, J. I. Taur, Y. Y. Lo, W. L. Lee, C. S. Chang, W. B. Su and C. I. Wu, *ACS Nano*, 2014, **8**, 1784–1791.
- 253 D. Y. Wang, I. S. Huang, P. H. Ho, S. S. Li, Y. C. Yeh, D. W. Wang, W. L. Chen, Y. Y. Lee, Y. M. Chang, C. C. Chen, C. T. Liang and C. W. Chen, *Adv. Mater.*, 2013, **25**, 4521–4526.
- 254 X. An, F. Liu, Y. J. Jung and S. Kar, *Nano Lett.*, 2013, **13**, 909–916.
- 255 F. H. L. Koppens, T. Mueller, P. Avouris, A. C. Ferrari, M. S. Vitiello and M. Polini, *Nat. Nano*, 2014, **9**, 780–793.
- 256 M. Zhu, X. Li, S. Chung, L. Zhao, X. Li, X. Zang, K. Wang, J. Wei, M. Zhong, K. Zhou, D. Xie and H. Zhu, *Carbon*, 2015, **84**, 138–145.
- 257 H. Y. Kim, K. Lee, N. McEvoy, C. Yim and G. S. Duesberg, *Nano Lett.*, 2013, **13**, 2182–2188.
- 258 A. Singh, M. A. Uddin, T. Sudarshan and G. Koley, *Small*, 2014, **10**, 1555–1565.
- 259 S. L. Li, K. Tsukagoshi, E. Orgiu and P. Samori, *Chem. Soc. Rev.*, 2016, **45**, 118–151.
- 260 X. Li, Z. Lv and H. Zhu, *Adv. Mater.*, 2015, **27**, 6549–6574.
- 261 X. Li, D. Xie, H. Park, M. Zhu, T. H. Zeng, K. Wang, J. Wei, D. Wu, J. Kong and H. Zhu, *Nanoscale*, 2013, **5**, 1945–1948.
- 262 Y. Lin, X. Li, D. Xie, T. Feng, Y. Chen, R. Song, H. Tian, T. Ren, M. Zhong, K. Wang and H. Zhu, *Energy Environ. Sci.*, 2013, **6**, 108–115.
- 263 X. Li, D. Xie, H. Park, T. H. Zeng, K. Wang, J. Wei, M. Zhong, D. Wu, J. Kong and H. Zhu, *Adv. Energy Mater.*, 2013, **3**, 1029–1034.
- 264 X. Miao, S. Tongay, M. K. Petterson, K. Berke, A. G. Rinzler, B. R. Appleton and A. F. Hebard, *Nano Lett.*, 2012, **12**, 2745–2750.
- 265 T. Cui, R. Lv, Z. H. Huang, S. Chen, Z. Zhang, X. Gan, Y. Jia, X. Li, K. Wang, D. Wu and F. Kang, *J. Mater. Chem. A*, 2013, **1**, 5736–5740.
- 266 Z. Kang, X. Tan, X. Li, T. Xiao, L. Zhang, J. Lao, X. Li, S. Cheng, D. Xie and H. Zhu, *Phys. Chem. Chem. Phys.*, 2016, **18**, 1992–1997.
- 267 G. Fan, H. Zhu, K. Wang, J. Wei, X. Li, Q. Shu, N. Guo and D. Wu, *ACS Appl. Mater. Interfaces*, 2011, **3**, 721–725.
- 268 X. Li, X. Zang, X. Li, M. Zhu, Q. Chen, K. Wang, M. Zhong, J. Wei, D. Wu and H. Zhu, *Adv. Energy Mater.*, 2014, **4**, 1400224.
- 269 C. Xie, X. Zhang, Y. Wu, X. Zhang, X. Zhang, Y. Wang, W. Zhang, P. Gao, Y. Han and J. Jie, *J. Mater. Chem. A*, 2013, **1**, 8567–8574.
- 270 X. Zhang, C. Xie, J. Jie, X. Zhang, Y. Wu and W. Zhang, *J. Mater. Chem. A*, 2013, **1**, 6593–6601.
- 271 L. Yang, X. Yu, M. Xu, H. Chen and D. Yang, *J. Mater. Chem. A*, 2014, **2**, 16877–16883.
- 272 K. Jiao, X. Wang, Y. Wang and Y. Chen, *J. Mater. Chem. C*, 2014, **2**, 7715–7721.
- 273 M. Zhong, D. Xu, X. Yu, K. Huang, X. Liu, Y. Qu, Y. Xu and D. Yang, *Nano Energy*, 2016, **28**, 12–18.
- 274 Y. Song, X. Li, C. Mackin, X. Zhang, W. Fang, T. Palacios, H. Zhu and J. Kong, *Nano Lett.*, 2015, **15**, 2104–2110.
- 275 E. Shi, H. Li, L. Yang, L. Zhang, Z. Li, P. Li, Y. Shang, S. Wu, X. Li, J. Wei, K. Wang, H. Zhu, D. Wu, Y. Fang and A. Cao, *Nano Lett.*, 2013, **13**, 1776–1781.
- 276 M. Zhu, X. Li, Y. Guo, X. Li, P. Sun, X. Zang, K. Wang, M. Zhong, D. Wu and H. Zhu, *Nanoscale*, 2014, **6**, 4909–4914.
- 277 X. Wang, Z. Cheng, K. Xu, H. K. Tsang and J.-B. Xu, *Nat. Photonics*, 2013, **7**, 888–891.

- 278 X. M. Li, M. Zhu, M. D. Du, Z. Lv, L. Zhang, Y. C. Li, Y. Yang, T. T. Yang, X. Li, K. L. Wang, H. W. Zhu and Y. Fang, *Small*, 2016, **16**, 595–601.
- 279 R. Lu, C. W. Ge, Y. F. Zou, K. Zheng, D. D. Wang, T. F. Zhang and L. B. Luo, *Laser Photonics Rev.*, 2016, **10**, 595–602.
- 280 L. B. Luo, H. Hu, X.-H. Wang, R. Lu, Y. F. Zou, Y. Q. Yu and F. X. Liang, *J. Mater. Chem. C*, 2015, **3**, 4723–4728.
- 281 X. Li, S. Lin, X. Lin, Z. Xu, P. Wang, S. Zhang, H. Zhong, W. Xu, Z. Wu and W. Fang, *Opt. Express*, 2016, **24**, 134–145.
- 282 A. V. Babichev, H. Zhang, P. Lavenus, F. H. Julien, A. Y. Egorov, Y. T. Lin, L. W. Tu and M. Tchernycheva, *Appl. Phys. Lett.*, 2013, **103**, 201103.
- 283 F. Lin, S. W. Chen, J. Meng, G. Tse, X. W. Fu, F. J. Xu, B. Shen, Z. M. Liao and D. P. Yu, *Appl. Phys. Lett.*, 2014, **105**, 073103.
- 284 V. Q. Dang, T. Q. Trung, D. I. Kim, L. T. Duy, B. U. Hwang, D.-W. Lee, B. Y. Kim, L. D. Toan and N.-E. Lee, *Small*, 2015, **11**, 3054–3065.
- 285 Z. Chen, X. Li, J. Wang, L. Tao, M. Long, S. J. Liang, L. K. Ang, C. Shu, H. K. Tsang and J.-B. Xu, *ACS Nano*, 2017, **11**, 430–437.
- 286 C. H. Liu, Y. C. Chang, T. B. Norris and Z. Zhong, *Nat. Nano*, 2014, **9**, 273–278.
- 287 Z. Chen, Z. Cheng, J. Wang, X. Wan, C. Shu, H. K. Tsang, H. P. Ho and J.-B. Xu, *Adv. Opt. Mater.*, 2015, **3**, 1207–1214.
- 288 D. H. Shin, S. Kim, J. M. Kim, C. W. Jang, J. H. Kim, K. W. Lee, J. Kim, S. D. Oh, D. H. Lee, S. S. Kang, C. O. Kim, S. H. Choi and K. J. Kim, *Adv. Mater.*, 2015, **27**, 2614–2620.
- 289 I. Nikitskiy, S. Goossens, D. Kufer, T. Lasanta, G. Navickaitė, F. H. L. Koppens and G. Konstantatos, *Nat. Commun.*, 2016, **7**, 11954.
- 290 M. Zhu, L. Zhang, X. Li, Y. He, X. Li, F. Guo, X. Zang, K. Wang, D. Xie, X. Li, B. Wei and H. Zhu, *J. Mater. Chem. A*, 2015, **3**, 8133–8138.
- 291 T. Yu, F. Wang, Y. Xu, L. Ma, X. Pi and D. Yang, *Adv. Mater.*, 2016, **28**, 4912–4919.
- 292 Q. J. Xiang, J. G. Yu and M. Jaroniec, *Chem. Soc. Rev.*, 2012, **41**, 782–796.
- 293 L. L. Tan, S. P. Chai and A. R. Mohamed, *ChemSusChem*, 2012, **5**, 1868–1882.
- 294 B. Xia, Y. Yan, X. Wang and X. W. Lou, *Mater. Horiz.*, 2014, **1**, 379–399.
- 295 D. Deng, K. S. Novoselov, Q. Fu, N. Zheng, Z. Tian and X. Bao, *Nat. Nano*, 2016, **11**, 218–230.
- 296 K. Nakada, M. Fujita, G. Dresselhaus and M. S. Dresselhaus, *Phys. Rev. B: Condens. Matter Mater. Phys.*, 1996, **54**, 17954–17961.
- 297 D. E. Jiang, B. G. Sumpter and S. Dai, *J. Chem. Phys.*, 2007, **126**, 134701.
- 298 D. Deng, L. Yu, X. Pan, S. Wang, X. Chen, P. Hu, L. Sun and X. Bao, *Chem. Commun.*, 2011, **47**, 10016–10018.
- 299 A. Shen, Y. Zou, Q. Wang, R. A. W. Dryfe, X. Huang, S. Dou, L. Dai and S. Wang, *Angew. Chem., Int. Ed.*, 2014, **53**, 10804–10808.
- 300 H. Jin, H. Huang, Y. He, X. Feng, S. Wang, L. Dai and J. Wang, *J. Am. Chem. Soc.*, 2015, **137**, 7588–7591.
- 301 Y. Jia, L. Zhang, A. Du, G. Gao, J. Chen, X. Yan, C. L. Brown and X. Yao, *Adv. Mater.*, 2016, **28**, 9532–9538.
- 302 J. Duan, S. Chen, M. Jaroniec and S. Z. Qiao, *ACS Catal.*, 2015, **5**, 5207–5234.
- 303 H. Cui, Z. Zhou and D. Jia, *Mater. Horiz.*, 2017, **4**, 7–19.
- 304 L. Qu, Y. Liu, J. B. Baek and L. Dai, *ACS Nano*, 2010, **4**, 1321–1326.
- 305 Z. Yang, Z. Yao, G. Li, G. Fang, H. Nie, Z. Liu, X. Zhou, X. a. Chen and S. Huang, *ACS Nano*, 2012, **6**, 205–211.
- 306 Z. H. Sheng, H. L. Gao, W. J. Bao, F. B. Wang and X. H. Xia, *J. Mater. Chem.*, 2012, **22**, 390–395.
- 307 Z. W. Liu, F. Peng, H. J. Wang, H. Yu, W. X. Zheng and J. Yang, *Angew. Chem.*, 2011, **123**, 3315–3319.
- 308 Z. Yao, H. Nie, Z. Yang, X. Zhou, Z. Liu and S. Huang, *Chem. Commun.*, 2012, **48**, 1027–1029.
- 309 Y. Okamoto, *Appl. Surf. Sci.*, 2009, **256**, 335–341.
- 310 L. Zhang and Z. Xia, *J. Phys. Chem. C*, 2011, **115**, 11170–11176.
- 311 L. Zhang, J. Niu, L. Dai and Z. Xia, *Langmuir*, 2012, **28**, 7542–7550.
- 312 L. Yu, X. Pan, X. Cao, P. Hu and X. Bao, *J. Catal.*, 2011, **282**, 183–190.
- 313 D. Deng, X. Pan, L. Yu, Y. Cui, Y. Jiang, J. Qi, W. X. Li, Q. Fu, X. Ma, Q. Xue, G. Sun and X. Bao, *Chem. Mater.*, 2011, **23**, 1188–1193.
- 314 D. Guo, R. Shibuya, C. Akiba, S. Saji, T. Kondo and J. Nakamura, *Science*, 2016, **351**, 361–365.
- 315 D. Usachov, O. Vilkov, A. Grüneis, D. Haberer, A. Fedorov, V. K. Adamchuk, A. B. Preobrajenski, P. Dudin, A. Barinov, M. Oehzelt, C. Laubschat and D. V. Vyalikh, *Nano Lett.*, 2011, **11**, 5401–5407.
- 316 J. Masa, W. Xia, M. Muhler and W. Schuhmann, *Angew. Chem., Int. Ed.*, 2015, **54**, 10102–10120.
- 317 Y. Jiang, L. Yang, T. Sun, J. Zhao, Z. Lyu, O. Zhuo, X. Wang, Q. Wu, J. Ma and Z. Hu, *ACS Catal.*, 2015, **5**, 6707–6712.
- 318 J. Masa, A. Zhao, W. Xia, Z. Sun, B. Mei, M. Muhler and W. Schuhmann, *Electrochem. Commun.*, 2013, **34**, 113–116.
- 319 Y. Feng, F. Li, Z. Hu, X. Luo, L. Zhang, X. F. Zhou, H. T. Wang, J. J. Xu and E. G. Wang, *Phys. Rev. B: Condens. Matter Mater. Phys.*, 2012, **85**, 155454.
- 320 S. F. Huang, K. Terakura, T. Ozaki, T. Ikeda, M. Boero, M. Oshima, J. i. Ozaki and S. Miyata, *Phys. Rev. B: Condens. Matter Mater. Phys.*, 2009, **80**, 235410.
- 321 S. Wang, L. Zhang, Z. Xia, A. Roy, D. W. Chang, J.-B. Baek and L. Dai, *Angew. Chem., Int. Ed.*, 2012, **51**, 4209–4212.
- 322 Y. Zheng, Y. Jiao, L. Ge, M. Jaroniec and S. Z. Qiao, *Angew. Chem.*, 2013, **125**, 3192–3198.
- 323 J. Liang, Y. Jiao, M. Jaroniec and S. Z. Qiao, *Angew. Chem., Int. Ed.*, 2012, **51**, 11496–11500.
- 324 J. Xu, G. Dong, C. Jin, M. Huang and L. Guan, *ChemSusChem*, 2013, **6**, 493–499.
- 325 C. H. Choi, M. W. Chung, H. C. Kwon, S. H. Park and S. I. Woo, *J. Mater. Chem. A*, 2013, **1**, 3694–3699.
- 326 G. Wu and P. Zelenay, *Acc. Chem. Res.*, 2013, **46**, 1878–1889.
- 327 D. Deng, X. Chen, L. Yu, X. Wu, Q. Liu, Y. Liu, H. Yang, H. Tian, Y. Hu, P. Du, R. Si, J. Wang, X. Cui, H. Li, J. Xiao, T. Xu, J. Deng, F. Yang, P. N. Duchesne, P. Zhang, J. Zhou, L. Sun, J. Li, X. Pan and X. Bao, *Sci. Adv.*, 2015, **1**, e1500462.

- 328 Y. Li, W. Zhou, H. Wang, L. Xie, Y. Liang, F. Wei, J. C. Idrobo, S. J. Pennycook and H. Dai, *Nat. Nano.*, 2012, **7**, 394–400.
- 329 K. Parvez, S. Yang, Y. Hernandez, A. Winter, A. Turchanin, X. Feng and K. Müllen, *ACS Nano*, 2012, **6**, 9541–9550.
- 330 F. Calle-Vallejo, J. I. Martinez and J. Rossmeisl, *Phys. Chem. Chem. Phys.*, 2011, **13**, 15639–15643.
- 331 Y. Okamoto, *Chem. Phys. Lett.*, 2006, **420**, 382–386.
- 332 M. N. Groves, A. S. W. Chan, C. Malardier-Jugroot and M. Jugroot, *Chem. Phys. Lett.*, 2009, **481**, 214–219.
- 333 I. Fampiou and A. Ramasubramaniam, *J. Phys. Chem. C*, 2012, **116**, 6543–6555.
- 334 Y. Tang, Z. Yang and X. Dai, *Phys. Chem. Chem. Phys.*, 2012, **14**, 16566–16572.
- 335 X. Liu, C. Meng and Y. Han, *J. Phys. Chem. C*, 2013, **117**, 1350–1357.
- 336 D.-H. Lim and J. Wilcox, *J. Phys. Chem. C*, 2011, **115**, 22742–22747.
- 337 M. Zhou, A. Zhang, Z. Dai, C. Zhang and Y. P. Feng, *J. Chem. Phys.*, 2010, **132**, 194704.
- 338 S. Zhang, Y. Shao, H.-g. Liao, J. Liu, I. A. Aksay, G. Yin and Y. Lin, *Chem. Mater.*, 2011, **23**, 1079–1081.
- 339 X. Chen, G. Wu, J. Chen, X. Chen, Z. Xie and X. Wang, *J. Am. Chem. Soc.*, 2011, **133**, 3693–3695.
- 340 H. Yin, H. Tang, D. Wang, Y. Gao and Z. Tang, *ACS Nano*, 2012, **6**, 8288–8297.
- 341 S. Guo and S. Sun, *J. Am. Chem. Soc.*, 2012, **134**, 2492–2495.
- 342 M. Liu, R. Zhang and W. Chen, *Chem. Rev.*, 2014, **114**, 5117–5160.
- 343 D. Higgins, P. Zamani, A. Yu and Z. Chen, *Energy Environ. Sci.*, 2016, **9**, 357–390.
- 344 S. Guo, S. Zhang and S. Sun, *Angew. Chem., Int. Ed.*, 2013, **52**, 8526–8544.
- 345 L. Dong, R. R. S. Gari, Z. Li, M. M. Craig and S. Hou, *Carbon*, 2010, **48**, 781–787.
- 346 Z.-S. Wu, S. Yang, Y. Sun, K. Parvez, X. Feng and K. Müllen, *J. Am. Chem. Soc.*, 2012, **134**, 9082–9085.
- 347 Y. Hu, J. O. Jensen, W. Zhang, Y. Huang, L. N. Cleemann, W. Xing, N. J. Bjerrum and Q. Li, *ChemSusChem*, 2014, **7**, 2099–2103.
- 348 Y. Liang, Y. Li, H. Wang, J. Zhou, J. Wang, T. Regier and H. Dai, *Nat. Mater.*, 2011, **10**, 780–786.
- 349 Y. Li, H. Wang, L. Xie, Y. Liang, G. Hong and H. Dai, *J. Am. Chem. Soc.*, 2011, **133**, 7296–7299.
- 350 X. Li, L. Zhang, X. Zang, X. Li and H. Zhu, *ACS Appl. Mater. Interfaces*, 2016, **8**, 10866–10873.
- 351 X. Li, L. Zhang, M. Huang, S. Wang, X. Li and H. Zhu, *J. Mater. Chem. A*, 2016, **4**, 14789–14795.
- 352 J. Duan, S. Chen, B. A. Chambers, G. G. Andersson and S. Z. Qiao, *Adv. Mater.*, 2015, **27**, 4234–4241.
- 353 H. Tang, K. Dou, C. C. Kaun, Q. Kuang and S. Yang, *J. Mater. Chem. A*, 2014, **2**, 360–364.
- 354 J. Deng, L. Yu, D. Deng, X. Chen, F. Yang and X. Bao, *J. Mater. Chem. A*, 2013, **1**, 14868–14873.
- 355 J. Deng, P. Ren, D. Deng, L. Yu, F. Yang and X. Bao, *Energy Environ. Sci.*, 2014, **7**, 1919–1923.
- 356 H. Wang, Y. Yang, Y. Liang, J. T. Robinson, Y. Li, A. Jackson, Y. Cui and H. Dai, *Nano Lett.*, 2011, **11**, 2644–2647.
- 357 D. Deng, L. Yu, X. Chen, G. Wang, L. Jin, X. Pan, J. Deng, G. Sun and X. Bao, *Angew. Chem., Int. Ed.*, 2013, **52**, 371–375.
- 358 H. T. Chung, J. H. Won and P. Zelenay, *Nat. Commun.*, 2013, **4**, 1922.
- 359 J. A. Varnell, E. C. M. Tse, C. E. Schulz, T. T. Fister, R. T. Haasch, J. Timoshenko, A. I. Frenkel and A. A. Gewirth, *Nat. Commun.*, 2016, **7**, 12582.
- 360 J. Wei, Y. Liang, Y. Hu, B. Kong, G. P. Simon, J. Zhang, S. P. Jiang and H. Wang, *Angew. Chem.*, 2016, **128**, 1377–1381.
- 361 M. Tavakkoli, T. Kallio, O. Reynaud, A. G. Nasibulin, C. Johans, J. Sainio, H. Jiang, E. I. Kauppinen and K. Laasonen, *Angew. Chem., Int. Ed.*, 2015, **54**, 4535–4538.
- 362 J. Deng, P. Ren, D. Deng and X. Bao, *Angew. Chem., Int. Ed.*, 2015, **54**, 2100–2104.
- 363 Y. Hu, L. Zhong, J. O. Jensen and Q. Li, *Asia-Pac. J. Chem. Eng.*, 2016, **11**, 382–385.
- 364 Y. Yao, Q. Fu, Y. Y. Zhang, X. Weng, H. Li, M. Chen, L. Jin, A. Dong, R. Mu, P. Jiang, L. Liu, H. Bluhm, Z. Liu, S. B. Zhang and X. Bao, *Proc. Natl. Acad. Sci. U. S. A.*, 2014, **111**, 17023–17028.
- 365 R. Mu, Q. Fu, L. Jin, L. Yu, G. Fang, D. Tan and X. Bao, *Angew. Chem., Int. Ed.*, 2012, **51**, 4856–4859.
- 366 N. Zhang, Y. H. Zhang, X. Y. Pan, X. Z. Fu, S. Q. Liu and Y. J. Xu, *J. Phys. Chem. C*, 2011, **115**, 23501–23511.
- 367 S. Dong, Y. Cui, Y. Wang, Y. Li, L. Hu, J. Sun and J. Sun, *Chem. Eng. J.*, 2014, **249**, 102–110.
- 368 P. Gao, A. Li, D. D. Sun and W. J. Ng, *J. Hazard. Mater.*, 2014, **279**(21), 96–104.
- 369 S. Q. Liu, Z. Chen, N. Zhang, Z. R. Tang and Y. J. Xu, *J. Phys. Chem. C*, 2013, **117**(4), 8251–8261.
- 370 W. J. Ong, L. L. Tan, S. P. Chai and S. T. Yong, *Chem. Commun.*, 2015, **51**(5), 858–861.
- 371 P. Gao, J. C. Liu, D. D. Sun and W. Ng, *J. Hazard. Mater.*, 2013, **250**(6), 412–420.
- 372 M. Ahmad, E. Ahmed, Z. L. Hong, J. F. Xu, N. R. Khalid, A. Elhissi and W. Ahmed, *Appl. Surf. Sci.*, 2013, **274**(12), 273–281.
- 373 H. Moussa, E. Girot, K. Mozet, H. Alem, G. Medjandi and R. Schneider, *Appl. Catal., B*, 2016, **185**(16), 11–21.
- 374 Z. Chen, N. Zhang and Y. J. Xu, *CrystEngComm*, 2013, **15**(18), 3022–3030.
- 375 X. Q. An, J. C. Yu, Y. Wang, Y. M. Hu, X. L. Yu and G. J. Zhang, *J. Mater. Chem.*, 2012, **22**(19), 8525–8531.
- 376 D. Zhao, G. Sheng, C. Chen and X. Wang, *Appl. Catal., B*, 2012, **111**(23), 303–308.
- 377 Q. J. Xiang, J. G. Yu and M. Jaroniec, *Nanoscale*, 2011, **3**(24), 3670–3678.
- 378 Y. Wang, W. Wang, H. Mao, Y. Lu, J. Lu, J. Huang, Z. Ye and B. Lu, *ACS Appl. Mater. Interfaces*, 2014, **6**(28), 12698–12706.
- 379 Y. Sun, B. Qu, Q. Liu, S. Gao, Z. Yan, W. Yan, B. Pan, S. Wei and Y. Xie, *Nanoscale*, 2012, **4**(29), 3761–3767.

- 380 W. J. Ong, L. L. Tan, S. P. Chai, S. T. Yong and A. R. Mohamed, *Nano Energy*, 2015, **13**(31), 757–770.
- 381 H. Zhang, X. J. Lv, Y. M. Li, Y. Wang and J. H. Li, *ACS Nano*, 2010, **4**, 380–386.
- 382 J. C. Liu, H. W. Bai, Y. J. Wang, Z. Y. Liu, X. W. Zhang and D. D. Sun, *Adv. Funct. Mater.*, 2010, **20**(39), 4175–4181.
- 383 A. Tayyebi, M. Outokeh, M. Tayebi, A. Shafikhani and S. S. Sengor, *J. Alloys Compd.*, 2016, **663**(17), 738–749.
- 384 E. P. Gao, W. Z. Wang, M. Shang and J. H. Xu, *Phys. Chem. Chem. Phys.*, 2011, **13**(26), 2887–2893.
- 385 X. Liu, L. Pan, T. Lv, G. Zhu, T. Lu, Z. Sun and C. Sun, *RSC Adv.*, 2011, **1**(37), 1245–1249.
- 386 Y. Liang, H. Wang, H. S. Casalongue, Z. Chen and H. Dai, *Nano Res.*, 2010, **3**, 701–705.
- 387 G. D. Jiang, Z. F. Lin, C. Chen, L. H. Zhu, Q. Chang, N. Wang, W. Wei and H. Q. Tang, *Carbon*, 2011, **49**(42), 2693–2701.
- 388 C. Liu, L. Zhang, R. Liu, Z. Gao, X. Yang, Z. Tu, F. Yang, Z. Ye, L. Cui, C. Xu and Y. Li, *J. Alloys Compd.*, 2016, **656**, 24–32.
- 389 S. D. Perera, R. G. Mariano, K. Vu, N. Nour, O. Seitz, Y. Chabal and K. J. Balkus, *ACS Catalysis*, 2012, **2**(34), 949–956.
- 390 Y. Fu, X. Sun and X. Wang, *Mater. Chem. Phys.*, 2011, **131**(27), 325–330.
- 391 J. S. Lee, K. H. You and C. B. Park, *Adv. Mater.*, 2012, **24**(23), 1084–1088.
- 392 H. Liu, X. Dong, X. Wang, C. Sun, J. Li and Z. Zhu, *Chem. Eng. J.*, 2013, **230**(32), 279–285.
- 393 H. i. Kim, G. h. Moon, D. Monllor-Satoca, Y. Park and W. Choi, *J. Phys. Chem. C*, 2012, **116**, 1535–1543.
- 394 N. Li, G. Liu, C. Zhen, F. Li, L. Zhang and H.-M. Cheng, *Adv. Funct. Mater.*, 2011, **21**(20), 1717–1722.
- 395 B. Qiu, M. Xing and J. Zhang, *J. Am. Chem. Soc.*, 2014, **136**, 5852–5855.
- 396 Z. Zhang, F. Xiao, Y. Guo, S. Wang and Y. Liu, *ACS Appl. Mater. Interfaces*, 2013, **5**, 2227–2233.
- 397 C. Hou, Q. Zhang, Y. Li and H. Wang, *J. Hazard. Mater.*, 2012, **205**, 229–235.
- 398 Y. Li, H. Zhang, P. Liu, D. Wang, Y. Li and H. Zhao, *Small*, 2013, **9**(30), 3336–3344.
- 399 J. J. Duan, S. Chen, M. Jaroniec and S. Z. Qiao, *ACS Nano*, 2015, **9**, 931–940.
- 400 C. Han, Z. Chen, N. Zhang, J. C. Colmenares and Y. J. Xu, *Adv. Funct. Mater.*, 2015, **25**(13), 221–229.
- 401 G. Lui, J. Y. Liao, A. Duan, Z. Zhang, M. Fowler and A. Yu, *J. Mater. Chem. A*, 2013, **1**(31), 12255–12262.
- 402 N. T. Khoa, S. W. Kim, D. H. Yoo, S. Cho, E. J. Kim and S. H. Hahn, *ACS Appl. Mater. Interfaces*, 2015, **7**(11), 3524–3531.
- 403 H. Liu, S. Liu, Z. Zhang, X. Dong and T. Liu, *Sci. Rep.*, 2016, **6**, 33839.
- 404 J. C. Spear, B. W. Ewers and J. D. Batteas, *Nano Today*, 2015, **10**, 301–314.
- 405 D. Berman, A. Erdemir and A. V. Sumant, *Mater. Today*, 2014, **17**, 31–42.
- 406 P. Wu, X. Li, C. Zhang, X. Chen, S. Lin, H. Sun, C. Lin, H. Zhu and J. Luo, *ACS Appl. Mater. Interfaces*, 2017, **9**, 21554–21562.
- 407 A. Smolyanitsky, J. P. Killgore and V. K. Tewary, *Phys. Rev. B: Condens. Matter Mater. Phys.*, 2012, **85**, 035412.
- 408 D. Yalin, *J. Phys. D: Appl. Phys.*, 2014, **47**, 055305.
- 409 S. W. Liu, H. P. Wang, Q. Xu, T. B. Ma, G. Yu, C. Zhang, D. Geng, Z. Yu, S. Zhang, W. Wang, Y.-Z. Hu, H. Wang and J. Luo, *Nat. Commun.*, 2017, **8**, 14029.
- 410 S. Li, Q. Li, R. W. Carpick, P. Gumbsch, X. Z. Liu, X. Ding, J. Sun and J. Li, *Nature*, 2016, **539**, 541–545.
- 411 A. S. de Wijn, *Nature*, 2016, **539**, 502–503.
- 412 D. Berman, A. Erdemir and A. V. Sumant, *Carbon*, 2013, **54**, 454–459.
- 413 D. Berman, A. Erdemir and A. V. Sumant, *Carbon*, 2013, **59**, 167–175.
- 414 Z. Wei, Z. Ming, Z. Hongwei, T. Yu, W. Kunlin, W. Jinquan, J. Fei, L. Xiao, L. Zhen, Z. Peng and W. Dehai, *J. Phys. D: Appl. Phys.*, 2011, **44**, 205303.
- 415 J. Lin, L. Wang and G. Chen, *Tribol. Lett.*, 2011, **41**, 209–215.
- 416 X. Dou, A. R. Koltonow, X. He, H. D. Jang, Q. Wang, Y.-W. Chung and J. Huang, *Proc. Natl. Acad. Sci. U. S. A.*, 2016, **113**, 1528–1533.
- 417 S. Choudhary, H. P. Mungse and O. P. Khatri, *J. Mater. Chem.*, 2012, **22**, 21032–21039.
- 418 C. C. Vu, S. Zhang, M. Urbakh, Q. Li, Q. C. He and Q. Zheng, *Phys. Rev. B: Condens. Matter Mater. Phys.*, 2016, **94**, 081405.
- 419 J. Yang, Z. Liu, F. Grey, Z. Xu, X. Li, Y. Liu, M. Urbakh, Y. Cheng and Q. Zheng, *Phys. Rev. Lett.*, 2013, **110**, 255504.
- 420 Z. Liu, J. Yang, F. Grey, J. Z. Liu, Y. Liu, Y. Wang, Y. Yang, Y. Cheng and Q. Zheng, *Phys. Rev. Lett.*, 2012, **108**, 205503.
- 421 D. Berman, S. A. Deshmukh, S. K. R. S. Sankaranarayanan, A. Erdemir and A. V. Sumant, *Science*, 2015, **348**, 1118.
- 422 S. Kawai, A. Benassi, E. Gnecco, H. Söde, R. Pawlak, X. Feng, K. Müllen, D. Passerone, C. A. Pignedoli, P. Ruffieux, R. Fasel and E. Meyer, *Science*, 2016, **351**, 957.
- 423 X. Zheng, L. Gao, Q. Yao, Q. Li, M. Zhang, X. Xie, S. Qiao, G. Wang, T. Ma, Z. Di, J. Luo and X. Wang, *Nat. Commun.*, 2016, **7**, 13204.
- 424 R. Mehta, S. Chugh and Z. Chen, *Nano Lett.*, 2015, **15**, 2024–2030.
- 425 E. Kim, N. S. Arul and J. I. Han, *J. Nanosci. Nanotechnol.*, 2016, **16**, 6061–6067.
- 426 I. A. Sahito, K. C. Sun, A. A. Arbab, M. B. Qadir and S. H. Jeong, *Carbohydr. Polym.*, 2015, **130**, 299–306.
- 427 A. Abbas, Y. Zhao, J. Zhou, X. Wang and T. Lin, *Fibers Polym.*, 2013, **14**, 1641–1649.
- 428 X. Jiang and L. T. Drzal, *Composites, Part A*, 2011, **42**, 1840–1849.
- 429 K. Krushnamurti, M. Rini, I. Srikanth, P. Ghosal, A. P. Das, M. Deepa and C. Subrahmanyam, *Composites, Part A*, 2016, **80**, 237–243.
- 430 M. Sanghermano, L. Calvara, E. Chiavazzo, L. Ventola, P. Asinari, V. Mittal, R. Rizzoli, L. Ortolani and V. Morandi, *Prog. Org. Coat.*, 2015, **86**, 143–146.

- 431 T. Luo and J. R. Lloyd, *Adv. Funct. Mater.*, 2012, **22**, 2495–2502.
- 432 G. Huang, J. Gao, X. Wang, H. Liang and C. Ge, *Mater. Lett.*, 2012, **66**, 187–189.
- 433 Y. Shi, X. Qian, K. Zhou, Q. Tang, S. Jiang, B. Wang, B. Wang, B. Yu, Y. Hu and R. K. K. Yuen, *Ind. Eng. Chem. Res.*, 2013, **52**, 13654–13660.
- 434 G. Huang, J. Yang, J. Gao and X. Wang, *Ind. Eng. Chem. Res.*, 2012, **51**, 12355–12366.
- 435 X. Zhang, Q. Shen, X. Zhang, H. Pan and Y. Lu, *J. Mater. Sci.*, 2016, **51**, 10361–10374.
- 436 S.-D. Jiang, Z.-M. Bai, G. Tang, Y. Hu and L. Song, *Ind. Eng. Chem. Res.*, 2014, **53**, 6708–6717.
- 437 D. Wang, K. Zhou, W. Yang, W. Xing, Y. Hu and X. Gong, *Ind. Eng. Chem. Res.*, 2013, **52**, 17882–17890.
- 438 C. Gao, T. Liu, C. Shuai and S. Peng, *Sci. Rep.*, 2014, **4**, 4712.
- 439 X. Wang, W. Xing, L. Song, H. Yang, Y. Hu and G. H. Yeoh, *Surf. Coat. Technol.*, 2012, **206**, 4778–4784.
- 440 S. S. Kandanur, M. A. Rafiee, F. Yavari, M. Schrammeyer, Z.-Z. Yu, T. A. Blanchet and N. Koratkar, *Carbon*, 2012, **50**, 3178–3183.
- 441 P. F. Li, H. Zhou and X. Cheng, *Surf. Coat. Technol.*, 2014, **254**, 298–304.
- 442 C. Zhao, S. Pandit, Y. Fu, I. Mijakovic, A. Jesorka and J. Liu, *RSC Adv.*, 2016, **6**, 38124–38134.
- 443 F. Gao, C. Xu, H. Hu, Q. Wang, Y. Gao, H. Chen, Q. Guo, D. Chen and D. Eder, *Mater. Lett.*, 2015, **138**, 25–28.
- 444 Y. Liu, Z. Dang, Y. Wang, J. Huang and H. Li, *Carbon*, 2014, **67**, 250–259.
- 445 Y. Liu, J. Huang and H. Li, *J. Therm. Spray Technol.*, 2014, **23**, 1149–1156.
- 446 M. Li, Q. Liu, Z. Jia, X. Xu, Y. Cheng, Y. Zheng, T. Xi and S. Wei, *Carbon*, 2014, **67**, 185–197.
- 447 A. Janković, S. Eraković, M. Mitić, I. Z. Matić, Z. D. Juranić, G. C. P. Tsui, C. y. Tang, V. Mišković-Stanković, K. Y. Rhee and S. J. Park, *J. Alloys Compd.*, 2015, **624**, 148–157.
- 448 A. Janković, S. Eraković, M. Vukašinović-Sekulić, V. Mišković-Stanković, S. J. Park and K. Y. Rhee, *Prog. Org. Coat.*, 2015, **83**, 1–10.
- 449 Y. Yan, X. Zhang, H. Mao, Y. Huang, Q. Ding and X. Pang, *Appl. Surf. Sci.*, 2015, **329**, 76–82.
- 450 K. S. Novoselov, V. I. Falko, L. Colombo, P. R. Gellert, M. G. Schwab and K. Kim, *Nature*, 2012, **490**, 192–200.